

Spontaneous Evolution of Long-range Correlations in Dynamical Systems

A Thesis submitted for the degree of
Doctor of Philosophy (Science)
in
Physics(Theoretical)

by
Biplab Bhattacharjee

Department of Physics
University of Calcutta
2017

Dedicated to

My Parents

Acknowledgement

I would like to thank my Ph.D. supervisor, Prof. Subhrangshu Sekhar Manna for his guidance, stimulating suggestions and encouragement. From briefing minute technicalities of simulations to make me understand the larger than life picture of physics, he has been an encouragement all along. I would also like to thank, Prof. Jayanta K. Bhattacharjee and Prof. Binayak Dutta Roy (late) for their aspiring classes that dragged me to the interesting and fascinating field of statistical physics. I am also very much thankful to Dr. Punyabrata Pradhan and Dr. Sakuntala Chatterjee who had been active faculty members of our statistical physics group and had been constant motivations for students with instructive and enjoyable comments and suggestions, especially in of our weekly journal club meetings.

Special thanks to my collaborators, Dr. Animesh Mukherjee, Dr. Sraddha Mishra, Prof. Amitava Datta and Kunal da. They all have been quite instructive and have enriched me with a lot of fruitful discussions and motivations. Few of my seniors specially Abhijit da and Amartya da owe a lot of gratitude.

I am quite privileged to have a bunch of talented yet quite gel along friends and group members, who always had been open to any kind of academic and non academic discussions. Arghya, my masters' room mate cum class mate and my masters' project colleague has been very supportive throughout my stay at SNB. Sumanta Kundu and Suman Aich, two of my juniors have also been quite influencing. A lot of academic, non academic, social and personal discussions with them have molded me not only as a good learner but also as a better person. I would also like to mention Subhasish, J. B, Debanjan, Arijit, Arnab, Anand and Ashu with whom I have spent quite a long, good and bad times together. Special thanks to Sayani, Shauri, Ishita, Chandreyee, and Amal for many special memories to cherish. Aritra, Monalisa, Indranil, Debasish, Subrata, Rakesh, Subhadip,

Rajkumar, Souvanik, Krishnendu, Aslam, Sarowar da and many others construct the infinite circle of friends and colleagues who have been more or less an influence in some way or the other.

I would also like to acknowledge my teachers during my school days, specially Saikat sir, Rupa di, Dilip sir, Raja da and Ashish sir. Their amicable and constant effort behind me the person, me the student, defines what I am now.

A special phase has been well spent with the members of Roy's Taekwondo Academy (RTA). Special thanks to Master Pradipta Kumar Roy and Master Ruma Roy Chowdhury. Its because of their motivation and passionate training that I am in love with the spirit of the game, Taekwondo, and it also helped me relax my body and mind during the stressful phases in the final year of my Ph.D.

Special mention to our college group, the extended G7 that includes Swagata, Samrat, Deepak, Subrata, Tanmoy, Somrita, Sayan and Nayan who made my B.Sc days a learning, enjoyable and memorable period.

Special thanks to Anjasha, for being a constant mental support in many critical situations and for bringing a fresh breath of air during stresses and in my life.

Finally, I would like to acknowledge my family members and especially my parents. They have been with me throughout, in every critical situation. Their efforts, support, and patience are beyond description. Not to forgot my little brother Sourav, with whom I have grown up and now share an in-depth empathy.

Biplab Bhattacharjee,
Senior Research Fellow,
Department of Theoretical Sciences,
Satyendra Nath Bose National Centre for Basic Sciences,
Block JD, Sector-III, Salt Lake, Kolkata-700106.

Publication List

1. *Information sharing and sorting in a community*,
Biplab Bhattacharjee, S. S. Manna and A. Mukherjee,
Phys. Rev. E 87, 062808,(2013).
2. *Cyclic and Coherent States in Flocks with Topological Distance*,
Biplab Bhattacharjee, K. Bhattacharya and S. S. Manna,
Frontiers in Physics 1, 35 (2014).
3. *Topological-distance-dependent transition in flocks with binary interactions*,
Biplab Bhattacharjee, S. Mishra and S. S. Manna,
Phys. Rev. E 92, 062134 (2015).
4. *Asymptotic properties of restricted naming games*,
B. Bhattacharjee, Amitava Datta and S. S. Manna,
Physica A 478, 177-187 (2017)
5. *Band structure of a flock in motion with quenched range of interaction*,
Biplab Bhattacharjee and S. S. Manna,
(submitted).

Contents

Acknowledgements	ii
Publication List	iv
Contents	v
1 Introduction	1
1.1 Complex systems	2
1.2 Collective behavior	4
1.2.1 The Vicsek model	5
1.2.2 Long-range order in 2D dynamical XY model	8
1.2.3 Transition: Continuous or Discontinuous	9
1.2.4 Band formation	11
1.2.5 Topological interaction	12
1.2.6 Plan of the thesis	13
1.3 Naming Game	16
1.3.1 Definition of Naming Game	16
1.3.2 Naming Game on regular lattices	18
1.3.3 Naming Game on random graphs	19
1.3.4 Degree dependence	20
1.3.5 Master equation approach and other studies	21
1.3.6 Plan of the thesis	22

1.4	Preliminaries of critical phenomena	24
1.4.1	Phase transitions	24
1.4.2	Long-range order	32
1.4.3	Importance of models	33
1.5	Complex networks	33
1.5.1	Random connected graphs	34
1.5.2	Small world networks	35
1.5.3	Degree Distribution	36
1.5.4	Clustering	37
2	Cyclic and coherent states in flocks with topological distance	39
2.1	Introduction	40
2.2	Model	43
2.3	Random geometric graphs	45
2.4	Stationary states	47
2.4.1	Single sink states	48
2.4.2	Cyclic states	48
2.4.3	Other states	51
2.5	Dynamics in presence of noise	54
2.6	The fastest refreshing rate of the interaction zone	60
2.7	Vortices on the square lattice	63
2.8	Summary	68
3	Topological distance dependent transitions in flocks with binary interactions	70
3.1	Introduction	71
3.2	Model	72
3.3	The results	74
3.3.1	The $n = 1$ case	74

3.3.2	The $n = 2$ case	77
3.3.3	The $n \geq 3$ cases	79
3.4	Studying different characteristic times	81
3.4.1	Persistence times	81
3.4.2	Information spreading times	83
3.5	Theoretical analysis	84
3.5.1	Hydrodynamic equations of motion for binary flocks	84
3.5.2	Linear stability of homogeneous polarized state close to order-disorder transition	86
3.6	Summary	89
4	Band structure in collective motion with quenched range of interaction	92
4.1	Introduction	93
4.2	Model	94
4.3	Description of the dynamical evolution	96
4.4	Results	99
4.4.1	System size $L = 128$	99
4.4.2	System size $L = 256$	105
4.4.3	System size $L = 512$	109
4.5	Summary	114
5	Information sharing and sorting in a community	116
5.1	Introduction	117
5.2	Model	119
5.3	Algorithm	121
5.4	Results	123
5.5	The largest cluster	125
5.6	Summary	128

6	Asymptotic properties of restricted naming games	129
6.1	Introduction	130
6.2	Restricted vocabulary	131
6.2.1	The model	132
6.2.2	Results	134
6.3	Symmetric naming game with limited number of distinct names .	136
6.3.1	Model and results	136
6.4	Summary	139

1 Introduction

1.1 Complex systems

What is a complex system? A complex system is characterized by some properties which add features driving complexity to a however simple looking system. Among many, few properties stand out [1]. Internal structure and subsystem hierarchy [2], stochastic evolution and dynamical adaptation [3], uncertainty and emergence of unpredictable features constructs the periphery of any complex dynamical system [4, 5].

Ecosystem [6] along with evolving social dynamics [7], financial markets [8], biological developments [9, 10], all are prototypical examples of complex adaptive systems. In these above-mentioned systems and many such other systems, localized interactions and stochastic selection processes develop emerging multilevel dynamics. The uncertain nature of the behavior of components, stochastic adaptation and dynamic evolution under different internal and external perturbations give rise to features, almost unpredictable, that become an integral part of such systems are known as emerging features. The components of the system follow some prefixed microscopic rules.

Ranging from evolving species to natural phenomena like earthquakes [11, 12], social organization and most of the observed natural structures have complexity built within. Quantifying the probabilistic features and determining how it propagates through the system is a key aspect of reliable prediction and control of complex systems. Thus, complex systems are identified by their feature of displaying emergent organization without a central organizing principle, that is what we call an emergence. Such systems can't be analyzed by decomposing the system into subsystem levels which break the scales that characterize the system. Here the construction of statistical tools for analyzing complex systems plays a vital role.

So the question that becomes important to answer is what lay the basis of understanding complex systems. From completely different interactive microscopic

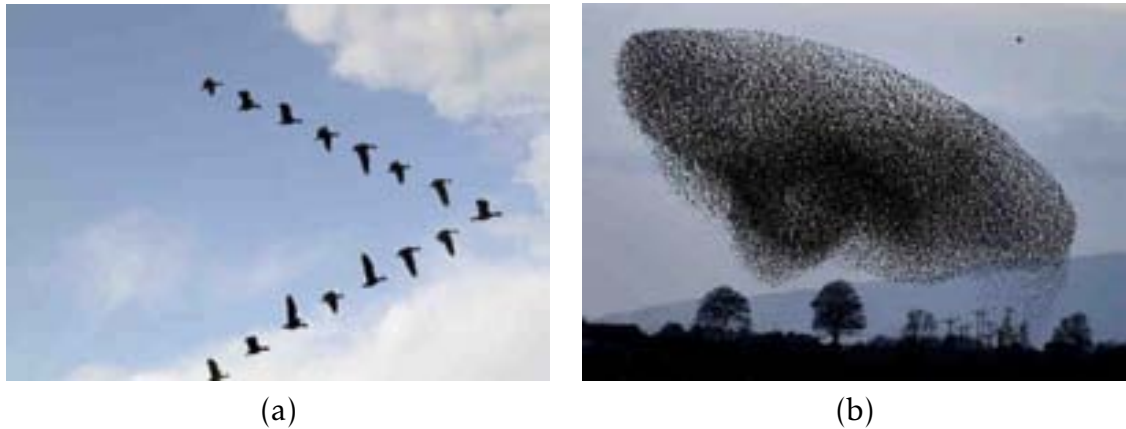


Figure 1.1: Examples of collective motion: (a) A small flock of birds ^a (b) a large flock of Starlings ^b

dynamics, complex systems give rise to macroscopic features that reflect in spontaneous evolution of long-range order, and consequently, universality classes of phase transitions emerge. The qualitative description of any complex system depends on how long-range order develops, i.e. how correlation among different quantities develop in systems. Under critical emergent behavior, in what scales the long-range correlation develops and the universality classes that each system belongs to, lay the foundation for studying complex natural systems.

In this chapter, we will discuss two of the most fascinating complex systems, i.e., the collective behavior of self-propelled creatures moving in free space, e.g., bird flocks [13, 14] and the dynamical process of naming games, displaying eye-catching emergent features like self-organization and global consensus, with local, spatially limited interactive mechanism. In the light of the most fascinating behaviors in natural systems, well supported by physical laws, models and universal constructions these two models will spearhead the analysis of the dynamical evolution of long-range order in dynamical systems and will define the course of the thesis.

^a Source: <https://www.tes.com/lessons/wHOPg5ggmf9pxw/ock-words>

^b Source: <https://www.theguardian.com/environment/gallery/2014/nov/06/starling-murmurations-in-pictures>

1.2 Collective behavior

Movements of flocks of birds (Fig. 1.1), schools of fishes, swarms of bees, bacterial colonies, etc. are common examples of collective motion in nature. These groups of creatures move together and along the same direction irrespective of their sizes. The topic of studying the properties and characteristics of such groups in motion has been popularly known as the ‘Collective motion’ or ‘Collective behavior’. Over last several decades, this topic has attracted the attention of the scientific community, for both experimental as well as theoretical research.

In the language of collective dynamics, the individual creatures are referred as ‘agent’. In a collection, agents are considered as short-sighted. An individual agent is influenced by a group of other agents within a well-defined neighborhood around the individual agents, who in turn interact with their own neighbors etc. Thus a pair of agents feels the influence of each other, even though they are positioned at a large distance of separation. Eventually, all agents in the entire flock become correlated, and the whole group acts in unison. In this way, even a short-range interaction among the agents leads to a unique global behavior of the entire collection. Such a flock pattern is called ‘cohesive’ when, on the average, a certain characteristic distance is maintained by each agent from other agents. At the same time, they are said to be ‘coherent’ since all agents travel along the same direction in space. Therefore, in this class of collective dynamical systems, the features of coherence and cohesion had been regarded as the signature of long-range correlation. These correlations emerge spontaneously from the dynamical rules of the model systems described by the microscopic interactions.

These collective features emerge spontaneously and are maintained by the system collectively, if not exposed to quite high perturbations. Even in the presence of some external perturbations, e.g. pressure from a nearby predator in the case of a school of fishes or a flock of birds, the system depicts adaptive mechanism, and up to a certain threshold of such external perturbation, the emergent struc-

tures are resilient. The question posed by T. Vicsek [15] and in the quite broader sense is often asked by biologists, physicists and chemists, is, "Are these observed motion patterns system specific?". Subsequent studies suggested that these kinds of qualitative phenomena have been observed in a large class of systems. These systems follow general and often simpler microscopic laws and similar complex qualitative features emerge spontaneously. All these class of systems is often said to belong to systems depicting "collective phenomena/behavior" (CB).

How such collective patterns emerge from local microscopic dynamics, what kind of models or local interaction rules ensure such global correlations and order-disorder transitions in the presence of noise defines the outline of the preliminary studies on collective dynamical systems. The simplest model, famously known as "Vicsek Model" [16] after the name of Tamas Vicsek, described the basic features of collective phenomena and is qualitatively followed by many in different variants of the problem.

1.2.1 The Vicsek model

The Vicsek model is a well-known model in collective behavior [16]. In its two-dimensional version, N agents are released at random locations, (x_i, y_i) within a square box of size $L \times L$ fitted with the periodic boundary condition. All agents move with a constant self-propulsion speed v_0 , and the directions θ_i of their velocities have been drawn from a uniform distribution between 0 and 2π . The agents are considered to be massless point particles, and hence hard core collisions do not take place. Each agent is associated with a range \mathcal{R} (Fig. 1.2(a)), same for all agents. Each agent interacts with $n_{\mathcal{R}}(t)$ agents, including itself, within this range \mathcal{R} . The time t is measured by the number of updates per agent.

At any arbitrary intermediate time t , during the dynamical evolution, the system passes through a series of microstates. Each microstate is defined by the specific positions and the directions of motion of all the N agents. Let us denote

the velocity vector of the i -th agent at time t as $\mathbf{v}_i(t)$ having the orientational angle $\theta_i(t)$. At the next time step ($t + 1$), the orientational angles $\theta_i(t + 1)$ are then estimated for all agents in a synchronous manner. The agent i interacts with all $n_{\mathcal{R}}(t)$ (Fig. 1.2(b)) agents within its neighborhood, including itself. The resultant direction $\theta_i(t + 1)$, of all the velocity vectors within \mathcal{R} , is determined and is assigned as the direction of the velocity of agent i at time ($t + 1$). The resultant is estimated as (Fig. 1.2(c)),

$$\theta_i(t + 1) = \tan^{-1} \left[\frac{\sum_{j \in \mathcal{R}} \sin \theta_j(t)}{\sum_{j \in \mathcal{R}} \cos \theta_j(t)} \right], \quad (1.1)$$

where the summation runs over all $n_{\mathcal{R}}(t)$ agents within \mathcal{R} . Since individual agents have distinctly different neighborhoods, even before the application of noise, different agents may have different directions of motion. With their constant self-propulsion speed v_0 , all the agents are then displaced along their updated velocity directions. This update takes place synchronously. The velocities of all the agents at the next time step ($t + 1$) are then determined using the velocities of all the agents at time t . Following the dynamics, after a transient phase, the system relaxes to a completely coherent phase in the noise-free case. The agents then depict coherent and cohesive structures, and the motion is purely ballistic.

However, with the introduction of scalar noise the Eqn. (1.1) is modified as:

$$\theta_i(t + 1) = \tan^{-1} \left[\frac{\sum_{j \in \mathcal{R}} \sin \theta_j(t)}{\sum_{j \in \mathcal{R}} \cos \theta_j(t)} \right] + \zeta(\eta). \quad (1.2)$$

The noise term $\zeta(\eta)$ quantifies the amount of error that is added to the orientational angle of each agent participating in an interaction. Qualitatively, any other kind of perturbation can be introduced in the microscopic rules governing the dynamics. Here η measures the strength of the noise and $\zeta(\eta)$ represents a random angle for each agent drawn from a uniform distribution within $[-\eta/2,$

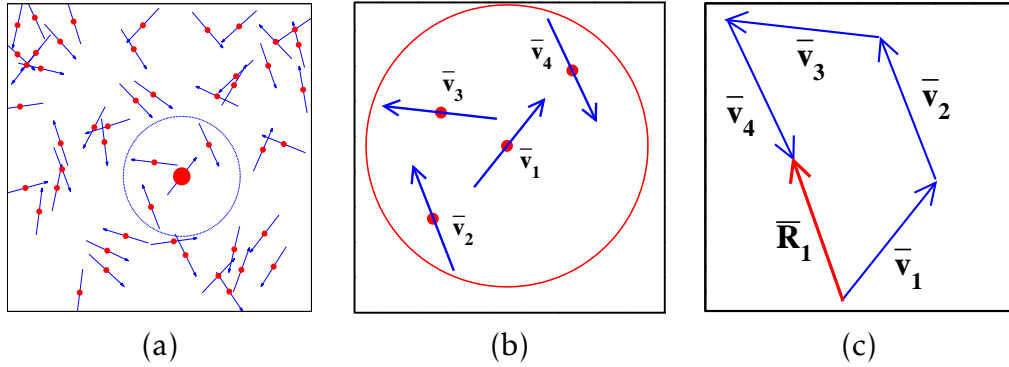


Figure 1.2: In (a) the red dots are the positions of the particles and the corresponding blue arrows are the associated velocity directions of each particle. The Vicsek interaction radius of a particle (big red dot) has been shown using a blue circle around the particle. In (b) the same interacting neighborhood of the particle with velocity \bar{v}_1 and its neighbors with velocities \bar{v}_2 , \bar{v}_3 and \bar{v}_4 have been depicted. The resultant velocity direction \bar{R}_1 , of the same particle has been shown in (c).

$\eta/2]$. Each agent is then displaced along its direction of motion $\theta_i(t+1)$. With the introduction of noise in the system, the completely coherent structures start to dismantle, and the amount of coherence systematically decays with increasing noise strength.

To quantify the amount of coherence or alternatively the amount of order, the instantaneous global order parameter $\Omega(t, \eta, L)$ is defined for the entire system as the magnitude of the velocity vector of an agent, averaged over all agents and scaled by the speed v_0 .

$$\Omega(t, \eta, L) = \frac{1}{Nv_0} \left| \sum_{j \in N} \mathbf{v}_j(t) \right|. \quad (1.3)$$

In the stationary state $\Omega(t, \eta, L)$ is estimated over a long duration of time and is averaged over time to find $\Omega(\eta, L)$.

With systematically increasing noise strength, the system shows a transition from an ordered phase with a high value of the order parameter to a disordered phase with almost zero value of the order parameter. The motions of individual

agents in the disordered phase, are diffusive. The transition, in the study of Vicsek et. al. is claimed to be of a continuous type, in the thermodynamic limit. The following set of equations in eqn. 1.4

$$\Omega(\eta, \rho) \sim \begin{cases} [\eta_c(\rho) - \eta]^\beta \\ [\rho - \rho_c(\eta)]^\delta \end{cases} \quad (1.4)$$

defines the behavior of the order parameter at criticality and are similar to the behavior of order parameter in case of a standard second order transition [17]. Here β and δ are the critical exponents that characterize the critical behavior of the model, η is the typical noise strength and ρ is the particle density. $\eta_c(\rho)$ and $\rho_c(\eta)$ are respectively the critical noise and critical density in the thermodynamic limit, $L \rightarrow \infty$. This more or less summarizes the model and its behavior around criticality.

1.2.2 Long-range order in 2D dynamical XY model

As soon as the Vicsek model was introduced, the observed symmetry breaking and the existence of a long-range ordered phase at high temperature like regimes depicted by the model with almost equivalent dynamical rules like 2D X-Y model where the velocity in the Vicsek model plays the similar role as that of spins in the XY model, draw interest of many in this direction. In the same year, 1995, J. Toner and Y. Tu [18] explained the behavior following a continuum description of such a model. They explained that what makes the long-range ordered state stable in this model is the existence of a convection term and is the essential difference with the equilibrium XY model where no long-range ordered phase is observed in 2D. The non-equilibrium effects of the nonlinear terms in the dynamical equation stabilize the long-range ordered state even in two dimensions. From Renormalization Group analysis they also claimed that this model is different from its equilibrium counterpart in all spatial dimension, $d < 4$. In a later

study [19] of the same dynamics, they have shown that Galilean invariance is not present in such a dynamics and presence of more than one non-zero sound speeds of propagation along the mean direction is possible. Also, anomalous scaling relations has also been predicted and are justified by showing attenuation effect of sound waves.

1.2.3 Transition: Continuous or Discontinuous

With the subsequent studies [18–20] focusing on the scaling relations of the transition observed, quite surprisingly, in the 2D Vicsek model, Chaté. et al. [21] came up with another twist in the tale. In their study, they investigated this fundamental aspect of collective motion rigorously and questioned the continuous nature of the transition. Quite elaborated numerical results were presented with the indication that there exists a “crossover” system size, L^* , beyond which, independent of the magnitude of the self-propulsion speed, the discontinuous character of the transition appears. It was also claimed that, in the thermodynamic limit, the discontinuous character of the critical transition in models of collective systems, is the “true” asymptotic behavior. It was argued in support of their observations that for the set of density and self-propulsion speed assumed in the Vicsek’s original paper, the crossover system size is larger compared to the sizes in which the simulations have been performed. With a very small density $\rho = 1/8$ and self-propulsion speed $v = 0.50$ it was shown [21] that the Vicsek model shows a discontinuous transition in the thermodynamic limit.

They introduced another kind of noise, the vectorial noise, in contrast to the angular/scaler noise incorporated in the Vicsek’s model. The argument in favor of a different kind of noise is as follows: The agents can make an error while estimating the velocity directions of its neighbors. The noise then adds up as an error with all individual agents velocity vector. The corresponding L^* is shown to be comparatively smaller and hence for high densities comparatively smaller

system sizes suffice to show the critical behavior in the thermodynamic limit.

In 2006, however, M. Nagy et. al., in support of the study of Vicsek [16] and the claim of a continuous transition, placed some critically analyzed arguments [22]. It was categorically shown in this study that, for larger self-propulsion speeds the boundary effects are predominant and as a result, the critical behavior for larger self-propulsion speeds are not conclusive. The discontinuous transition is an artifact of the larger speeds. There exist a smaller speed regime, $v_0 \leq 0.10$, where the diffusion is isotropic, the boundary effects are negligible, and hence the critical behavior is conclusive, and in this regime, the transition is found to be continuous. However, for the speed regime $v_0 \geq 0.30$ the strongly anisotropic diffusion has been observed due to the strong boundary effects. Nagy et. al. has claimed that in this regime the boundary effects are so strong that the observed discontinuous transitions might not be the actual critical behavior of the problem. Further it was also stated, “the motion of the particles in such systems are quasi-continuous, i.e., usually the reaction time of the birds are significantly faster than the characteristic time that is needed to travel through their interacting neighborhood. This condition imposes the following constraint on the update time Δt in the numerical simulations: $\Delta t \ll R/v$ ” [16], where v is the self-propulsion speed. This constraint is satisfied in the small velocity regime. The large velocity regime $\Delta t \gg 0.30$, assumed by Chaté et. al. [21], might be a reasonable approximation in case of rare flocking processes (e.g., ‘turbulent’ motion of escaping birds during predator attack), however, due to strong boundary effects in those situations, any conclusive critical behavior is almost impossible.

Baglietto and Albano [23] also exhibited that for smaller v , even in the limit when the speed goes to zero (only except when it is exactly equal to zero), the disorder to order transition is continuous and is independent of the actual value of the self-propulsion speed v in this regime.

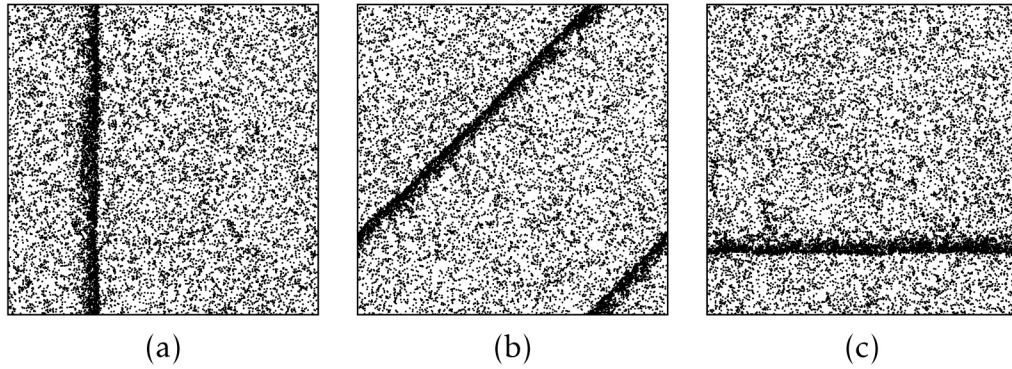


Figure 1.3: Pictorial depiction of band formation in flocks. The (a) (b) and (c) shows the parallel diagonal and perpendicular moving bands wrt the y -axis. The sharp edge of the bands are the respective moving front.

1.2.4 Band formation

While demonstrating the strong boundary effects for comparatively larger self-propulsion speeds, in their study, [22], Nagy. et. al. observed some high density bands moving vertical (Fig. 1.3(a)), horizontal (Fig. 1.3(b)) or diagonal (Fig. 1.3(c)) to the boundaries. These are argued to be the artifact of strong boundary effects and are then identified as the signature of a discontinuous transition. In further studies, Chaté et. al. [24], with the help of extensive numerical simulations verified the existence of high density highly ordered bands in the ordered phase, close to the transition point. These bands are highly ordered and depict ballistic motion with speed almost equal to the self-propulsion speed v . However, the particles outside the bands, i.e. in the comparatively lesser density regimes are completely disordered and follows diffusive motion. From the power-spectra analysis of the density profiles, they further added that these band-like structures, in the asymptotic limit, are not regular wave trains characterized by a single wavelength, rather a collection of irregularly spaced localized traveling long lived metastable (or possibly stable) objects characterized by multiple wave lengths.

In a subsequent study [25] of flocking phenomena via the corresponding hy-

hydrodynamic description, reverified the existence of high density band-like structures. The critical analysis in their study identified three flocking states, namely the “Fluctuating Flocking state” in the low speed high density regime, the “striped phase” with properly formed bands in the high density and high speed regime and an “isotropic stable state” in the low density regime, for any speed. They claimed that there exist a critical self-propulsion speed $v_c(\rho)$ that separates the polarized moving state with large anomalous fluctuations (below $v_c(\rho)$) from striped phase moving with high speed (above $v_c(\rho)$). These states are however separated from the stable isotropic state by a critical density $\rho_c(v)$. From the stability analysis, it has been observed that the fluctuating flocking states are the result of giant number fluctuations around the criticality. Due to the convective nonlinearities, the stability of the propagating front wave solutions that correspond to the high density band formation, sets in.

1.2.5 Topological interaction

From binary collision model to model with a repulsive term, with acceleration dependent alignment, many variants of the Vicsek model has been studied aiming to understand the critical behavior of collective phenomena. The consequent numerical and analytic studies were aimed at identifying the type of the transition and the microscopic features driving the system to form stable long-range order in the system. However, with the Starflag group [26] presenting their experimental results debriefing some astonishing results, propelled the study of collective behavior in another direction. In their study, they claimed that the density dependent metric interaction (neighborhood specified by an interaction radius R) is far from being practical. Observing the angular density distribution of neighboring birds in flocks of Starlings, it has been found to be anisotropic. It implies that it is more likely for a Starling to keep its nearest neighbor at its two sides instead of keeping them on the front and back and that eventually defines

their neighborhood. Fishes [27] have also been found to interact with neighbors determined by topological rules. The neighborhood forms a Voronoi geometric structure that is topologically unique and hence the neighborhood is termed as the “topological neighborhood” which fixes the number of neighbors that the individual birds can interact with. The order-disorder transition observed in the models of collective motion with the topological interactions [28–30] and the observed ordered phase at the finite density regime is found to be different from that of its metric counterpart [31].

1.2.6 Plan of the thesis

As stated in the above discussion, the phenomenon of collective behavior is being studied with great interest in systems exhibiting non-equilibrium phase transition under driven noise [15, 18, 20, 32–37]. With tuning the noise parameter to a vanishingly small value, such a system of co-moving agents, spontaneously arrives at an ordered state while evolving dynamically from any arbitrary initial state. On the other hand for stronger noise, the order parameter vanishes [16]. In some studied models in the literature, the nature of the associated transition has been suggested to be ‘continuous’ [16, 26, 38–40] whereas in some other examples ‘discontinuous’ transitions have been claimed [24, 41] to exist. The interaction of an agent with other agents in its local neighborhood determines the dynamical behavior of the agent. Here the neighborhood is determined in terms of Euclidean distance [16] or topological distance [26, 28, 30]. Moreover in the low noise regime, occurrence of facets like high density traveling bands was revealed in later studies [21, 24] and arguments were put forward in favor of a discontinuous transition. Further, it has also been argued that by tuning the self-propulsion speed of agents one can switch over from continuous to discontinuous transitions [22].

Almost all models studying collective phenomena found in literature has as-

sumed that the flock moves in a space having a periodic boundary. Helical, hexagonal and other boundaries have also been considered but only in the context of band formation. A periodic boundary condition is, however, a jargon and quite non-physical for a system limited to a small regime in infinite space. Also, as stated previously that the field study by the StarFlag group indicated in support of the topological distance interactions in co-moving systems rather than metric distance [26], citing the observations on the flocks of Starlings. The birds in the Starling flock prefer to keep its nearest neighbor at its two sides instead of keeping them on the front and back, and that eventually defines their neighborhood. Fishes [27] have also been found to interact with neighbors determined by topological rules.

These studies prompted us to study the collective motion of flocking phenomena in two dimensions using the interactions depending on the topological distance under open boundary conditions.

In Chapter 2, a detailed numerical analysis of the topological distance dependent model for collective motion under open boundary conditions with and without noise has been described [40]. Few interesting and new features such as cyclic and other stationary states, observed in our model, would be debriefed. A simple mapping of our model to a 2D X-Y model has also been discussed, and formation of vortex-antivortex pairs have been studied on the square lattice as well [40].

The basic features of flocking, i.e. coherence and cohesion, has been extensively observed via different interactive mechanism among collectively moving agents. Two such grossly studied interactive mechanisms are the metric distance interaction model [16] and the topological distance interaction model [29]. Though similar in basic features like coherence and cohesion, these models show quite drastic differences in their critical behavior. As discussed above, in the presence of noise the system goes from an ordered state to a disordered state with

increasing noise strength. In the models employing the metric distance interaction, the transition from an ordered state to a disordered one is found to be a discontinuous one, with all features of typical discontinuous transition e.g negative dip in fourth order Binder cumulant [42–44], double hump order parameter distribution, flip flop between the metastable states near the transition point etc. On the other hand, a continuous transition has been observed for models with topological distance interactions. The basic differences between two such interactions are up for debate, and many extensive studies have been performed on such behaviors. As a result, astonishing properties like high density band formation has been observed and that prompted the researchers to somewhat conclude that density fluctuation defines the type of transition in such collectively moving systems.

In Chapter 3, a binary interaction model of flocking has been introduced [45]. In a binary interaction model, agents modify their directions according to the direction of its n^{th} neighbor following some specific rules. This n is a parameter of the model. Tuning this parameter and analyzing the system near criticality, a crossover from a discontinuous transition to a continuous transition has been observed with increasing the parameter value n . Stability analysis around the criticality, using hydrodynamic description of the model, for different n values in this binary interaction model, has also be performed and discussed elaborately in the light of the density fluctuation driven transitions in collective phenomena [45].

In chapter 4, a modified version of the Vicsek Model, would be described, with a quenched range of interactions. Here, in contrast with all other models, the range of interactions are quenched in space in the form of an underlying lattice structure, and particles within each interaction zone interact. With this simple modification, a set of non-trivial band structures has been observed. A formulation of characterizing different band structures has been proposed using three

numbers associated with each structure, i.e., the number of bands simultaneously moving, the intersection number of each band with the x-axis and the intersection number with the y-axis. The discontinuous transition, with increasing system sizes, become more prominent in this version of the model and here we summarize that the non-trivial band structures with increasing length, increasing width, increasing wrapping numbers or even intersecting independently moving band structures emerge as a signature of establishment of long-range correlation in such dynamical systems [46].

1.3 Naming Game

Evolution of human language, from scratch to a well developed communication scheme has been an astonishing feature of language dynamics. A class of very simple models that describe such evolving dynamics are known as Language games from which a subset of dynamical models to describe naming of objects has been put forth and are known as naming games (NG). Collective dynamics of agents with memory and feedback dependent interactions, the dynamics evolve and lead to a self-organized emergence of a communication system. The idea of memory and feedback is pretty new in this area and is overwhelmingly accepted by different classes of models dealing with the naming dynamics.

1.3.1 Definition of Naming Game

A. Bronchelli et. al. [47] first introduced Naming game models which aims to describe how consensus among agents is achieved about the name of a given object to a community of agents. In such models each individual has a vocabulary, initially empty, where they can keep different names [48–52]. The agents in such a dynamics can interact among themselves via some interactive mechanisms, which are model specific. In each interaction, a pair of distinct agents

are randomly selected and are allowed to interact. The negotiation takes place between the two selected agents via a sequence of pre-specified steps as follows: one of the agents (termed as a speaker) draws attention of the other agent (termed as the hearer) toward the external meaning of a specific object given to the community, either by production of new forms or by comparison of available conventional forms. In case of the hearer is able to understand the attempt of the speaker the interaction is said to be a ‘success’. Both the agents update their form-meaning repertoire by removing all competing forms corresponding to the meaning except the ‘winning’ one currently uttered by the speaker. Else, if the hearer produces a wrong interpretation, the interaction is termed as a ‘failure’, and the hearer learns the proper form-meaning association from the speaker. Following a sequence of such interactions, the interacting (Fig. 1.4) agents reshape their internal form-meaning association, and the adjustment of such successive individual associations collectively lead to the emergence of a global consensus.

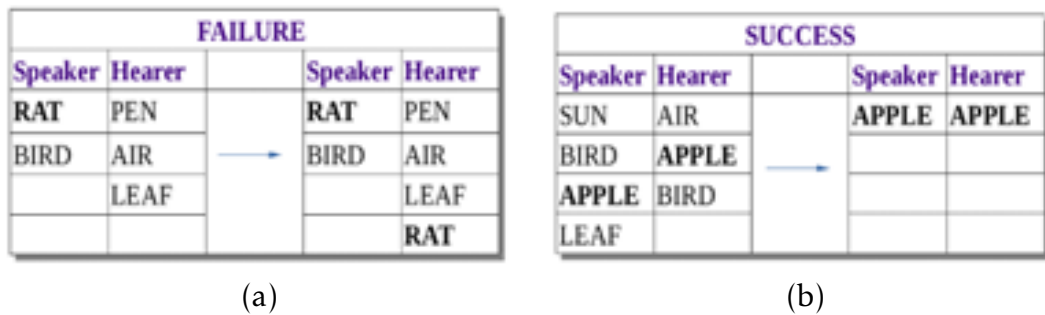


Figure 1.4: The interaction rules for (a) Failure and (b) Successful moves.

The dynamics evolve following such a sequence of bipartite interactions in a community of N agents. A ‘pseudo’ time t is defined for the convenience of following the dynamics and is equal to the number of bipartite interactions taking place. At any intermediate time, the vocabulary of each agent i is likely to have some entries and is denoted by the set $\{\ell_i(t)\}$ of length $\ell_i(t)$. Commonly, the naming dynamics is described in terms of a few quantities. For example, the total number of names $W(t, N) = \sum_{i=1}^N \ell_i(t)$ with all agents at time t is a well-known

quantity to look at. Typically, this number initially grows with time, reaches a maximum, then gradually decreases and finally converges to N . The maximum value of W after the configuration averaging grows with N as a power law like

$$\langle W_m(N) \rangle \sim N^\gamma. \quad (1.5)$$

At the same time, it is also customary to define two different time scales associated with the evolution dynamics. One is the time t_m when W reaches its maximum value. Again, a configuration averaged value of this quantity grows like

$$\langle t_m(N) \rangle \sim N^\alpha. \quad (1.6)$$

Secondly, one defines the convergence time t_f when every agent has only one name in its vocabulary, the same name for all agents and therefore the entire community has only N names. The averaged value of such a time scale is also assumed to vary like

$$\langle t_f(N) \rangle \sim N^\beta. \quad (1.7)$$

The three exponents in the power, namely α , β and γ , characterize the naming game. In a mean field dynamics [47], where any agent can interact with any other agent independent of their spatial location, all the characteristic exponents, i.e. α , β and γ are found out to be ~ 1.50 . This implies that the system needs a total memory of the order of $N^{1.5}$ to reach a consensus in a time scale of the order of $\sim N^{1.50}$.

1.3.2 Naming Game on regular lattices

The same analysis on the 1D and the 2D lattices has also been done [51]. In lattices, however, in contrast with the mean field models, the agents can interact with any of its randomly selected neighbor and hence the interactions are spa-

tially localized by construction. The analysis of the exponent α for both 1D and 2D lattices are found to be 1.0 and hence suggesting a faster growth to the state where the system has a maximum number of names for a single object, compared to the mean field model. The convergence time exponent, β is obtained to be ≈ 3.0 and ≈ 2.0 for $d = 1$ and $d = 2$ respectively, where d stands for the dimensionality of the lattice. In the same study, it has also been concluded that more generally the exponent β can be given as $\beta(d) \sim N^{1+2/d}$ and $d = 4$ is the upper critical dimension of this class of models. To describe the dynamics more concretely, it can be stated that initially small clusters of names grow locally around its maximum of $N/2$ words. Then the interfaces start diffusing. When two interfaces meet, the cluster situated in between the interfaces disappears, and the two interfaces coalesce. Such a coarsening leads to the well-known growth of the typical size ξ of the clusters as $t^{1/2}$. The density of interfaces, at which unsuccessful interactions can take place, decays as $1/\sqrt{t}$. Moreover, starting from a lattice in which all agents have no words, a time N is needed to reach a size of order 1 so that in fact ξ grows as $\sqrt{t/N}$, which explains the exponent of the convergence time $\beta \sim 3$ needed to reach consensus, i.e., $\xi = N$.

1.3.3 Naming Game on random graphs

However for heterogeneous networks, the dynamics are quite different from the above mentioned homogeneous networks. In networks like Barabasi-Albert (BA) the dynamical activity pattern of a node depends on its degree. High-degree nodes have a fundamental role but require larger memory capacity. They govern the dynamics acting as spreaders of linguistic conventions. The average degree, the clustering co-efficient of such networks also plays a big role in determining the time scales of the problem.

The prototype of homogeneous networks is the uncorrelated random graph model proposed by Erdős and Rényi [53, 54]. The construction consists of draw-

ing undirected edges between all possible pairs with. These edges are drawn with a constant probability p between each possible pair out of N given vertices. The graph, as a result, shows a binomial degree distribution with average $\langle k \rangle \simeq Np$, converging to a Poissonian distribution for large N . If p is sufficiently small (order $1/N$), the graph is sparse and presents locally tree-like structures. In order to account for degree heterogeneity, other constructions have been proposed for random graphs with arbitrary degree distributions. The BA networks have small clustering, in contrast with social networks. It turns out that growing networks can as well be constructed with a large clustering. A comparison of the models on the *ER* and the *BA* network for average degree $\langle k \rangle = 4$ has been performed [52]. Because of the finite average connectivity, the memory peak scales linearly with the system size N , and is reached after a time $O(N)$, in contrast with mean field $\sim O(N^{1.5})$ for peak height and maximum time but similarly to the finite-dimensional case. With respect to the slow coarsening process observed in finite-dimensional lattices, on the other hand, the small-world properties of the networks, i.e., the existence of short paths among the nodes, speeds up the convergence towards the global consensus. Therefore, complex networks exhibiting small-world properties constitute an interesting trade-off between mean-field “temporal efficiency” and regular lattice “storage optimization”. For both *ER* and *BA* networks, the convergence time scales as N^γ with $\gamma \sim 1.4 \pm 0.1$. This suggests that the small-world property allows inhomogeneous and sparse networks to recover the high temporal efficiency observed in the mean-field system.

1.3.4 Degree dependence

The maximal memory used by a node of degree k is proportional to \sqrt{k} . For the mean-field case, all agents have degree $k = (N - 1)$ and the maximal value of the total memory N_w scales as $N\sqrt{k} = N^{3/2}$. The knowledge of the average maximal memory of a node of degree k is not sufficient to understand which degree classes

play a major role in driving the dynamics towards the consensus. Two competing effects take part in determining the differences between nodes: high-degree nodes require more memory than low-degree nodes, but their number is much smaller. As a result, low-degree classes have, in fact, overall a larger number of different words. The role of the hubs, then, is that of diffusing words throughout the network and their property of connecting nodes with originally different words helps the system to converge. On the other hand, however, playing mostly as hearers, the hubs are not able to promote actively successful words, and their convergence follows that of the neighboring low-degree sites. In fact, once the low-degree nodes have successfully eliminated most of the different words created initially, the system globally converges on a faster time scale. We note that the average memory $N_w(k, t)/N_k$ converges slightly faster than $N_d(k, t)$ and $N_d(k, t)$ converges faster for larger k .

1.3.5 Master equation approach and other studies

With different studies pointing that the non-equilibrium dynamical behavior of the model presents very different features depending on the underlying topological properties of the system, study of microscopic activity patterns [55] via master equation approach suggested that the negotiation process between agents is at the origin of a very rich internal activity in terms of variations of the inventory size. The analysis depending on $P_n(k | t)$ that an agent of degree k has an inventory of size n at time t have been able to explain its behavior in function of both the global temporal evolution and the underlying topology of the system. The dynamics have been divided into three phases. Starting with an initial transient phase, the dynamics of the naming game follows two temporal regions, the reorganization, and the convergence phases.

Some studies on the analytic description of such models [48] has verified the exponents obtained in the mean-field version of the models. Apart from that, it

suggested that the variation of the convergence time scale is not exactly 1.50 but in the large system size limit, it shows a $N \log N$ behavior. The authors have also stated that the winning word is chosen by symmetry breaking process. Starting from an artificial situation of two names A and B distributed (A with n_A fraction and B with n_B fraction) among the agents in the community, and removing the influences of the invention process, they have shown that the process still ends up in the usual state with a global agreement.

The naming game models, starting from the simplest examples of a framework progressively leading to the establishment of human-like languages and to understand the role of self-organization in the evolution and change of human languages [49, 50], then, has acquired a paradigmatic role in the novel field of semiotic dynamics that primarily investigates how language evolves through the invention and successive adoption of new words and grammatical constructions.

The basic construction has been, then, profitably used in order to understand the origin and the evolution of language, and have found an important field of application in artificial intelligence, where the ultimate goal consists of modeling the self-organized collective learning processes in populations of artificial agents.

It finds wide applications in various fields ranging from artificial sensor network as a leader election model [56] to the social media as an opinion formation model [57]. More advanced models [58, 59] attempting to explain further complex processes like categorization and color naming have also been built on top of the basic naming game framework.

1.3.6 Plan of the thesis

Thus, we have literature, so rich on naming game, with many studies devoted to the understanding of the dynamics as well as a larger part of the studies devoted to its direction of applications on artificial intelligence, categorization and color naming. In the versions of the naming game models, we have observed that the

values of the set of characteristic exponents depend on the detailed features of the dynamical rules and on the microscopic features of the underlying networks.

The interaction rules in almost all the models observed in the literature assume that, in an interaction, the speaker utters a randomly selected word among many present names in its inventory. The hearer looks for the uttered name in its inventory. In a failure, where the name is not common and is basically the learning ground of the dynamics, the interaction mechanism gives undue privilege to the hearer who learns the name uttered by the speaker. However, the speaker ends up learning nothing after a failure. Also, there might be other common names present in their inventories, but because those words were not randomly selected by the speaker, defines the interaction, a potential successful interaction, a failure. The naming game dynamics is basically a process of learning where individual agents learn different names from their interacting partners and reshape their memories. And learning more often than not being a symmetric and bi-directional process, the construction of the basic naming game models on unidirectional rules are far from being practical.

In chapter 5, we will reconstruct the basic model of naming game by redefining the interaction rules, in order to address the reciprocity of learning process by having a model with symmetric rules of interactions [60]. The study will also keep the room for retaining all successful names in a single successful interaction and hence no common name present in the inventories of the interacting agents would be deleted.

On another aspect of the problem, the sizes of the vocabularies of the agents have been assumed to be infinite in the models studied for the dynamics of naming games in the literature, [49,58,59]. It has been observed that the memories of individuals play a vital role in the microscopic dynamics [52]. Realistic studies suggest that an individual agent has only a finite amount of memory. Both short

term memory and long term human memory have been found to be quite limited. Artificial memories, e.g. memory chips, etc. also have their size limitations, and hence memory allocations to artificially created systems of robots do face the same problem of memory restriction. Hence, the assumption of infinite memory is too stringent and in contrast to its practical counterpart. Therefore, it would be quite appropriate to study the effect of finiteness of the vocabulary sizes in the dynamics of naming games.

In chapter 6, the naming game problem will be analyzed with the vocabulary size of every agent, assumed to be finite and restricted to a certain fixed, suitably tunable, cut-off value [61].

1.4 Preliminaries of critical phenomena

1.4.1 Phase transitions

Dynamical systems with emerging long-range correlation are often characterized by transitions [62] from one phase to another via some perturbation. These phases are often distinguishable from each other due to completely different features in each phase and spontaneous symmetry breaking across the transition.

There are a number of substances in different phases around us [17]. A phase can be defined as the state of matter with uniform macroscopic physical properties on a macroscopic length scale. The example of ice, liquid water, and water vapor is quite common where all of these are distinct phases of water as a collection of macroscopic numbers of H_2O molecules.

A phase, often characterized by thermodynamic functions, typically the free energy F , a thermodynamic function of a few macroscopic parameters e.g. the temperature and the pressure and is determined by the values of these thermodynamic quantities. With these parameters as axes, if we plot the different phases specified by the values of the parameters, is commonly termed as the “phase di-

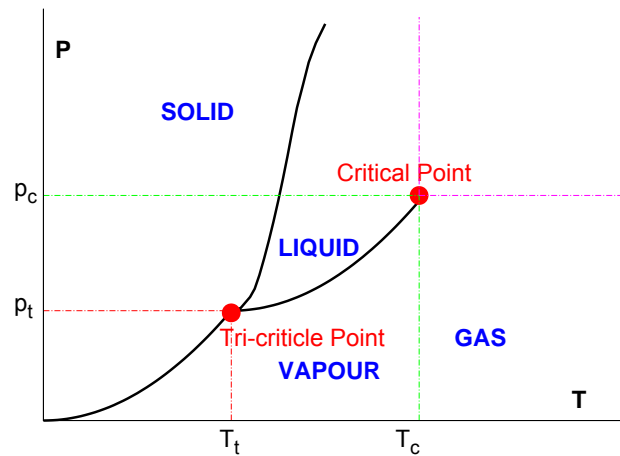


Figure 1.5: Schematic pictorial depiction of a typical phase diagram of water. The phases are determined by values of the control parameters i.e. the temperature T and pressure p . (T_c, p_c) and (T_t, p_t) denotes the values of the control parameters at the critical point and the triple point respectively.

agram”, as shown in Fig. 1.5. Here we can see that a phase diagram has few specific features.

Phase boundary: A phase boundary is a line in the 2D parameter space which separates two different phases, uniquely identified by different characteristics. Crossing the line, from one side to the other, is associated with spontaneous symmetry breaking and emergence of long-range order in the system. Across the phase boundary, any change in parameters like the temperature, results in a sudden change in the phase of a substance. The solid phase drastically changes into a liquid phase at the melting temperature of any liquid. This is known as “phase transition”.

Critical point: In the phase diagram, phase boundary sometimes disappears at certain values of the parameters, denoted by a point in the 2D parameter space, where the two phases become indistinguishable, is known as the “critical point” (Fig. 1.5).

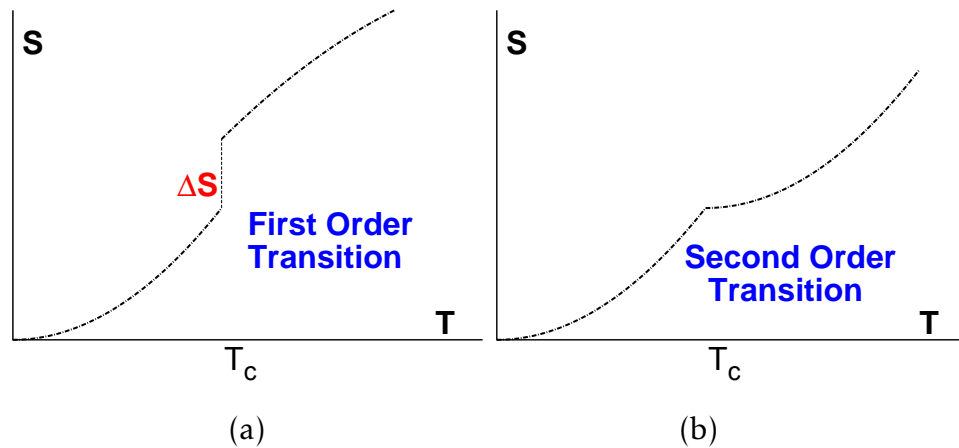


Figure 1.6: The variation of the entropy S around the transition point T_c for (a) First order transition with $\Delta S \geq 0$ and (b) Second order transition with $\Delta S = 0$.

Triple/Tri-critical point: Some substances, for example, say water, often describes more than one transitions. In case of transitions, one followed by another, there are certain values of the control parameters, at which the features of the three phases co-exist. This particular point in the 2D parameter space is denoted by a point of three connecting lines, is termed as the “Triple point” or the “Tri-critical point”(Fig. 1.5).

To describe the dynamics of a system via the phase diagram, each phase needs to be uniquely characterized. The “order parameter” is of great importance, which measures how ordered or how similar in state the microscopic constituents (elements) of the phases are and is associated with the breaking of a symmetry of the system under consideration and measures the degree of asymmetry in each phase. In the broken symmetry phase i.e. the ordered phase the order parameter is non-zero implying a higher degree of asymmetry and vanishes in the highly symmetric disordered phase. Hence, the change from a non-zero to a zero value of the order parameter characterizes the phase transition.

Continuous and Discontinuous phase transitions

In a phase transition, associated with many features measurable in terms of thermodynamic quantities, a drastic change between thermodynamic phases occurs with the variation of the thermodynamic control parameters like the temperature and the pressure. Theoretical description of a familiar example of melting of ice at 0°C near 1 atm, shows a drastic change of microscopic properties associated with emergence of singularities (non-analyticities) in functions representing physical quantities. In Fig. 1.6, variation of one of the quantity i.e. the entropy S has been shown across the transition. Other quantities that show similar emergence of singularities are the volume V and the specific heat C . Such singularities are often observed as a discontinuity (jump), a cusp or a divergence in the parameter space. In melting of ice, the entropy jumps (Fig. 1.6(a)) across the transition when latent heat is supplied to the system. While boiling, the volume changes discontinuously. The inter-competition between the (internal) energy E and the entropy S controls the phase of a system. The free energy, defined as, $F = E - TS$, hence, determines the features and consequently the phase transitions are often described in terms of the free energy itself. While the internal energy (E), favors order, the entropy privileges disorder. The external parameters like the temperature T , determines which one of the two terms would dominate.

Depending on the occurrence of singularities, the conventional classification of phase transitions roughly divides transitions into two separate classes. When the first-order derivative of the free energy F , i.e. the entropy S , shows a discontinuity at the transition point, this is known as the first order or a discontinuous transition, shown in Fig. 1.6(a). If the first order derivative of the free energy is continuous across the transition but the second or the higher order derivatives (e.g. the specific heat C) shows a discontinuity or divergence, the transition is known as a continuous transition(Fig. 1.6(b)). The nomenclature of transitions by order of the derivative of the order parameter that first shows a discontinuity

or divergence is also pretty common. For example, the melting of ice accompanies latent heat and is associated with a jump in entropy ($\Delta S \neq 0$). Such a transition is known as the first order transition, since the entropy is the first order derivative of the free energy $S = -(\frac{\partial F}{\partial T})_V$.

If the entropy is continuous across the transition but the specific heat C (second derivative of the free energy) is discontinuous, then the transition is said to be a “second order” transition. In many second-order transitions, the specific heat diverges at the transition temperature.

We describe the continuous phase transition and the critical phenomena on the same line and are often synonymous. The anomaly of co-existing indistinguishable phases occurs around such transition. Striking similarities in behavior near the critical point among systems that are otherwise quite different in nature is one of the vital reasons of our interest in such systems. The degree of singularity or divergence of the magnetisation and the corresponding susceptibility can be described by functions of a dimensionless quantity $t = (T - T_c)/T_c$, which is the difference between the control parameter (here the temperature) and its critical value, normalised properly, as:

$$m \approx \begin{cases} t^{\beta_m} & \text{if } T < T_c \\ t^{1/\delta_m} & \text{if } T = T_c \end{cases} \quad (1.8)$$

and

$$\chi \approx \begin{cases} t^{-\gamma_\chi} & \text{if } T < T_c \\ t^{-\gamma'_\chi} & \text{if } T > T_c \end{cases} \quad (1.9)$$

respectively, where the $\{\beta_m, \delta_m\}$ and the $\{\gamma_\chi, \gamma'_\chi\}$ are the critical exponents associated with the parameters m and χ .

Other such important quantity, is $G(r)$: the connected two-point correlation function defined as $G(r) = \langle S_i S_{i+r} \rangle - \langle S_i \rangle \langle S_{i+r} \rangle$ with two spins, S_i , S_{i+r} , separated

by a distance r , ξ : the correlation length, can also be described by their respective critical exponents $\{\tau_g, \eta_g\}$ and $\{\nu, \nu'\}$ as:

$$G(r) \approx \begin{cases} r^{-\tau_g} e^{-r/\xi} & \text{if } T \neq T_c \\ r^{2-(d+\eta_g)} & \text{if } T = T_c \end{cases} \quad (1.10)$$

$$\xi \approx \begin{cases} t^{-\nu_\xi} & \text{if } T < T_c \\ t^{-\nu'_\xi} & \text{if } T > T_c \end{cases} \quad (1.11)$$

Here d is the space dimensionality of the system. Hence, the degree of singularity of physical quantities near the critical point is described by critical exponents. Experiments show that physical quantities generally have power law singularities as functions of the difference between the control parameters (such as temperature) and their critical values. Critical exponents are very basic quantities to characterize critical phenomena, and an important goal of the theory of critical phenomena is to develop a systematic method to calculate the values of critical exponents. Most importantly, there are simple relations between exponents (scaling law), which allow one to determine an exponent given the values of other exponents (i.e. not all exponents are independent). For example, the Rushbrooke scaling law is $\alpha_c + 2\beta_m + \gamma_\chi = 2$. Here α_c is the exponent of the specific heat.

First order transitions are often associated with a negative dip in the fourth order cumulant of the order parameter, constructed by K. Binder and is coined by his name as the ‘‘Binder Cumulant’’. If m is the order parameter of any system in consideration under thermodynamic transition, the Binder cumulant is defined as $U = 1 - \frac{\langle m^4 \rangle}{3 \langle m^2 \rangle^2}$, where $\langle .. \rangle$ denotes the average over configurations.

It’s immediately noticeable that from the viewpoint of statistical mechanics, the free energy lays the basis of thermodynamics and is determined by the parti-

tion function Z , defined as:

$$Z = e^{-F/\kappa_B T} = Tr[e^{-H/\kappa_B T}]. \quad (1.12)$$

Here κ_B is Boltzmann's constant, and the trace $Tr[]$ represents a sum over all the degrees of freedom entering the Hamiltonian H of the system under study. Because of the fact that Z is a sum of exponentials of $-H/(\kappa_B T)$, the non-analyticities of the free energy can only occur in the thermodynamic limit satisfying the condition that V and N , the volume of the system and the number of degrees of freedom (e.g. spins in magnetic materials) respectively, grow to infinity, such that its ratio remains constant, i.e. $N/V \rightarrow const.$

Depending on conditions a material may depict both first and second order transitions.

Scaling

The group of scientists, Widom, Domb and Hunter, Kadanoff [63], Patashinskii and Pokrovskii [64], and Fisher ([65, 66]) had independently developed the scaling hypothesis and discussed the same in diverse directions. The hypothesis can be divided into two sub-categories [67], i.e., the emergence of a set of scaling-relations and data collapse. Near the transition, the critical exponents can be described by some functional forms or laws, known as scaling laws. One of such is the relation α_c , $2\beta_m$, and γ_χ as defined in eqn. (1.8, 1.11) and α_c is the similar exponent of the specific heat can be given by $\alpha_c + 2\beta_m + \gamma_\chi = 2$. Data collapse, however, can be explained easily in terms of our simple example of a simple ferromagnet. The order parameter m can be written as a the function of two variables, the magnetic field h and the temperature t as $m = m(h, t)$. If we consider the m vs. t variation for a set of family of h values, the scaling hypothesis suggests that all the curves will fall on top ("data-collapse") of each other with a proper

scaling of the m and the t axes. The scaling relations around transition are found out to be power laws and the scaling relations looks like $m(h, t) \rightarrow m(h, t)/h^{\alpha_m^0}$ and $t \rightarrow t/h^{\alpha_t^0}$.

Both these hypothesis has been supported by a wide range of experimental justifications from diverse systems and also numerical calculations. The exponents are found out to be exact for a class of systems. Moreover, the general principles of scale invariance used here have proved useful in interpreting a number of other phenomena, ranging from elementary-particle physics ([68]) to galaxy structure [69].

Universality

Kadanoff, in the year 1970 at the Enrico Fermi Summer School, was the first to clearly put forward the concept of universality classes of critical behavior based on earlier works of a list of eminent scientists including Griffiths, Jasnow and Wortis, Fisher, Stanley, and many others [67]. A large number of diverse systems can be said to belong to a single universality class if their critical exponents and the scaling relations are found out to be same. The exponents are then termed as universal for the set of systems belonging to the class, the "Universality class". In the same line, a small set of universal classes can describe almost all diverse systems.

From experimental studies, $m - h - t$ data on five diverse magnetic materials near their respective critical points has been shown in the article of Stanley [67]. The data collapse of five diverse magnetic materials, $CrBr_3$, EuO , Ni , YIG and Pd_3Fe , none of which is an idealized ferromagnet. Where $CrBr_3$ has considerable lattice anisotropy, and EuO has significant second-neighbor interactions, Ni is an itinerant-electron ferromagnet, YIG is a ferrimagnet, and Pd_3Fe is a ferromagnetic alloy. The data collapse of these, diverse materials, around the transition via universal scaling relations and exponents supports the scaling hypothesis.

Systems with the same values of critical exponents and scaling functions are said to belong to the same universality class. Hence all these five, however diverse materials, belongs to the same universality class because of the fact that they follow the same scaling laws and have the same critical exponents. This apparent universal behavior of critical phenomena near transition provides enough motivation for the study of critical phenomena to determine the important factors determining the universality classes.

1.4.2 Long-range order

A number of important events occur at the critical point independent of the characteristics of the substance undergoing the transition. Studying such substance near the critical point provides enormous insight on criticality. Universality is one such important property exhibited by substances undergoing phase transition. Universality implies that materials undergoing phase transition will have common specific characteristics regardless of any other properties and conditions. While passing from a disordered to an ordered phase, consequently, a material exhibits the development of long-range order. In the disordered phase, the system depicts no correlation between its constituents, i.e., the interacting atoms. However, while passing through the transition, the system develops high correlation between its constituents. For example, a disordered magnet has spins pointing in random directions with vanishingly small magnetization. However with the temperature falling below the Curie temperature, all the spins get aligned depicting a finite and non-zero magnetization. The molecules in a liquid crystal similarly show random orientation in the disordered state, but below the transition temperature, all spins get aligned. The two-point correlation function that measures the correlation, diverges at the transition point as in eqn. 1.10.

Long-range correlation specifically refers to the slow decay of the (temporal or spatial) correlation function of the observable $A(x)$ defined as $G(x_0) = \langle A_i(x)A_i(x+$

$x_0) >_{i,x}$. Accordingly, the correlation length ξ , that quantifies the correlation, diverges as the deviation, $(t = T_c - T)$, from the critical point, T_c , tends to vanish as shown in eqn. (1.11).

1.4.3 Importance of models

With the very idea of universality classes, physicists are often in search of models that are not only easy to work with but are rich in its understanding of various systems. With many systems from various fields to aim at, studying a model with rich behavior of a universality class that describes the behavior of many systems near criticality, is an asset to the scientific community. Starting from the Ising model [17, 62, 70–72], the n -vector model [73–75] to q -state Pott's model [76, 77], Voter model [78–80] etc. often describes unique universality classes that many natural, social, financial and physical systems belong to.

1.5 Complex networks

As we know, emergence of magnetism from the collective behavior of millions of spins, or spectacular phenomena as Bose-Einstein condensation or superfluidity from quantum particles are all quite well explained. The idea of complex networks plays a vital role in many such descriptions. Starting from cellular networks to chemical networks linked by reactions, the internet web, computers connected by physical links, etc. and a wide range of many such natural systems are often described by complex networks. Complex network description not only has helped in understanding the topological evolution of such networks but also has given insights into the organizing principles of many evolving networks.

The success of modeling various systems, depends on the unique identification of the strength of time and space varying particle-particle interactions and are easily accessible. To deal with such natural systems, in the past few years, devel-

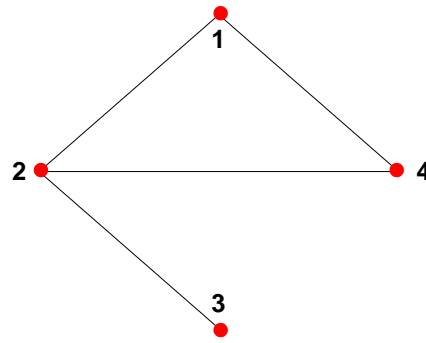


Figure 1.7: A graph with $N = 4$ nodes and $n = 4$ edges has been displayed. $P = \{1, 2, 3, 4\}$ and $E = \{(1, 2), (1, 4), (2, 3), (2, 4)\}$ are the set of nodes and edges respectively.

opments of framework has been done on the tools of statistical mechanics in this direction, and quite unexpectedly, links between major topics, ranging from percolation to Bose-Einstein condensation, in condensed-matter physics have been well established thereafter.

1.5.1 Random connected graphs

The study of graph theory includes the understanding of complex networks. A network is represented by a graph in mathematical terms. A graph is constructed of a pair of sets $G = \{P, E\}$. Here P and E are respectively a set of N nodes P_1, P_2, \dots, P_N represented by dots and a set of edges E_1, E_2, \dots represented by lines. Each element of the set E connects a pair of elements of P i.e., any two dots in the graph are joined by a line if the corresponding nodes are connected.

Graph theory, originating from the work of Leonhard Euler, focusing on small graphs showing high degree of regularity. With interest on diverse networks, the study of random graphs with randomly distributed edges became rich field of study. The theory of random graphs was developed and introduced by Paul Erdős and Alfréd Rényi [53, 54] after getting fascinated by the fact that probabilistic methods were quite useful and often simpler in tackling problems of

graph theory. In a random graph N nodes are connected by n edges, chosen randomly from the $N_0 = N(N - 1)/2$ possible edges ([53, 54]). In total there are $C_{N_0}^n$ graphs with N nodes and n edges that form a probability space where every realization is equally probable. The binomial model is an equivalent definition of random graphs. In this model, among N existing nodes, each pair of node is being connected with probability p . The total number of present edges in the graph is a random variable with the expectation value $E(n) = pN_0$. A graph G_0 of N nodes, P_1, P_2, \dots, P_N and n consequent edges, can be obtained by this process with a probability $P(G_0) = p^n(1 - p)^{N_0 - n}$. For some probability p there will be well connected paths between any two nodes. For this p and beyond the graph is known as a *connected graph*.

Random-graph theory is often used to study various complex networks because of the fact that networks with pretty complex topologies and unknown organizing principles often appear random.

With this model, our thinking about complex networks has been centered around this for decades since its introduction. But with the growing interest in complex systems, researchers had been prompted to look for tools beyond the study of random graphs to understand more diverse and complex systems whose topology deviates from random graphs. With the intuition, that complex systems must display some organizing principles, which should be at some level encoded in their topology, the development of tools and measurements to capture in quantitative terms the underlying organizing principles of diverse networks kick started.

1.5.2 Small world networks

Small-world describes the fact that in most networks there is almost always a relatively shorter path between any two nodes despite often being large size networks. Here the distances between any two nodes are defined as the number of

edges along the shortest paths connecting them. The popular manifestation of small world networks is the “six degrees of separation” concept, uncovered by the social psychologist Stanley Milgram [81]. He concluded that there is an associated path between most pairs of people in the United States of typical length of about six degrees. Starting from the network of actors in Hollywood, having on an average three co-stars from each other, chemicals in a cell with typically separated by three reactions, small-world property seems to characterize most of the complex networks. As indicated by Erdős and Rényi, the typical distance between any pair of node scales as the logarithm of the number of present nodes, in random graphs. Hence, random graphs [54] are small worlds as well [82]. Thus, though the concept of small-world seems quite intriguing, it doesn't point toward any particular organizing principle.

With new concepts and measures proposed, consequent in depth investigation had taken place in the last few decades, motivated by the current developments and circumstances. However, few concepts occupy a prominent place in contemporary thinking about complex networks. Here we define and briefly discuss them, and the idea of few of these will be used in the thesis and are briefly described below.

1.5.3 Degree Distribution

All nodes in a network don't have the same number of edges (termed as the node degree) associated with it. Hence there is a spread in the node degree and is characterized by a distribution function $P(k)$. This is equal to the probability that any randomly selected node will have exactly k edges. Edges are randomly placed in random graphs which in turn ensures approximately same degree for the majority of the nodes in the graph. This number is close to the average degree $\langle k \rangle$ of the random network. The degree distribution of a random graph is a Poisson distribution having its peak at $P(\langle k \rangle)$. However, for most of the large networks,

the degree distribution deviates, significantly, from a Poisson distribution. Starting from the World Wide Web [83], the Internet [84], metabolic networks [85] and for many large numbers of networks the degree distribution has a power-law tail,

$$P(< k >) \sim k^{-\gamma_k}. \quad (1.13)$$

Such networks are known as scale-free [86] networks.

With these discoveries, a revival of network modeling has been initiated in the next few years that resulted in the introduction and study of three main classes of modeling paradigms. First is the random graphs, which are the variants of the Erdős-Rényi model, were still widely used in many fields, serving as the benchmark for many modeling and empirical studies. Secondly a class of models motivated by clustering, collectively called small-world models, had also been put forward. These models interpolate between the random graphs and the highly clustered regular lattices. Finally, with the discovery of the power-law degree distribution, various scale-free models had been constructed focusing on the network dynamics, aiming to offer a universal theory of network evolution.

1.5.4 Clustering

Social networks depict a common property of forming cliques, which represents that within a circle of friends every member knows every other member. This tendency of clustering, inherent in social networks, is quantified by the clustering coefficient [87]. This concept has its root in sociology appearing under “fraction of transitive triples” [88].

Let us consider a selected node i in the network, with k_i edges to connect it with other k_i nodes. There would be $k_i(k_i - 1)/2$ edges between any two nearest neighbors of the original node i if they are part of a clique. But if the network doesn't form a clique, there might be lesser number of edges, say E_i , between any

such pair. The ratio of the present edges E_i and the number of possible edges $k_i(k_i - 1)/2$, between a pair of neighbor of the original node i , gives the clustering coefficient of node i ,

$$C_i = \frac{2E_i}{k_i(k_i - 1)}. \quad (1.14)$$

Thus the local clustering coefficient quantifies how close the neighbors of a particular node are of being a clique. The average of all individual C_i 's, is defined as the clustering coefficient of the whole network. An alternative definition of C has also been discussed in [89, 90].

2 Cyclic and coherent states in flocks with topological distance

2.1 Introduction

Collective behavior, briefly described in Chapter 1, is well known phenomena, observed in systems like collectively moving bird flocks or swarming bees, are often modeled by groups of self-propelled mobile agents [16, 18, 91]. They are ‘cohesive’ and ‘coherent,’ i.e. each agent maintains a characteristic distance from other agents and at the same time they move along a common direction. The generic feature of collective motion is, agents are short-sighted. Agent’s can interact with a small group of local agents around it. However, the whole group behaves in unison. In other words, a short-range interaction among the agents may lead to a unique global behavior of the entire flock signifying the existence of a long-range correlation among the agents.

Given a random initial configuration of agents with random positions and velocity directions what kind of short-range dynamics can lead to global correlation reflected in cohesion and coherence among the agents was explored in an assembly of self-propelled particles by T. Vicsek et. al. in their model, known as the Vicsek model [16]. Here particles (agents) are released at random locations within a unit square box on the $x-y$ plane with periodic boundary condition and with random velocities. However, in the deterministic motion the direction of velocity of each agent i is oriented along the resultant velocity direction θ_i of all agents within an interaction zone (IZ) of range \mathcal{R} around i as:

$$\theta_i(t+1) = \tan^{-1} \left[\frac{\sum_{j \in \mathcal{R}_i} \sin \theta_j(t)}{\sum_{j \in \mathcal{R}_i} \cos \theta_j(t)} \right]. \quad (2.1)$$

The corresponding position update rules are as follows:

$$x_i(t+1) = x_i(t) + v_0 \cos \theta_i(t+1) \quad (2.2)$$

$$y_i(t+1) = y_i(t) + v_0 \sin \theta_i(t+1) \quad (2.3)$$

In reality, each agent may make an error in judging the resultant direction of motion, and this has been introduced in the stochastic version of the model where noise is introduced by topping the angle of orientation, θ_i , by a random amount $\Delta\theta$. Each individual agent is then moved along the updated velocity direction.

A coherent phase is observed in the noise-free case with high agent densities. Moreover, a continuous phase transition is observed on increasing the strength of noise where the mean flock speed continuously decreases to zero. Facets like high density traveling bands occurring at low noise were revealed in later studies [21, 24] and arguments were put in favor of a discontinuous transition. Further, it has been argued that by tuning the magnitude of the velocity of agents one can switch over from continuous to discontinuous transitions [22].

A number of studies have been done where the interacting neighborhood is determined using the topological distance. In [92] an agent interacts only with its Voronoi neighbors, thus when the agent density is very low, and the typical distance between the agents is quite large, an agent interacts with its topological neighbors. The behavior of such a flock is different from the one defined in terms of the metric distance. Also, the metric free topology was used in the hydrodynamic description of self-propelled agents where the neighbors are determined by the topological distance [30]. Such flocks often travel over long durations covering distances much larger than the size of the flocks and therefore the flocking is inherently a zero density problem in infinite space. Here we present a model of a 2D flock with topological distance interactions under open boundary condition, based on our work in [40].

In a recent field study by the StarFlag group, it has been argued that the animal collective behavior depends on topological rather than metric distance [26]. Observing flocks of Starlings the angular density distribution of neighboring birds have been found to be anisotropic, e.g., a bird is more likely to keep its nearest neighbor at its two sides rather than on the front and back. Fishes [27] have also

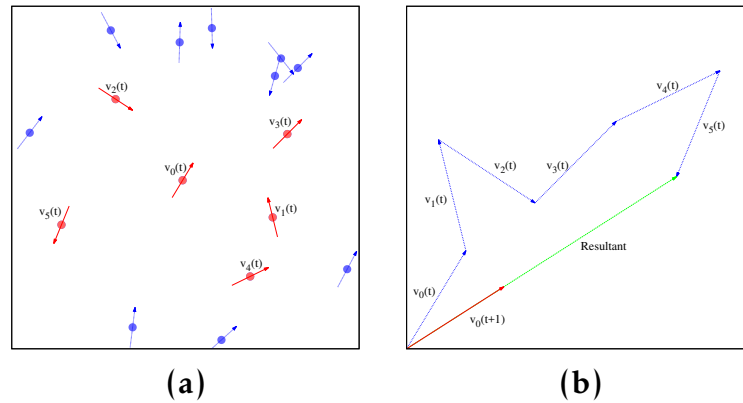


Figure 2.1: (a) A flock of $N = 16$ agents with $n = 5$ neighbors in the interaction zone and at any arbitrary time t . The central agent is denoted by the subscript 0, and the velocity vectors of this agent and its five neighbors in the interaction zone are shown using red arrows. (b) In the next time step, the velocity of agent 0 is calculated by Eqn. 2.1 which is along the resultant of all $n + 1$ velocity vectors and has the magnitude v .

been found to interact with neighbors determined by topological rules. Theoretical investigations [28, 30] revealed that the behavior of topology based models is very different from metric based models [31].

The concept of graph theory based topology was, however, used [97] to analyze the Vicsek model itself from the perspective of control theory. The metric distance based interactions were modeled using graphs with “switching topology”. Such studies also derived the conditions for the formation of coherent flocks for agents with fixed topologies [98]. The relevance of underlying graphs or networks on the nature of collective motion has also been studied [41, 99].

The observations of the StarFlag group prompted us to study the collective motion of flocking phenomena in two dimensions using the interactions depending on the topological distance. Most crucially we have obtained very interesting stationary states which have not been observed before, mainly the cyclic states. At the same time, an increasingly large number of states are found to be completely cohesive and coherent.

This chapter is organized as follows. In section 2 we describe our topological

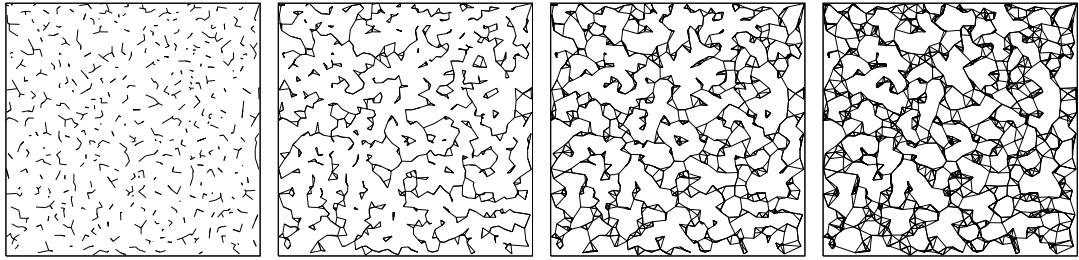


Figure 2.2: The undirected RGG with $N = 1000$ nodes distributed randomly within a square box with a free boundary condition. Each node is linked to its n nearest neighbors; $n = 1, 2, 3$ and 4 increasing from left to the right. For small n there are many components of the graph which merge with one another as n increases. The largest component has sizes 9, 150, 988, 1000.

distance dependent model for collective motion. The connectivity among such a collection of agents has been studied as the Random Geometric Graph in section 3. The stationary states of such flocks have been studied in section 4, the two most prominent states being the Single Sink State and the Cyclic State. The effect of the noise on the dynamics and the critical point of transition have been studied in section 5. In chapter 6, the same model under fastest refreshing of the neighbourhood has been discussed. A simpler version of the model with its vortex-antivortex states has been studied on the square lattice in section 7. Finally, we summarize and discuss in section 8.

2.2 Model

In our model, the interaction zone has been defined in the following way. During the flight, each agent i interacts with a short list of n other selected agents that constitute the IZ. It updates its velocity direction using the Eqn. 2.1, following a synchronous dynamics. In general, the agent often refreshes the group of agents in IZ. For example, at the early stage, when the flock is relaxing to arrive at the stationary state and also during some stationary states, the inter-agent distances change with time. Every time the IZ is refreshed, we assume the criterion of se-

lecting n agents is that they are the first n nearest neighbors of i . We introduce at this point a “refreshing rate” which controls how frequently an agent updates its IZ. We studied two limiting situations when these rates are slowest and fastest. In the slowest rate, the agents do not change at all the list of other n agents in their IZs. The IZ for each agent, constructed at the initial stage, remains the same ever after, even if n initial neighbors of an agent no longer remain nearest neighbors as time proceeds. The other limiting case is when the refreshing rate is the fastest, the IZ is refreshed for every agent at each time step. The slowest case has been discussed in sections 4 and 5. The fastest refreshing rates have been discussed in section 6. For the spins on the square lattice discussed in section 7, these two cases actually mean the same since the spins are firmly fixed at their lattice positions.

The number n of agents in IZ is considered as an integer parameter of the model. As in Vicsek model [16] the system is updated using a discrete time dynamics. While the speeds v of all agents are always maintained to be the same, the orientational angles θ_i of their velocities are updated by the direction of the resultant of velocity vectors of all n agents in the interaction zone and the agent i itself (Fig. 2.1),

$$\theta_i(t+1) = \tan^{-1}[\Sigma_j \sin \theta_j(t)/\Sigma_j \cos \theta_j(t)] \quad (2.4)$$

where the summation index j runs over all $(n+1)$ agents in IZ. No periodic boundary condition is imposed in our model and the whole flock moves in the infinite space. Compared to the Vicsek model, use of the free boundary condition makes our model less restrictive. Following this dynamics, the flock reaches the stationary state after a certain period of relaxation time. It is observed that the stationary state depends on the initial positions, initial velocities of the agents, as well as the neighbor number n . Though a number of different stationary states have been observed, often the state is a fixed point or a cycle. We have studied the statistical properties of these fixed points and cycles and observed that cohesion

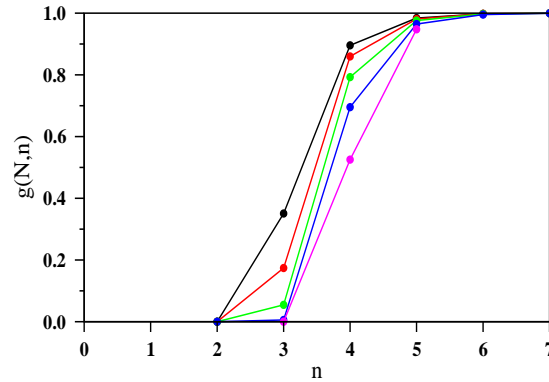


Figure 2.3: The fractions $g(N, n)$ of single component connected graphs, in a sample of 1000 RGGs, are plotted against n . For N agents this fraction grows as the number of neighbors n is gradually increased. System sizes N are 256 (black), 512 (red), 1024 (green), 2048 (blue) and 4096 (magenta), increased from left to right. The number of independent configurations used for each value of n is 1000.

and / or coherence are indeed present in different stationary states.

2.3 Random geometric graphs

At the initial stage, N agents are uniformly distributed at random locations within a unit square box on the $x-y$ plane without periodic boundary condition. A random geometric graph (RGG) [100] is constructed whose vertices are the agents. At the same time for any arbitrary pair of vertices i and j , j is defined as a neighbor of i if it is among the n vertices nearest to i . Then an edge is assumed to exist from i to j . This implies that the edges are in general ‘directed’ since if j is the neighbor of i then i may or may not be the neighbor of j . Therefore the resulting graph is inherently a directed graph. However one can also define a simplified version of the graph by ignoring the edge directions and consider the graph as an undirected graph. In the following, we refer such an undirected graph as the RGG.

In Fig. 2.2 we exhibit the pictorial representation of an undirected RGG for $N = 1000$ as n is increased step by step. For small values of n , the graph has

many different components. As n is increased the components grow gradually in size, merge into one another, and finally, the RGG becomes a single component connected graph covering all vertices for a certain value of n . Here we have shown four figures for $n = 1, 2, 3$ and 4 . The randomly selected positions of all vertices are exactly the same in these figures. The size of a component is measured by the number of vertices in that component. In this figure, the RGG becomes fully connected for $n = 4$.

The structure and connectivity of RGG depend on the initial positions of N vertices. Therefore we have first studied how the fraction $g(N, n)$ of connected graphs grows with n when the flock size N is increased. For a particular RGG, the connectivity is checked using the ‘Burning Algorithm’ [101] where the fire, initiated at an arbitrary vertex, propagates along the edges and finally burns all vertices if and only if the RGG is a single component connected graph.

In Fig. 2.3 we show the plots of $g(N, n)$ against n for different values of N . To find out if a minimum value of the neighbor number n exists, one can artificially prepare a linear initial configuration of agents where each agent has its right neighbor as the nearest one. This corresponds to $n = 1$ but occurrence of such a configuration by random selection of positions of the agents is extremely improbable. Numerically we find that for small n the $g(N, n)$ takes vanishingly small values. However, on increasing n , $g(N, n)$ increases very rapidly and when n is around 7, $g(N, n) \approx 1$ i.e., nearly all configurations become connected. With increasing flock size N the curves slowly shifts to higher values of the neighbor number n .

Only those flocks whose RGGs are single component connected graphs are considered for their dynamical evolution. The initial neighbor list is maintained for the entire dynamical evolution of the flock and is never updated even if all n initial neighbors of an agent no longer remain nearest neighbors as time evolves. This means that the set of agents’ velocities $\{\vec{v}_i(t+1)\}$ is fully determined using the

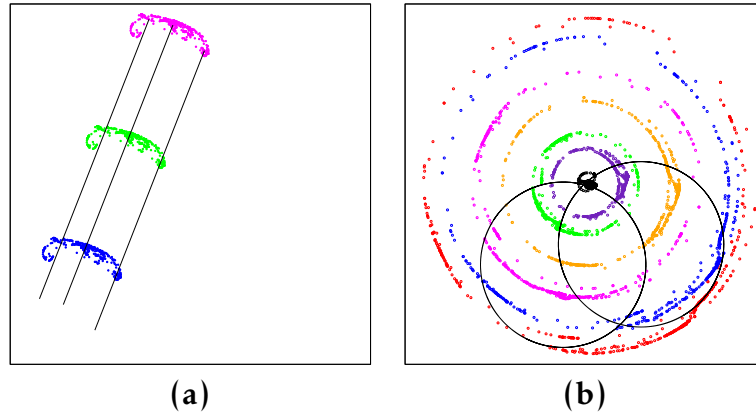


Figure 2.4: Flocks of size $N = 512$ and $n = 10$, moving with the speed of $v = 0.03$ without noise. (a) Single sink state: The fully cohesive and coherent motion of the flock is exhibited by its position at three different instants: 10000 (blue), 11000 (green) and 12000 (magenta). Three straight line trajectories of individual agents are also shown. The frame size is 90×90 units. (b) Cyclic state: The stationary state pulsating flock has been shown at different time instants: 173,000 (black), 176000 (red), 180000 (green), 188000 (blue), 192000 (brown), 197000 (violet) and 200000 (magenta). The time period is 28835. Two individual agents' circular trajectories with radius ≈ 137.67 are also shown. The frame size is 600×600 units.

detailed knowledge of the set $\{\vec{v}_i(t)\}$. The implication of this is, the positions and velocities are completely decoupled during the time evolution since the actual positions of agents do not play any role to determine the velocities. Therefore the topological connectivity of RGG remains invariant and is a constant of motion.

2.4 Stationary states

As the dynamics reach a steady state, the system eventually collapses to some steady states and remain in there ever after. There are few such states have been observed, and the list may not be exhaustive.

2.4.1 Single sink states

Initially, the N agents are randomly distributed with uniform probabilities within the unit square box on the $x - y$ plane. If the corresponding RGG is fully connected then, all agents are assigned the same speed v but along different directions. The angles θ_i of the velocity vectors with respect to the $+x$ axis are assigned by drawing them randomly from a uniform probability distribution between 0 and 2π . As time proceeds, the agents soon come out of the initial unit square box and spread out in the open two-dimensional space. After some initial relaxation time, the flock arrives at the stationary state. One of the most common stationary states is the one where the flock is completely coherent and cohesive. The entire flock moves along the same direction without changing the flock's spatial cohesive shape, and therefore $\theta_i(t) = C$ for all i and are independent of time. We call these states as the 'Single Sink States' (SSS). Therefore this stationary state is a fixed point of the dynamical process. A picture of such a flock has been shown in Fig. 2.4(a).

2.4.2 Cyclic states

In cyclic states, the velocity directions θ_i of all agents change at a constant rate in the absence of noise. Therefore the angular velocity $\dot{\theta}_i(t) = D$ for all agents is a constant of motion. Each agent moves in a circular orbit of its own depending on its initial position, but their radii and time periods are the same. Consequently, the magnitude of the resultant velocity of the whole flock in the CS has also a constant value but its direction changes with the same angular velocity. In addition, typically the shape of the flock is another circle though with some irregularities and interestingly its radius changes periodically with the same period of individual agents. Therefore the whole circular flock pulsates, i.e., periodically expands and contracts where each agent moves on its own fixed circular trajectory. We explain this motion in Fig. 2.4(b) by plotting the flock at different instants of

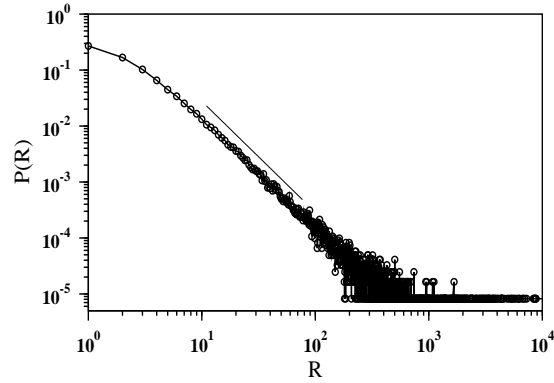


Figure 2.5: The probability distribution of the radii of the individual agent's circular orbits in the cyclic states. The power law has an exponent of $\tau = 1.99(2)$.

time and also show two individual agent trajectories. We call these states as the 'Cyclic States' (CS).

For an arbitrary CS, let the probability that the radius of individual agent's circular trajectory between R and $R + dR$ be $P(R)dR$. Given that the uniform speed of the agents is v and their angular velocities is $\dot{\theta}$, the radius of the circular trajectory is $R = v/\dot{\theta}$. We have studied a large number of such cyclic states and measured the radii of the agents' orbits. In Fig. 2.5 we show the probability distribution of these radii which follows a power law distribution $P(R) \sim R^{-\tau}$ with $\tau = 1.99(2)$.

Throughout this section we have used only one value of the agent speed, i.e., $v_0 = 0.03$. If the speed is reduced by a certain factor a CS state remains CS but all the characteristic lengths are reduced by the same factor. The radius of the circular orbit of every agent and also the size of the flock are reduced by the same factor. Therefore it appears that even in the continuous limit of $v_0 \rightarrow 0$, the characteristic features of the flocks reported here remain same.

Starting from the initial state, when the random positions and velocities are assigned to all agents, the fractions of stationary states that exhibit the SSS and CS are estimated and are denoted by $g_{SSS}(N, n)$ and $g_{CS}(N, n)$ respectively. In Fig. 2.6

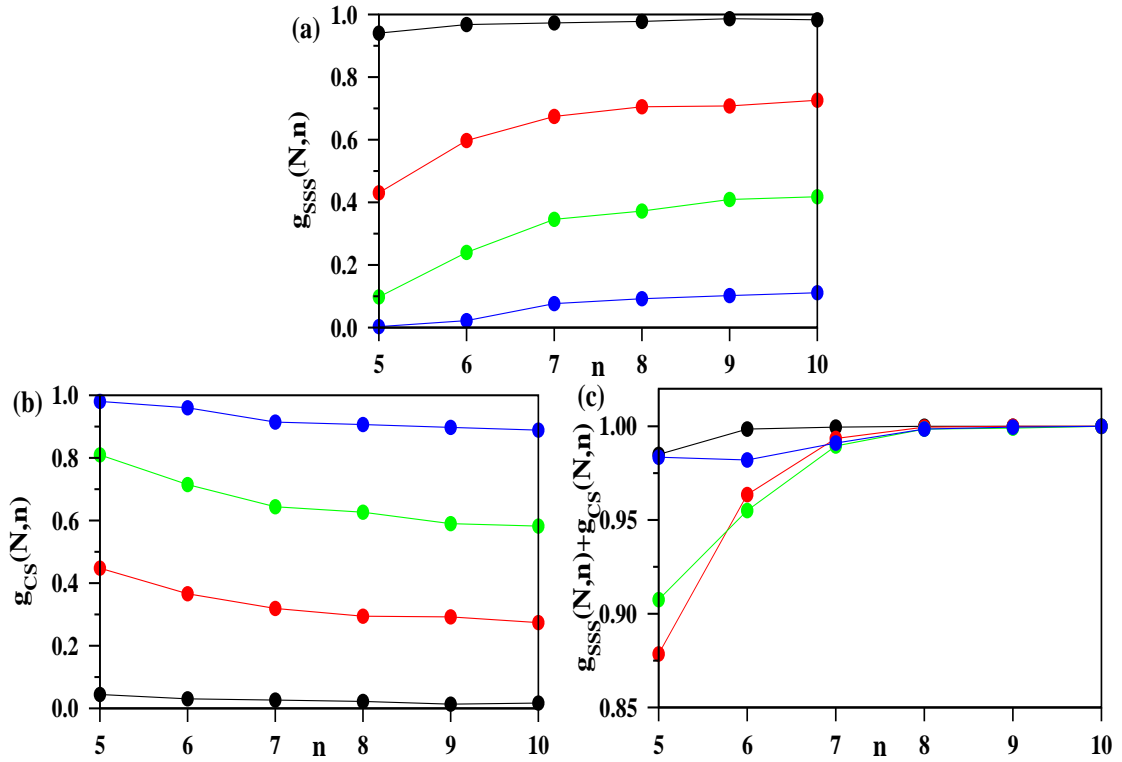


Figure 2.6: The occurrence of two most prominent stationary states when the neighbor number n has been varied over a range from 5 to 10 and for different flock sizes $N = 64$ (black), 256 (red), 512 (green) and 1024 (blue). (a) The fraction $g_{SSS}(N, n)$ of SSS has been plotted against n . (b) The fraction $g_{CS}(N, n)$ of CS has been plotted against n . (c) The sum of $g_{SSS}(N, n) + g_{CS}(N, n)$ has been plotted and it is seen that beyond $n \approx 8$ the sum is approximately unity.

these two quantities are plotted against the neighbor number n for different flock sizes N . For a certain N , $g_{SSS}(N, n)$ gradually increases with increasing n (Fig. 2.6(a)). For a given flock size N , however large, if the neighbor number n is increased to $N-1$, then on using the dynamics mentioned in Eqn. 2.4 the stationary state flock must be both cohesive and perfectly coherent i.e., $g_{SSS}(N, N-1) = 1$. No stationary state other than SSS can exist in this limiting situation. On the other hand when $n < N-1$ but n is increased, then $g_{SSS}(N, n)$ also gradually increases and approaches the value of unity for any arbitrary value of N . At the same time, $g_{CS}(N, n)$ decreases with n for a fixed N but increases with N for a fixed n (Fig. 2.6(b)). Finally in Fig. 2.6(c) we plot the sum $g_{SSS}(N, n) + g_{CS}(N, n)$

which is less than unity for small n , but on increasing n , this sum gradually increases and reached ≈ 1 for $n = 8$ for all N . It is therefore concluded that if the neighbor number is increased all other states gradually disappear and only SSS and CS states mostly dominate but ultimately for even larger value of n it is the SSS state that only survives.

2.4.3 Other states

In addition there are a number of other stationary states, few of them are described below, but the list may not be exhaustive.

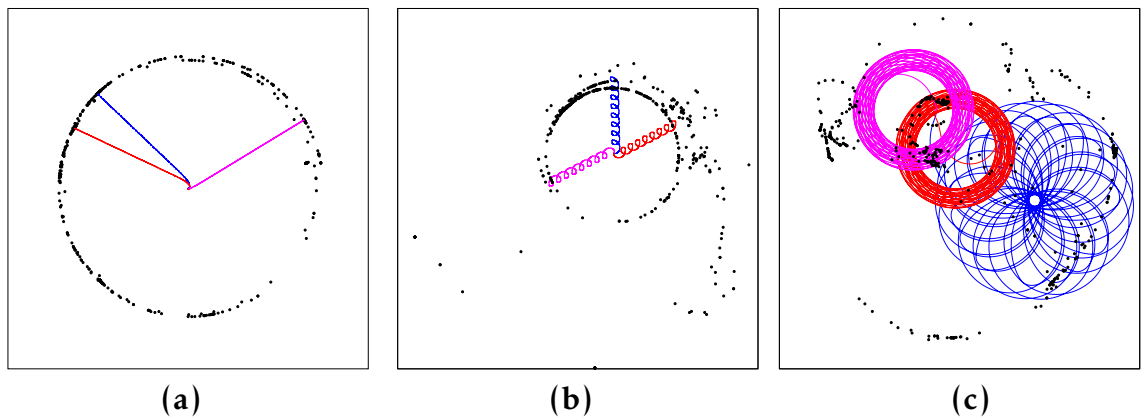


Figure 2.7: Flocks of size $N = 512$ and $n = 5$, moving with the speed of $v = 0.03$ without noise. The positions of the agents are marked by black dots and three individual agent's trajectories are shown in each case by red, blue and magenta colors. (a) Distributed sink state: Every agent moves along a fixed direction $\theta_i = C_i$ of its own which is different in general from the directions of motion of other agents. (b) Cycloid state: In the stationary state the trajectory of each agent is a cycloid. (c) Space-filling state: The trajectory of an agent never repeats itself but gradually fills up the space between two concentric circles. The frame sizes are 40000, 15000 and 350 units respectively.

(i) Each agent has a constant velocity, but their directions are different for different agents. For example the i -th agent has its direction of velocity $\theta_i = C_i$. In this case, the agents, after some relaxation time, move outward radially. The shape of the flock is approximately circular, again with some irregularities, and

the radius of the flock increases at a uniform rate. We call these states as the ‘Distributed Sink States’(DSS). In Fig. 2.7(a) an example of the DSS has been shown. The position of the flock is shown at $t = 500000$, and three agents’ trajectories have been shown using different colors.

(ii) In another type of stationary state, the trajectories of the individual agents are very similar to cycloids. Each agent moves radially outward in a nearly cycloidal motion (Fig. 2.7(b)). A considerable number of agents form a flock of a circular shape, but others are scattered around this circular flock. We call these as ‘Cycloid States’.

(iii) Thirdly there can be rosette type stationary states. The trajectory of each agent is like a rosette which never closes and lies between two concentric circles. Consequently, in the long time limit, the trajectories fill the space between the two circles. This means that the mean separation between consecutive intersections of the agent trajectory with a radial section gradually vanishes as the trajectory evolves for a longer time. We call these as ‘Space-Filling States’. Three such rosette trajectories and the position of the flock have been shown in Fig. 2.7(c).

Few points may be mentioned here about the characteristics of the different stationary states. For example, a possible anisotropic effect on the stationary states may exist due to the choice of the unit square box for releasing the agents. Initially, the positions of the agents are selected randomly within a unit square box on the two-dimensional plane. We have compared that if the agents’ locations are selected randomly within a circle of radius $1/2$, no appreciable change has been observed in the fractions of different stationary states.

The center of mass of the entire flock has different kinds of trajectories in different stationary states. In SSS, the center of mass moves in a straight line exactly similar to all other agents. In CS, the trajectory of the center of mass is also a circle, but it’s radius is not the same as the radius of the orbit of the individual

agents, but it is somewhat larger. In DSS the dynamics of the center of mass is similar to that of the agents. Although the shape of the flock is approximately circular, the fact that, at any instant, the positioning of the agents on the circumference is not uniform, makes the center of mass move radially outwards in a straight line. Motion is indeed unbounded. In cycloid states, the trajectory of the center of mass is also a cycloid and radially outwards. The motion here is also unbounded. In space filling states, the trajectory of the center of mass is rosette type. In this case, the trajectory is bounded.

How sensitive are the final stationary states on the choice of the random initial values of $\{x_i, y_i\}$ and $\{\theta_i\}$ for the N agents? To study this point, we tried with a flock that evolves from a certain initial configuration that evolves to a CS. Now we again evolve the same flock, but this time we slightly change the initial configuration randomly by $x_i = x_i + a \cdot 10^{-4} \cdot r$ and $y_i = y_i + a \cdot 10^{-4} \cdot r$, where r is a random number. The directions $\{\theta_i\}$ of the velocity vectors are maintained the same. We then tune a and found that with $0 < a < 1.70$ the stationary state is still a CS, but with different values of the orbit radius. When $a \geq 1.75$, the stationary state becomes SSS. We conclude that with some amount of perturbation the character of the stationary state remains same, but with even stronger perturbation the stationary state changes.

A preliminary calculation with our model in three dimensions shows the following features. In general, to obtain connected graphs, the value of n needs to be large compared to what is required in two dimensions. Almost always the dynamics lead to an SSS in the steady state. We did not find any other state starting from random initial conditions.

2.5 Dynamics in presence of noise

Studying the role of noise on the dynamics of the flock is very crucial. It is assumed that every agent makes a certain amount of error in judging the angle of its velocity vector at each time step. More precisely given the angles $\theta(t)$ of velocity vectors of all $n + 1$ agents within the interaction zone at time t , it first calculates the resultant of these vectors using the Eqn. 2.4. It then tops up this angle by a

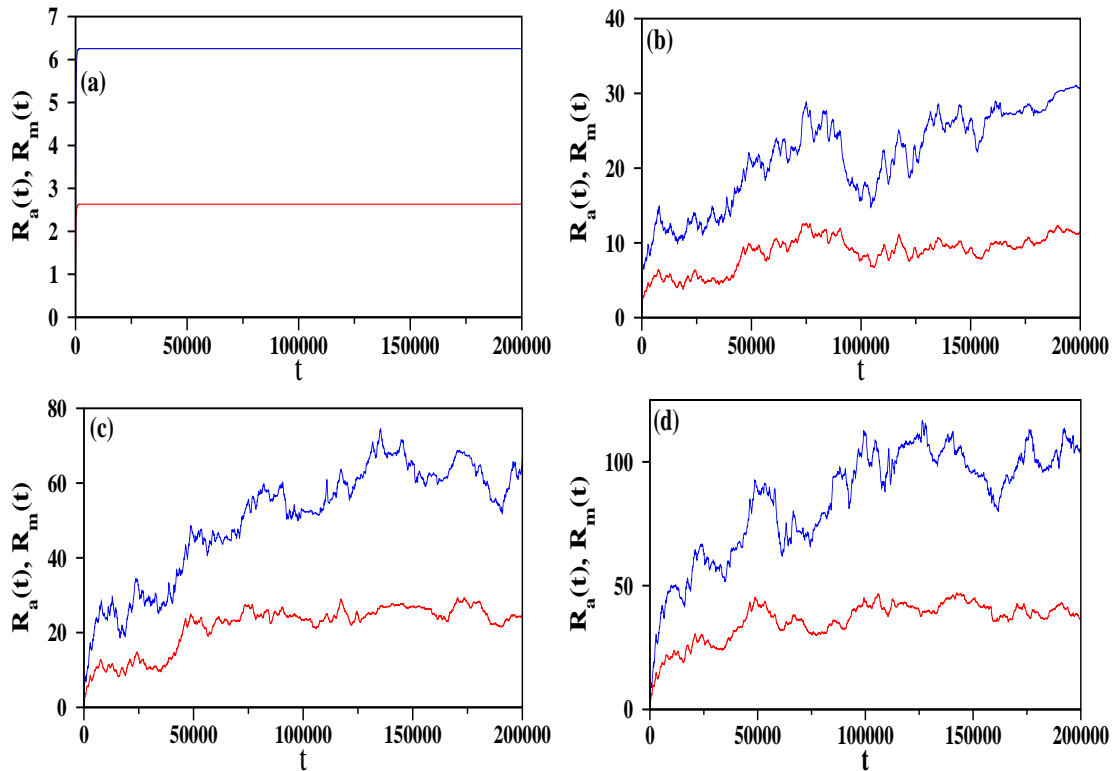


Figure 2.8: Effect of noise is exhibited on a single flock ($N = 512$ agents, each having $n = 10$ neighbors) which goes to a single sink state without any noise. Variation of the maximal radius R_m (blue) and the average radius R_a (red) have been shown with different strengths of the noise parameter: (a) $\eta = 0$, (b) 0.2, (c) 0.5 and (d) 1. The initial positions and velocities are same in all four cases.

random amount $\zeta(\eta)$ which is uniformly distributed within $\{-\eta/2, \eta/2\}$. Therefore the modified Eqn. 2.4 reads as:

$$\theta_i(t+1) = \tan^{-1}[\Sigma_j \sin \theta_j(t) / \Sigma_j \cos \theta_j(t)] + \zeta(\eta). \quad (2.5)$$

The role of the noise is to randomize the deterministic dynamics and quite expectedly the stationary state structures of the flocks exhibited in the SSS and CS patterns are gradually lost. We have studied the effect of noise on both these states by gradually increasing the strength of the noise η . In both cases we use a flock of $N = 512$ agents, each of them interacts with $n = 10$ nearest neighbors and travel with speed $v = 0.03$. Initially all of them are released within the square box of size unity. We first run the dynamics without any noise, i.e., $\eta = 0$ and ensure

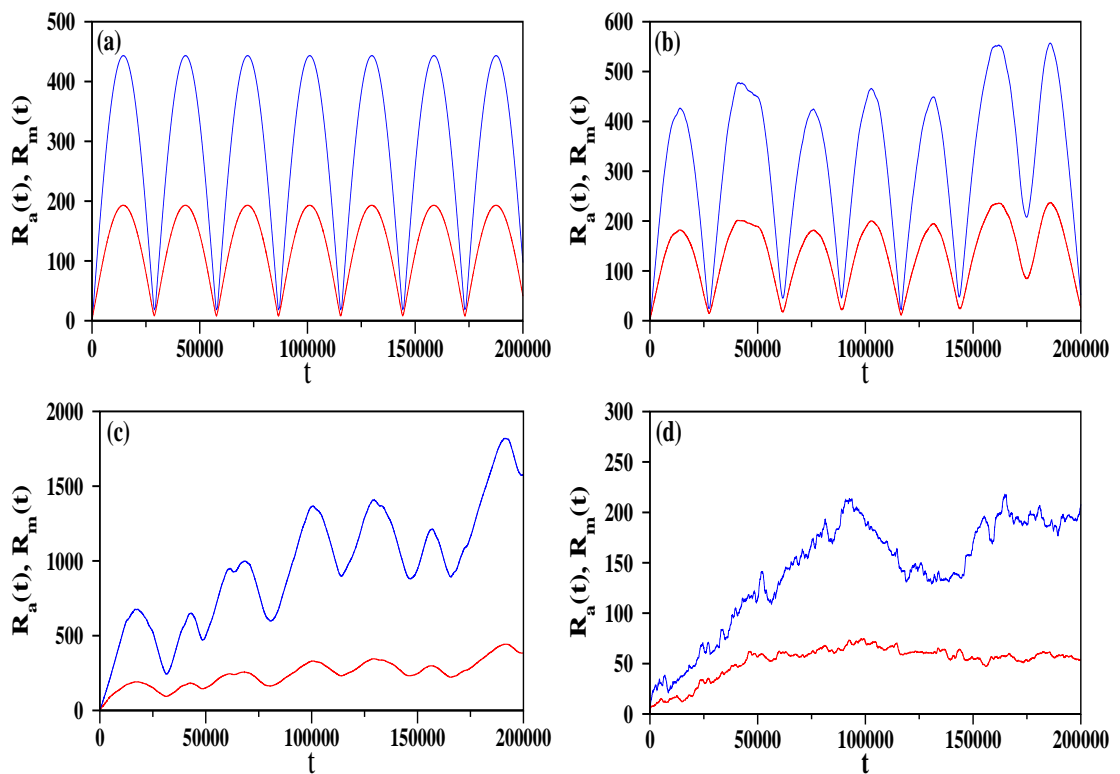


Figure 2.9: Effect of noise is exhibited on a single flock ($N = 512$ agents, each having $n = 10$ neighbors) which goes to a cyclic state without any noise. Variation of the maximal radius R_m (blue) and the average radius R_a (red) have been shown with different strengths of the noise parameter: (a) $\eta = 0$, (b) 0.2, (c) 0.5 and (d) 1. The initial positions and velocities are same in all four cases.

that the stationary state pattern is indeed a single sink state. As the dynamics proceeds we calculate the maximal distance $R_m(t)$ and the average distance $R_a(t)$ of an agent from the center of mass $(x_c(t), y_c(t))$ of the flock. In Fig. 2.8(a) we plot

these two quantities against time, and they are exactly horizontal curves which are the signatures of the SSS state. These simulations are then repeated for $\eta > 0$ and the variations of $R_m(t)$ and $R_a(t)$ have been shown in Figs. 2.8(b), 2.8(c) and 2.8(d) for $\eta = 0.2, 0.5$ and 1 respectively. In all four cases, the flock starts with the same positions and velocities of the agents. It is seen that on increasing the strength of noise the stochasticity gradually sets in and the variations of $R_m(t)$ and $R_a(t)$ gradually become random.

A similar plot has been exhibited in Fig. 2.9 for the CS but for only a single flock. The Fig. 2.9(a) shows the zero noise case, and the curves are periodic. However, when the noise level is increased (Figs. 2.9(b)-(c)), it distorts the periodicity. With small values of η the variations are slightly distorted from the periodic variations, however, with a larger strength of noise, the distortion is much more. Finally for $\eta = 1$ the fluctuations look random and similar to those in the SSS (Fig. 2.9(d)).

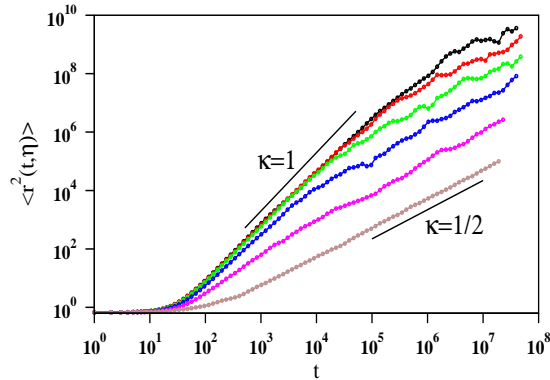


Figure 2.10: The mean square displacement $\langle r^2(t, \eta) \rangle$ of an agent from the origin has been plotted against time for different values of the noise parameter $\eta = 0.2$ (black), 0.5 (red), 1.0 (green), 2.0 (blue), 3.0 (magenta) and 4.0 (brown). The flock size $N = 512$ and the neighbor number $n = 10$. Two short straight lines are the guides to the eye whose slopes are $\kappa = 1/2$ and 1.

Next we calculated the mean square displacement $\langle r^2(t, \eta) \rangle$ from the origin as time passes. The averaging has been done for a single agent within a flock and over many such independent flock samples. The noise strength has been varied

over a wide range of values. In Fig. 2.10 we have displayed the variation of $\langle r^2(t, \eta) \rangle$ against the time t using a log–log scale for six different values of η . Here again we consider flocks with fully connected RGGs. On the other hand with zero noise these configurations may lead to any of the possible stationary states. Simulating up to a maximal time of $T = 10^8$ we observed a cross-over behavior in the mean square displacement. When η is very small $\langle r^2(t, \eta) \rangle \sim t^{2\kappa}$ with $\kappa \approx 1$ which implies that the flock maintains a ballistic motion at the early stage, i.e., the coherence is still maintained during this period. On the other hand after a long time one gets $\kappa = 1/2$ which indicates the diffusive behavior. This implies that even if a little noise is applied for a long time, the effect of the noise becomes so strong that the flock can no longer maintain a cohesive and coherent structure any more and agents diffuse away in space. Therefore for any value of η there is a cross-over from the ballistic to diffusive behavior. Consequently a cross-over time $t_c(\eta)$ can be defined such that for short times $t \ll t_c(\eta)$ the dynamics is ballistic with $\kappa = 1$ and for $t \gg t_c(\eta)$ the dynamics is diffusive with $\kappa = 1/2$. In Fig. 2.10 we show this behavior and observe that the crossover time depends explicitly on the value of η and diverges as $\eta \rightarrow 0$. The value of $t_c(\eta)$ has been estimated by the time coordinate of the point of intersection of fitted straight lines in the two regimes of Fig. 2.10: for $t \ll t_c(\eta)$ and for $t \gg t_c(\eta)$. The value of $t_c(\eta)$ so estimated diverges as $t_c(\eta) \sim \eta^{-2.52}$.

This transition is more explicitly demonstrated using a plot of the Order Parameter (OP) $M(\eta)$ against η (Fig. 2.11). The OP is defined as the time averaged magnitude of the resultant of all agents' velocity vectors, scaled by its maximum value

$$M(\eta) = \langle |\sum_{j=1}^N \mathbf{v}_j| \rangle / (Nv) \quad (2.6)$$

where $\langle \dots \rangle$ denotes the time average over a long period of time in the stationary state. In Fig. 2.11 (a) we have plotted $M(\eta)$ against η at an interval of $\Delta\eta = 0.1$ for different system sizes from $N = 64$ to 1024. In these simulations, the initial

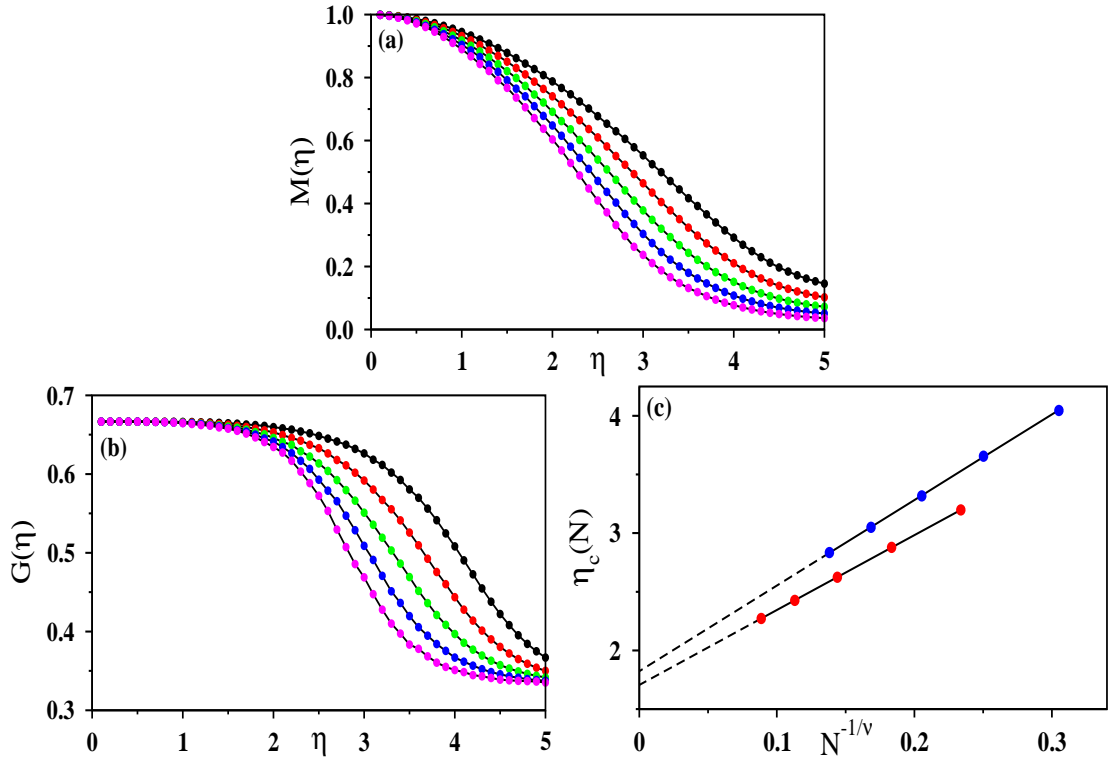


Figure 2.11: (a) The stationary state order parameter $M(\eta)$ and (b) the Binder cumulant $G(\eta)$ have been plotted for the system sizes $N = 64$ (black), 128 (red), 256 (green), 512 (blue) and 1024 (magenta) where all agents start with their initial velocities in the same direction. System size increases from right to left. (c) Extrapolation of $\eta_c(N)$ values determined from (a) and (b). We obtained $\eta_c(N) = 1.70 + N^{-1/2.86}$ and $\eta_c(N) = 1.82 + N^{-1/3.50}$ respectively.

conditions are chosen to be completely coherent so that the velocity vectors of all agents are in the same direction. In the absence of noise, this situation is maintained and $M(0) = 1$ at all times for all system sizes. However for $\eta > 0$ noise sets in, but in the stationary state one still gets a non-zero OP. On further increasing η the OP decreases monotonically and ultimately vanishes. Therefore there exists a critical value $\eta_c(N)$ of the noise parameter where the transition from the ordered state to disordered state takes place. It is observed in Fig. 2.11(a) that as the system size N is enlarged the transition becomes more and more sharper and shifts to the regime of small η . Further we have calculated the Binder cumulant $G(\eta) = 1 - \langle M^4(\eta) \rangle / 3 \langle M^2(\eta) \rangle^2$ and plotted against η in Fig. 2.11(b) for the same

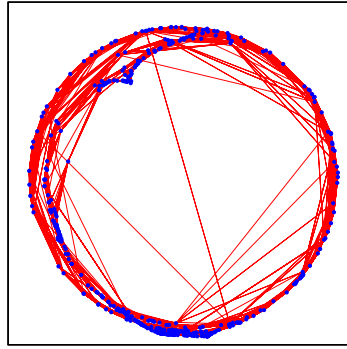


Figure 2.12: The position of a flock ($N = 512$, $n = 10$) in CS by blue dots and links by red lines. The frame size is 150 units.

system sizes [22]. The value of $G(\eta)$ drops from a constant value of around $2/3$ at the small η regime to about $1/3$ for large values of η .

The transition point η_c can be estimated in the following way. For each curve in Fig. 2.11(a) we calculate the value of $\eta_{1/2}(N)$ for which $M(\eta) = 1/2$. We define $\eta_{1/2}(N)$ is the characteristic noise level where the transition takes place. By interpolation of the plots in Fig. 2.11(a) of the points around $M(\eta) = 1/2$ we have estimated $\eta_{1/2}(N)$. These estimates are then extrapolated in Fig. 2.11(c) as:

$$\eta_{1/2}(N) = \eta_{1/2}(\infty) + AN^{-1/\nu}. \quad (2.7)$$

On tuning the trial values of ν very slowly, we found that for $\nu \approx 2.86$ the error in the least square fit of the above finite-size correction formula is minimum. Therefore the extrapolated $\eta_{1/2}(\infty) \approx 1.70$ is the critical noise strength η_c according to our estimate. A similar calculation has also been done using the Binder cumulant. From this calculation we estimated $\eta_c = 1.82$ and $\nu = 3.50$. The difference between the two estimates is considered as the error in the measured values which are 0.12 and 0.64 for η_c and ν respectively.

Since the agents are uniformly distributed initially, the edges of RGG also are homogeneously distributed as shown in Fig. 2.2(d). However with time evolution, these edges change their positions, but their connectivity does not change,

i.e., the end nodes of every edge are always fixed since the neighbor list does not change. How they look in the stationary state has been exhibited in Fig. 2.12. This is the picture of the circle shaped flock in the cyclic state. The blue dots represent the agents, and the red lines represent the edges. What is interesting to note is that the system self-organizes itself so that not only agents but also the edges are constrained to be within a very limited region of the space. Very few edges criss-cross the flock from one side to the opposite side. Initially, each agent had its n neighbors at its closest distances. After passing through the relaxation stage and arriving at the stationary state, when the shape of the flock is completely different from its initial shape, most of the agents maintain their connections with other agents in their local neighborhood only.

2.6 The fastest refreshing rate of the interaction zone

Here we consider the case corresponding to the fastest refreshing rate of the interaction zone, i.e., when every agent updates its n nearest neighbors at every time step. Consequently, the RGG is no longer a constant of motion in this case and is updated at each time step. While performing simulations of this version, we first notice that in the long time stationary state the entire flock becomes fragmented with probability one into different clusters. For a flock of N agents with neighbor number n , the minimum number of agents in a cluster is $n + 1$. An agent of a particular cluster has all n neighbors who are members of that cluster only. In the stationary state, all agents of a cluster have exactly the same direction of velocity, and the entire cluster moves along this direction with uniform speed v . Therefore, the velocity direction θ of a particular cluster can be looked upon as the identification label of that cluster. The shape of the flock is approximately circular since each cluster travels outward with the same speed (Fig. 2.13(a)).

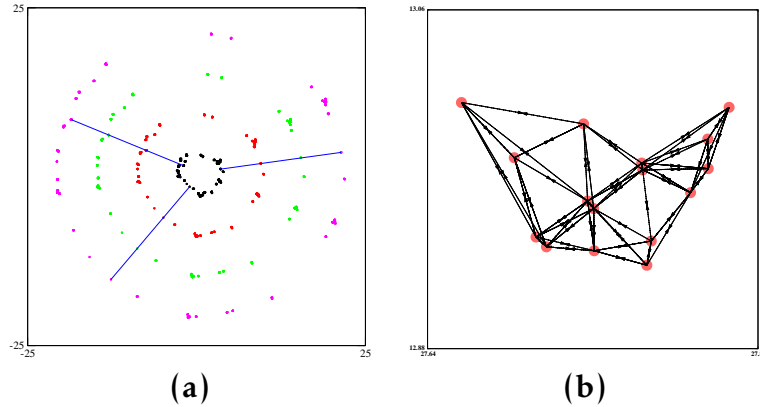


Figure 2.13: (a) Positions of a flock of $N = 512$ agents with $n = 5$ neighbors in the interaction zone and at four different time instants: 100 (black), 200 (red), 300 (green) and 400 (magenta). The RGG has been updated at every time step. Three individual agents' straight line trajectories have also been shown. There is a total of 29 clusters. (b) The sub-graph of the RGG corresponding to a specific cluster of 16 agents have been shown. An arrow has been drawn from the agent i to the agent j if j is one of the n neighbors of i . There is a total of $16 \times 5 = 80$ distinct links, and each link is directed in both directions. It may also be noted that whole set of links are restricted to the nodes of the cluster only.

Moreover, within a cluster, if the agent i is a neighbor of the agent j then j is also a neighbor of i . Therefore the sub-graph of the entire RGG specific to a cluster is completely undirected, and the corresponding part of the adjacency matrix is symmetric (Fig. 2.13(b)). This immediately implies that the $N \times N$ adjacency matrix of the entire flock can be written in a block-diagonal form by assigning suitable identification labels of different agents. A natural question would be how the probability distribution $D(s)$ of different cluster sizes depends on the cluster size s . To answer this question a large number of independent flocks have been simulated and each of them was evolved to its stationary state. In the stationary state the sizes of the individual clusters are measured using the burning method. In Fig.2.14(a) a plot of $D(s)$ vs. s for $s > n$ has been shown on a semi-log scale for $N = 512$ and $n = 5$, the data being collected using a sample size of 20000 independent flocks. Apart from some noise at the tail end and a maximum around the

smallest value of s the plot fits well to a straight line, implying an exponentially decaying form of the probability distribution. We conclude $D(s) \sim \exp(-s/s_c)$ where $s_c \approx 7.2(1)$.

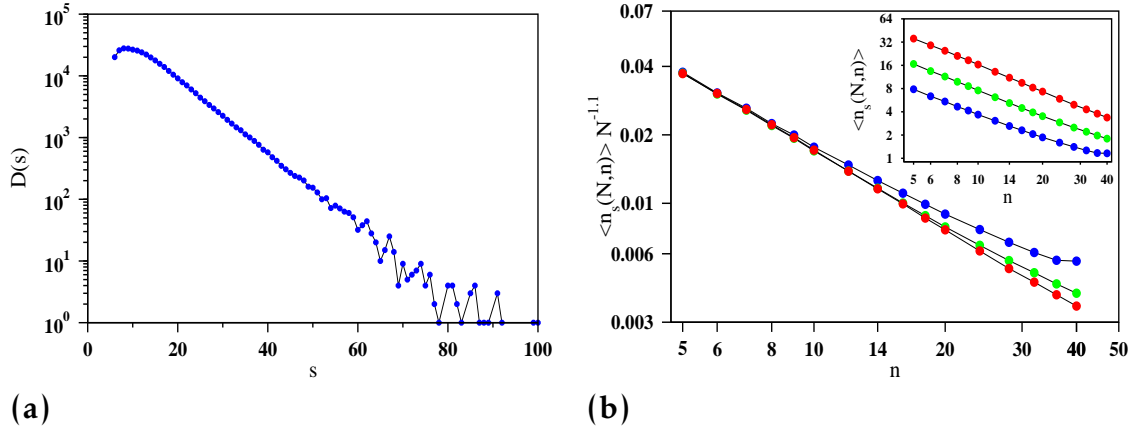


Figure 2.14: (a) The probability distribution $D(s)$ of the cluster sizes s seems likely to have an exponentially decaying form $\exp(-s/s_c)$ where $s_c \approx 7.2$. (b) The inset shows the plot of the average cluster size $\langle s(N, n) \rangle$ for $N = 512$ and $n = 5$ with neighbor number n on a log–log scale: $N = 128$ (blue), 256 (green) and 512 (red). In the main plot the vertical axis has been scaled by $N^{1.1}$ which leads to a data collapse.

Next, the average number of clusters $\langle n_s(N, n) \rangle$ has been calculated and plotted in the inset of Fig. 2.14(b) for $N = 128, 256$ and 512 and $n = 5$ on a log–log scale. Again, apart from the tail end, the plots fit very nicely to parallel straight lines, the slopes of which are estimated to be $1.168(5)$. In the main part of Fig. 2.14(b) a scaling has been shown which exhibits a nice data collapse, corresponding to the following form

$$\langle n_s(N, n) \rangle N^{-1.1} \sim n^{-1.168}. \quad (2.8)$$

This implies that as the neighbor number n increases, there would be fewer clusters in the stationary state. On the other hand, for a specific valued of n , the average cluster number grows with the flock size as $N^{1.1}$. Assuming that the above scaling relation holds good for the entire range of n , for a given N one can define a cut-off value of $n = n_c$ such that $\langle n_s(N, n_c) \rangle = 1$ which leads to

$n_c(N) \sim N^{1.1/1.168} = N^{0.94}$. However, our simulations suggest that due to the presence of an upward bending at the tail end, the above scaling relation does not work at this end and $n_c(N)$ is actually of the order of N .

2.7 Vortices on the square lattice

In this section we studied a simpler version of our model where every agent is a spin vector. They are no more mobile, their positions are completely quenched at the sites of a regular lattice, but the directions $\theta_i(t)$ of the spins are the only dynamical variables that evolve with time following Eqn. 2.4. More specifically, spins are placed on a square lattice with different choices for the first n neighbors and we study the spatio-temporal patterns that emerge during the time evolution of the angular variables $\{\theta_i(t)\}$. The arrangement of the spins allows to draw a parallel with the dynamics of planar spins in the two dimensional XY model. The connections between the Vicsek model [16] and the $2d$ XY model [102] have been explored since long [18, 32, 41]. It is well known that in the limit of speed $v \rightarrow 0$ the dynamics of the Vicsek model would exactly map on to the finite temperature Monte Carlo dynamics of the $2d$ XY model. However, in the latter model, any long-range ordered phase is absent. Instead, a quasi-long-range ordered phase appears at the low temperatures, and the transition to the disordered phase is associated with the simultaneous unbinding and increase of vortex-antivortex (VAV) pairs. In the low temperature phase, VAV pairs are to be found in tightly bound states. We find that our model defined on the square lattice also gives rise to VAV pairs and we determine the density of such pairs, as a function of the noise amplitude η .

We define the IZ of an agent with respect to its n nearest neighbors on the square lattice of size $L \times L$ with the periodic boundary condition. For $n = 2$, the IZ includes the top and the right nearest neighbors. For $n = 3$, the left nearest

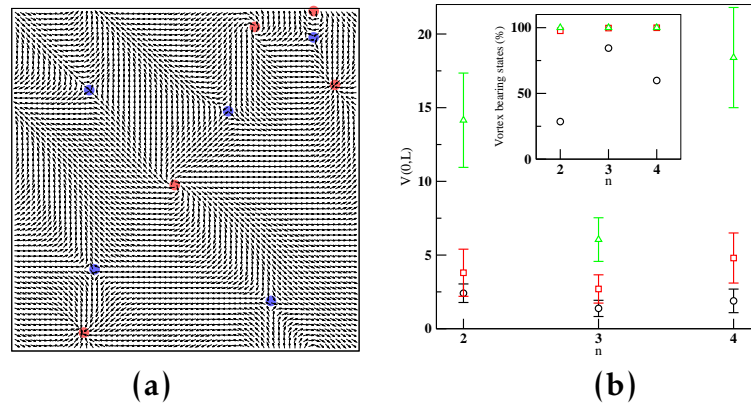


Figure 2.15: (a) Vortex-antivortex pairs of the spin systems in the stationary state in a square lattice with size $L = 64$ and $n = 2$ with zero noise. The orientations of the spins change with time in such a way so that the entire spin pattern with vortices and the antivortices move with a uniform speed from the top-right corner to the bottom-left corner. Vortices and antivortices are marked by filled red and blue circles. (b) The number $V(0,L)$ of vortex-antivortex pairs at zero noise for different values of n in lattices of three different sizes: $L = 32$ (circles), 64 (squares) and 128 (triangles). The bars indicate the standard deviation in the values obtained from around 100 configurations in each case. In the inset, the percentage of configurations which lead to steady states with vortex pairs is plotted against n .

neighbor is also included, and in the case of $n = 4$, all the four nearest neighbors are included. We notice that for the $n = 4$ case, the Vicsek model with spins similarly placed on the square lattice and interact with a range $R = 1$ and our model are same. As before we study the dynamics of the spin system with and without noise.

In the absence of noise, beginning from arbitrary initial conditions for θ_i 's, the dynamics results in the formation of VAV pairs. For $n = 2$ and 3 , the interactions are anisotropic. Consequently the entire spin pattern in the stationary state as well as all VAV pairs are mobile and in general all the spin orientations θ_i 's change with time. In comparison, for $n = 4$, all the θ_i 's remain frozen in time which also implies that all the VAV pairs are anchored. We find that the choice of the IZ, in addition to the periodic boundary condition, fixes the direction of

motion of the VAV pairs. In the Fig. 2.15(a) an instantaneous configuration of the spins is plotted for a lattice with $L = 64$ and $n = 2$. In general for the $n = 2$ case the entire spin pattern moves on the average along the diagonal direction from top-right to bottom-left. For the case, $n = 3$, the vortices travel from the bottom to the top.

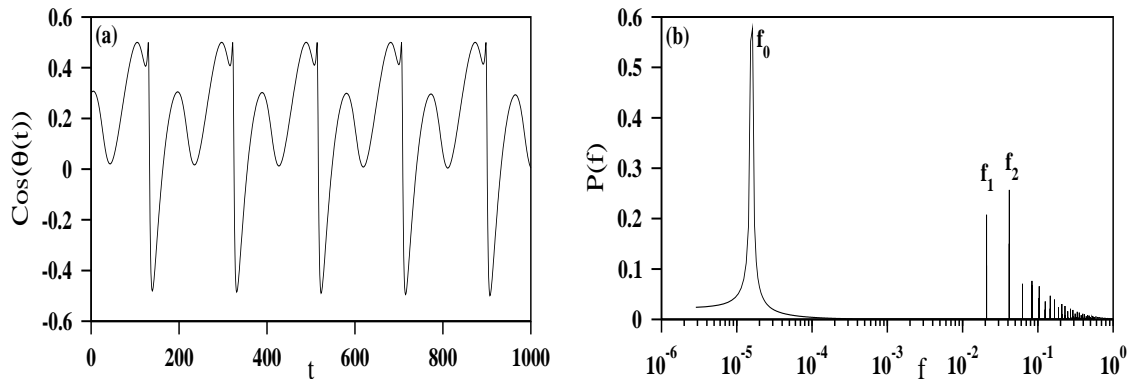


Figure 2.16: (a) The x -component of a typical spin vector is plotted against time for lattice with $L = 64$ and $n = 2$ at zero noise. (b) The corresponding power spectrum indicates the presence of three basic frequencies $f_0 = 1/(4096L)$, $f_1 = 1/(3L)$ and $f_2 = 2/(3L)$. The higher frequencies can be expressed as combinations of the f_1 and f_2 and essentially become harmonics of f_1 since $f_2 = 2f_1$.

Let the $V(\eta, L)$ be the number of VAV pairs observed at noise η in a lattice of size L . The number of VAV pairs observed at zero noise, $V(0, L)$ is plotted against the value of n in the Fig. 2.15(b) for different lattice sizes. We observed during the time evolution of a given initial condition that the number of VAV pairs initially decays and then becomes stationary. However, different initial conditions lead to different values at the stationary states. The bars indicate the dispersion that is observed for different initial conditions which lead to a non-zero number of VAV pairs. For the lattice size $L = 128$ we wait for 10^5 steps before calculating the number of VAV pairs. The inset to the Fig. 2.15(b) shows the percentage of initial conditions that lead to a non-zero number of VAV pairs. We find as lattice size increases, arbitrary initial conditions, almost always, lead to states with VAV

pairs.

The nature of the time variation of the spin angle θ_i 's for the cases $n = 2$ and $n = 3$ are found to be quite complex. In the Fig. 2.16(a) we plot the time series corresponding to the oscillation of the x -component of a typical spin vector for $L = 64$ and $n = 2$. The corresponding power spectrum apparently reveals the presence of three basic frequencies f_0 , f_1 and f_2 all of which are rational multiples of $1/L$ (Fig. 2.16(b)). The time evolution can be explained as a periodic oscillation with f_1 and f_2 (since $f_2 = 2f_1$) riding on a very slow mode. These features carry over to $L = 128$ as well. We find that in the case of $n = 3$, the spectrum is similar, but the frequencies are not simple multiples of $1/L$.

It is known that metastable vortices are produced at low temperatures in the $2d$ XY model when equilibrium is achieved beginning from arbitrary initial conditions. However, these vortices are not responsible for the VAV unbinding transition [103]. Therefore, we study the effect of noise by “cooling down” [104] the system to zero noise level starting from a high value of noise. At each noise level

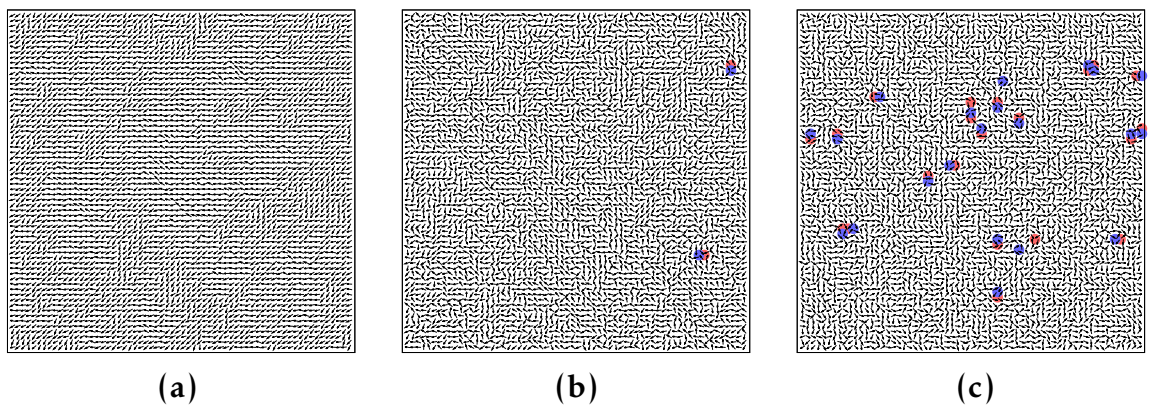


Figure 2.17: The figure shows proliferation of vortices as noise is increased in a square lattice of length $L = 64$ with $n = 4$. (a) For $\eta = 0.15$ there are no vortices, (b) for $\eta = 0.35$ vortices begin to appear, there are only two vortex-antivortex pairs and (c) for $\eta = 0.40$ twenty one vortex-antivortex pairs can be seen. Filled circles of two different colors, red for vortices and blue for antivortices, have been drawn around the vortex centers.

the system initially passes through 10^5 time steps; after this relaxation it passes

through an additional 10^4 time steps and then moves to the next lower level of noise. We begin around the value of noise given by $\eta = 3.7$ and decrease η by an amount 0.07 in each step. This method suppresses the generation of the VAV pairs at low noise. At zero noise the vortices are absent in contrast to the statistics discussed in the previous paragraphs where the cooling down method was not employed.

At zero noise we find the spin system reaches the globally ordered state where all the spin vectors are oriented in the same direction. We believe that this is due to the finite size effect of the lattice. The spin configuration at the low noise of $\eta = 0.15$ has been shown in the Fig. 2.17(a) for $L = 64$ and $n = 4$ where not only vortices are absent but the long-range order is also not present. At the higher noise levels, VAV pairs start appearing, and there is a rapid increase in the number of pairs with further increase in noise. All the VAV pairs appearing initially are tightly bound, i.e., lattice spacing is small between the members in a pair as in Fig. 2.17(b)) but at higher noise members in a pair are seen to unbound (Fig. 2.17(c)).

The order parameter $M(\eta)$ tends to unity as $\eta \rightarrow 0$ as shown in the Fig. 2.18(a). In Fig.2.18(b) we plot the vortex-pair density, defined as $\rho = V/L^2$. The natural collapse of the plots belonging to different system sizes indicates a functional dependence of ρ on n and η independent of L . To understand this behavior we obtain the collapse of the logarithm of $1/\rho$ in Fig.2.18(c) for different values of L and n . The plot reveals that in the region where VAV pairs start proliferating $\rho \sim \exp(-\frac{An^{\beta_0}}{\eta_0^\alpha})$, where A , β_0 and α_0 are constants. We estimate α_0 by averaging slope of individual curves which yields $\alpha_0 = 2.68 \pm 0.13$. This gives $\beta_0 = \gamma_0 \alpha_0 = 0.75$. This result is in contrast to the relation $\rho \sim \exp(-\frac{a}{T})$, where a is VAV pair energy and T is the temperature for the $2d$ XY model [104].

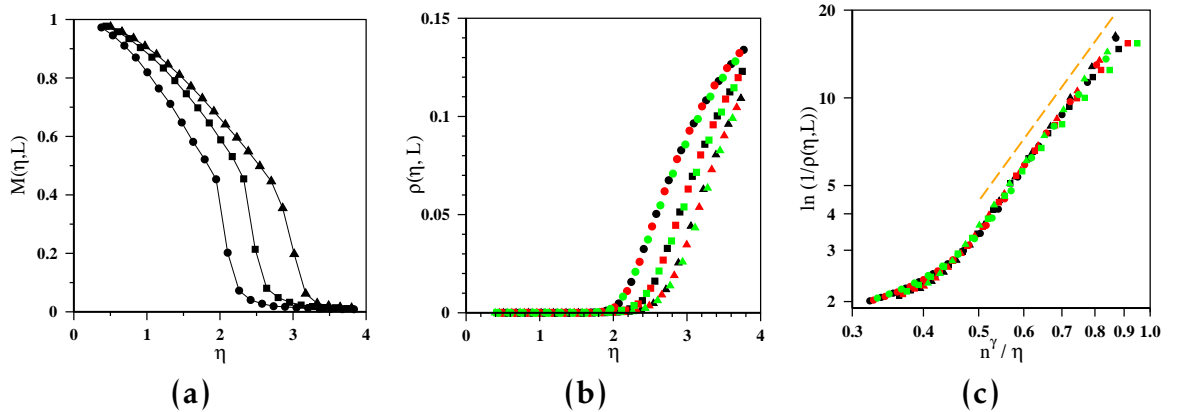


Figure 2.18: The behavior of different quantities against noise for lattice sizes $L = 32$ (black), 64 (red) and 128 (green) with values of $n = 2$ (circle), 3 (square) and 4 (triangle). (a) The variation of the order parameter $M(\eta, L)$ against noise η are shown for $L = 128$ and for $n = 2, 3$ and 4. (b) The vortex-pair density $\rho(\eta, L)$ against η . (c) Scaling collapse of $\ln(1/\rho(\eta, L))$ against n^{γ_0}/η . For the collapse we use $\gamma_0 = 0.28$. The dashed straight line, having slope $\alpha_0 = 2.68$, is a guide for the eye and indicates the power-law nature in the low noise regime.

2.8 Summary

To summarize, we have studied a model of the collective behavior of N interacting mobile agents which travel in the open free space. Each agent interacts with a group of n selected agents around it. The selection criterion is to choose the first n neighbors. We studied two limiting situations, i.e., when the refreshing rates are fastest and the slowest. We first studied when the refreshing rate is slowest, i.e., when the IZ for each agent is determined at the beginning and is never updated. All the agents follow the interaction rule in Vicsek model. It has been observed that in the absence of noise, starting from a small localized region of space the agents gradually spread as time passes, so that after some relaxation time the flock arrives at a stationary state. The most prominent stationary states are the single sink state and the cyclic state. Using numerical methods, we claim that the frequencies of occurrence of other stationary states like the distributed sink states, cycloid states, and the space-filling states go to zero as the neighbor

number increases to about 8. Beyond $n = 8$ only the SSS and CS states dominate. Finally as n approaches the flock size N , only the SSS states dominate. Further, on the application of noise, a crossover takes place from the ballistic motion to the diffusive motion and the crossover time depends on the strength of the noise η , which diverges as $\eta \rightarrow 0$. Further, the calculation of the Order Parameter $M(\eta)$ and the Binder cumulant $G(\eta)$ lead us to estimate the critical noise η_c required for the continuous transition from the ordered to the disordered phase. Secondly, when the refreshing rate is fastest, each agent freshly determines its neighbors in the interaction zone at every time step. In the stationary state, the flock gets fragmented into a number of smaller clusters of different sizes. The agents in a cluster move completely coherently, and different cluster has different direction of motion.

A simpler version of the model has also been studied in the limit of the speed $v_0 \rightarrow 0$ when the positions of spins are completely frozen at the sites of a square lattice, but their orientational angles $\theta_i(t)$ evolve with time again by the Vicsek interaction. Here for $n = 4$ the spin configuration is completely static. On the other hand for $n = 2$ and 3, the entire spin configuration moves along the diagonal and parallel to the asymmetry axis respectively. Further, we have observed that the density of vortex-antivortex pairs increases with the increasing strength of the noise and fits to a nice finite-size scaling behavior.

Overall, our findings suggest that complex spatio-temporal patterns may emerge in the interplay between an underlying network structure and collective motion. We believe that our study would also be relevant in the general problem of consensus development in networked agents [105] and as such issues like undesired synchronization observed in real-world networks [106]. We observed that multiple frequencies develop during oscillations of different dynamical variables. Whether there is a possibility that a cascade of frequencies develops eventually leading to chaotic behavior remains an open question.

3 Topological distance dependent transitions in flocks with binary interactions

3.1 Introduction

The study of Collective Behavior (CB) in systems exhibiting non-equilibrium phase transition under driven noise [15–20, 32–37, 107] is of great interest to the scientific community. Such systems, evolving dynamically from any arbitrary initial state, spontaneously arrives at an ordered state, when the noise parameter is tuned to a vanishingly small value. On the other hand, the order parameter vanishes [16] for stronger noises. In many models studied in the literature, the nature of the associated transition has been suggested to be ‘continuous’ [16, 26, 31, 38–40] whereas in other examples ‘discontinuous’ transitions have been claimed [24, 41, 108]. The dynamical behavior of an agent is determined by its interaction with other agents in its local neighborhood, where the neighborhood is determined in terms of Euclidean distance [16] or topological distance [26, 40].

With the essential idea of collective motion, being discussed in the previous chapters elaborately, in this chapter we present the dynamics of a binary flocks with angular noise, where an agent interacts only with its n -th topological neighbor, based on our work in [45]. Our extensive numerical study indicates that for $n = 1$ and 2, the order to disorder transition is discontinuous, but it is continuous for $n \geq 3$. We describe our binary flocking model in section 2. Subsequently, the simulation results for five different cases, namely from $n = 1$ to 5, are described in section 3. In section 4 we have discussed the phenomenon of persistence as well as the information spreading processes associated in this model and the subsequent time scales. Describes the theoretical analysis using hydrodynamic equations of motion for our binary flock in section 5, we summarize in section 6.

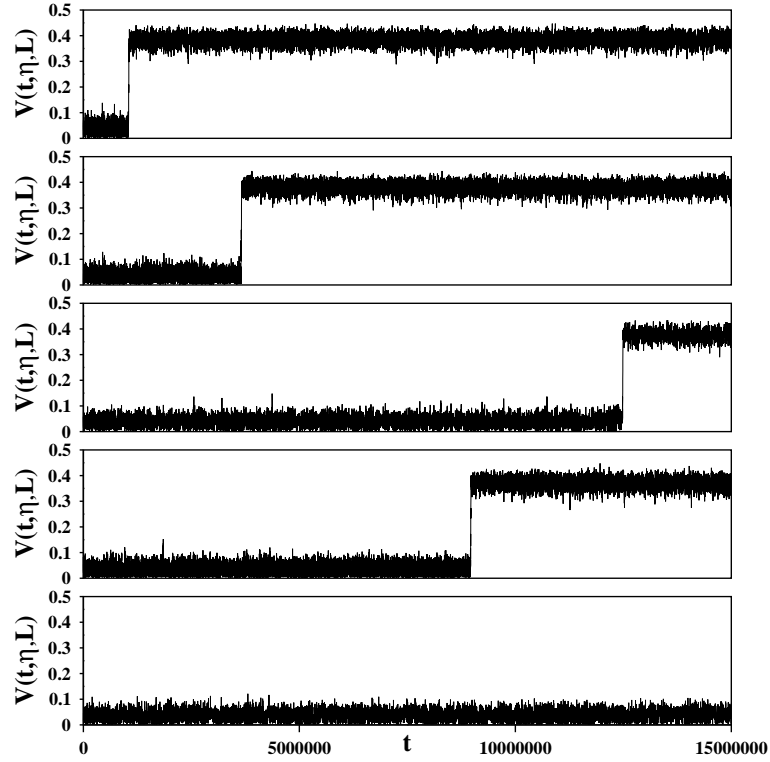


Figure 3.1: For $n = 1$, $L = 512$ and $\rho_0 = 1/8$. Plot of the order parameter $V(t, \eta, L)$ against time t . The switching times and their corresponding noise strengths are $t_c = 1047100$ ($\eta = 0.1184$), 3650100 (0.1188), 12484400 (0.1190) and 8964900 (0.1196) and for $\eta = 0.1200$ the system never switched over to the ordered state.

3.2 Model

In our binary flock, the direction of the velocity of any arbitrary agent i depends on the direction of the velocity of its n -th nearest neighbor j and its own velocity. Let us assume that with respect to any arbitrary reference direction, the velocity directions in time t of the i -th and j -th agents are $\theta_i(t)$ and $\theta_j(t)$ respectively. Then, in the next time step $t + 1$, the updated velocity direction will be,

$$\theta_i(t + 1) = \tan^{-1} \left[\frac{\sin(\theta_i(t)) + \sin(\theta_j(t))}{\cos(\theta_i(t)) + \cos(\theta_j(t))} \right] + \Delta\theta \quad (3.1)$$

where $\Delta\theta$ is a random top-up angle, that represents the noise variable. Its value is drawn freshly from the uniform distribution within the range $\{-\eta/2, \eta/2\}$, η being

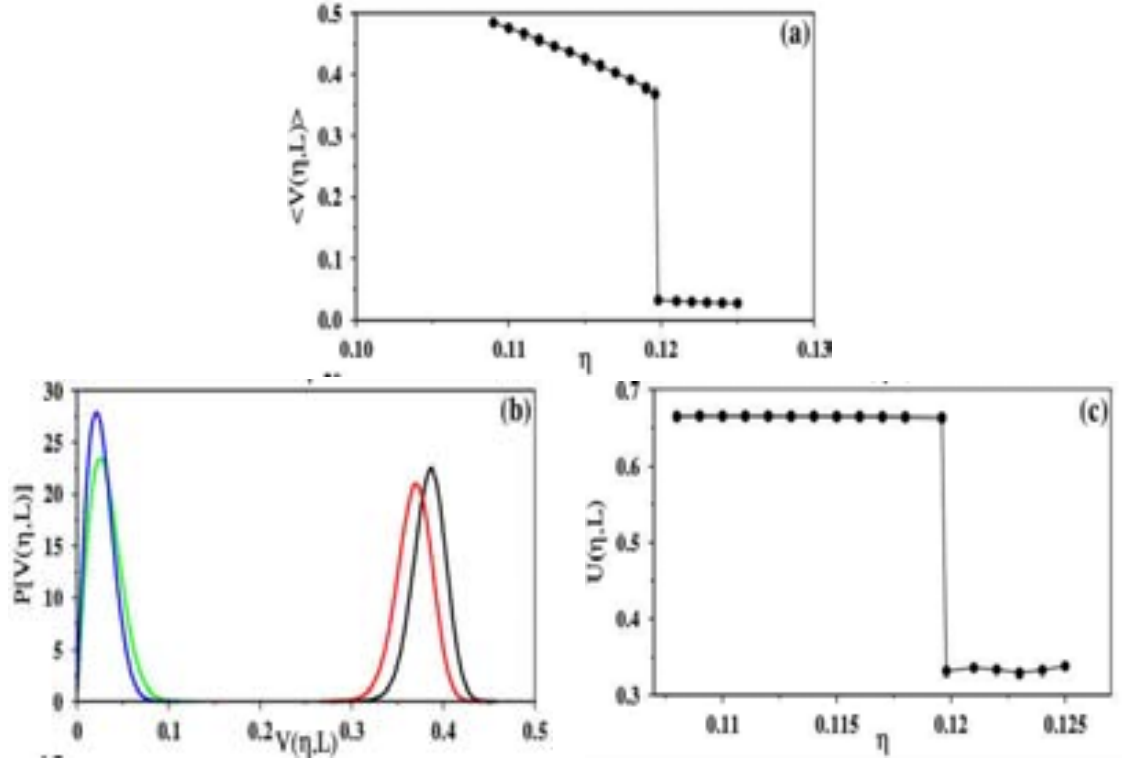


Figure 3.2: For $n = 1$, $L = 512$ and $\rho_0 = 1/8$. (a) Plot of the order parameter $\langle V(\eta, L) \rangle$ against noise parameter η exhibits a discontinuous jump at $\eta = 0.1197$. (b) The probability density of the order parameter $P[V(\eta, L)]$ plotted against $V(\eta, L)$; for the ordered state: $\eta = 0.1184$ (black) and 0.1196 (red) and for the disordered state $\eta = 0.1198$ (green) and 0.1250 (blue) in the sequence from right to left. (c) Binder cumulant $U(\eta, L)$ plotted against η jumps discontinuously from ≈ 0.663 to ≈ 0.332 at $\eta_c = 0.1197$.

the continuously tunable strength of the noise parameter. The agents' velocities are updated synchronously. Therefore the entire set of the velocity angles $\theta_i(t+1)$ are determined simultaneously using the complete set of $\theta_i(t)$ for all i . The order parameter is determined by the magnitude of the resultant velocity vector, scaled by the speed v_0 and averaged over all N agents,

$$V(t) = \frac{1}{Nv_0} |\Sigma_i \mathbf{v}_i(t)|. \quad (3.2)$$

In the following, we have considered five different cases for five different values of n , namely 1 to 5. Within our numerical accuracy we present evidence to claim

that the system undergoes an order to disorder phase transition with respect to the noise parameter η , the system has discontinuous transitions for $n = 1$ and 2 ; where as for $n \geq 3$ the nature of transition is continuous.

Numerical simulations have been performed on a $L \times L$ planar area. The density and the speed of agents are kept fixed at $\rho_0 = 1/8$ agents per unit area and $v_0 = 1/2$ in all calculations. In all simulations, we have kept the density constant but varied the system size L .

3.3 The results

3.3.1 The $n = 1$ case

For $n = 1$, every agent's velocity is determined by its own velocity and that of its first nearest neighbor. In general, if the j -th agent is the first nearest neighbor of the i -th agent, that does not necessarily imply that i is also the first nearest neighbor of j . However, with a small probability, this may actually happen, when both the i -th and the j -th agents are mutually dependent on each other for a while. Typically this happens when they are spatially close to each other but at the same time far away from all other agents. In this situation, they would form a very strongly bound pair. For example, for $\eta = 0$, both of them are completely synchronized and move along the same direction in parallel straight lines with exactly the same velocity, until they come in the close proximity to a third agent so that i and j cease to be mutually nearest neighbors any longer. On the other hand, for small values of $\eta > 0$, though their motion is random, yet they perform a nearly synchronized motion.

We start exhibiting the variation of the order parameter $V(t, \eta, L)$ against time at different noise levels η in Fig. 3.1. The time evolution of the system starts from the same initial configuration of the agents at time $t = 0$, that is, the same spatial locations as well as their random velocities, are used for all values of η . For small

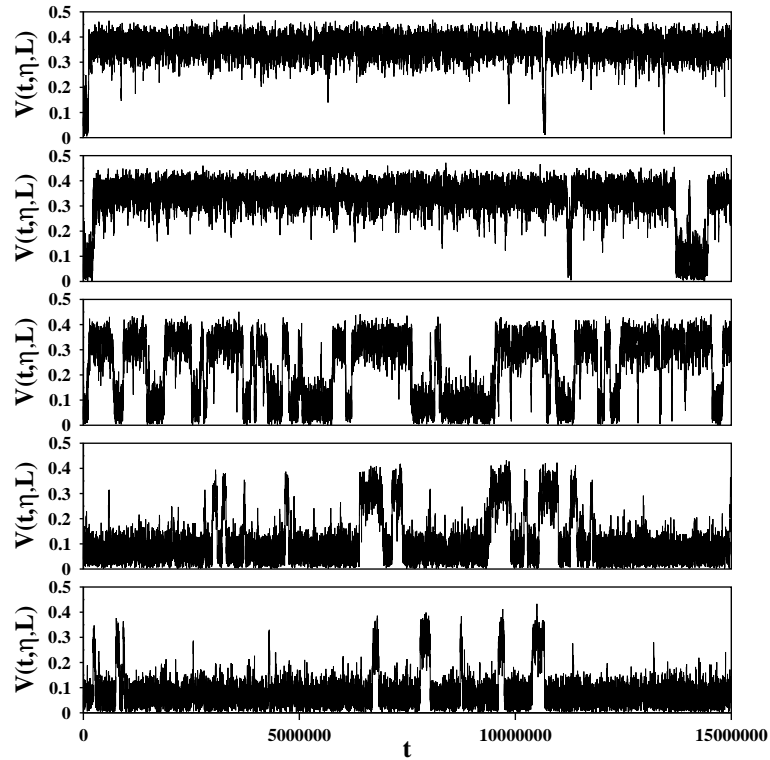


Figure 3.3: For $n = 2$, $L = 512$ and $\rho_0 = 1/8$, order parameter $V(t, \eta, L)$ against time t for $\eta = 0.138, 0.139, 0.140, 0.141$ and 0.142 exhibited from top to bottom. The top and bottom ones are almost completely in the ordered and the disordered phases respectively. Three intermediate plots show existence of metastable stationary states.

values of η , the system is in the ordered phase with a relatively large value of the $V(t, \eta, L)$ that fluctuates around a steady mean value in the stationary state. On the other hand, as η is gradually increased, the system moves into the disordered phase, the mean value $\langle V(t, \eta, L) \rangle$ of the order parameter gradually decreases. The order to disorder transition takes place in between these two regimes. It has been observed that typically the system starts in a disordered state but after some time, say t_c , it switches over to the ordered state when η is comparatively small. It is also noticed that the switching time becomes increasingly larger as η is gradually tuned to larger values.

In usual discontinuous transition and close to the critical point, the system is expected to be in multiple metastable states. Therefore, while in the station-

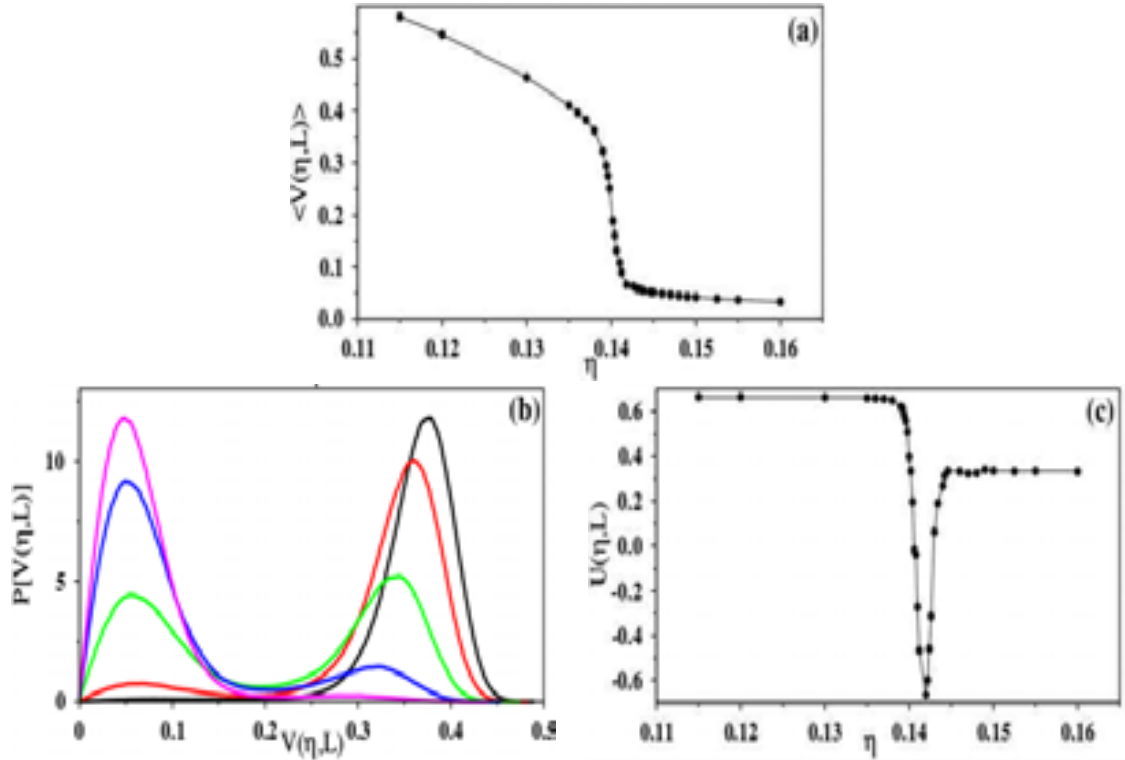


Figure 3.4: For $n = 2$, $L = 512$ and $\rho_0 = 1/8$. (a) The average value of the order parameter $\langle V(\eta, L) \rangle$ plotted against the noise parameter η . The plot exhibits a sharp, yet continuous variation at $\eta = 0.1400$. (b) The probability density of the order parameter $P[V(\eta, L)]$ for $\eta = 0.1380$ (black), 0.1390 (red), 0.1400 (green) and 0.1410 (blue) and 0.1420 (magenta), in the sequence from right to left. (c) Binder cumulant $U(\eta, L)$ plotted against η . At $\eta_c = 0.1400$ its value drops from ≈ 0.66 to ≈ -0.7 .

ary state, the system often switches back and forth between different metastable states [109]. In contrast, here the behavior of the system is very much different from this picture. Here the system resides in one of the two possible states, i.e., either in the ordered state or in the disordered state. Our finite but large time simulation indicates that once one of these two states are selected, the system remains in that state ever after. Therefore, the averaged value of the order parameter $\langle V(\eta, L) \rangle$ has been measured after the switching time t_c . Consequently, a plot of $\langle V(\eta, L) \rangle$ against η in Fig. 3.2(a) exhibits a clear discontinuous jump at the value of $\eta_c = 0.1197(1)$ exhibiting that it is indeed a discontinuous transition.

The probability distribution of the order parameter $P[V(\eta, L)]$ against $V(\eta, L)$

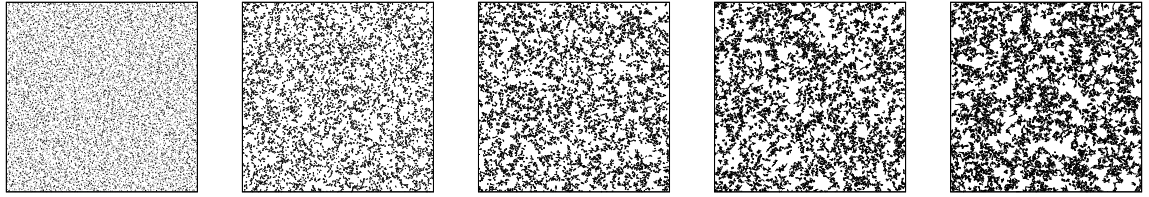


Figure 3.5: The spatial network of interaction links for $L = 512$, $\rho_0 = 1/8$ and $\eta = \eta_c(L)$. Every agent is connected to its n -th neighbor. Snapshots have been shown for $n = 1$ to 5 (from left to right).

has been studied next (Fig. 3.2(b)). The distribution is observed to be a single peaked curve. The position of the peak is large for the ordered state and small for the disordered state. The probability distribution abruptly shifts to the small values of V as the noise parameter η is gradually increased. In two such plots for $\eta = 0.1184$ and 0.1196 , the system is in the ordered state. However, when η is increased by the smallest amount of 0.0002 to the value 0.1198 , the system makes a transition to the disordered state and the distribution discontinuously shifts a large amount to the small regime of V .

The fourth order Binder cumulant $U(\eta, L)$ is defined as

$$U(\eta, L) = 1 - \frac{\langle V^4(\eta, L) \rangle}{3\langle V^2(\eta, L) \rangle^2}. \quad (3.3)$$

Fig. 3.2(c) shows the variation of $U(\eta, L)$ against η . It is very much consistent with the limiting values, that is, $U(\eta, L) \approx 2/3$ for $\eta < \eta_c$ and $U(\eta, L) \approx 1/3$ for $\eta > \eta_c$. The specific value of η where the jump in U takes place is $\eta_c = 0.1197$ and this is recognized as the critical value η_c of the noise parameter.

3.3.2 The $n = 2$ case

Here, the velocity of an agent i is determined by the velocity of its second nearest neighbor j and its own velocity. Therefore, the presence of a third agent, say the k -th agent, is necessary. For both i -th and j -th agents, the k -th agent may act as

their first neighbor. In turn, for the k -th agent, the j -th agent may be the first neighbor and the i -th neighbor may be the second neighbor. This is one special combination in which all three agents mutually depend on one another and form a stable cluster. However, at every time step, the noise feeds in fresh randomness. When a fourth agent comes close to this cluster, the cluster may not be stable any longer.

It is first observed that unlike the $n = 1$ case, very close to the critical point η_c , the order parameter $V(t, \eta, L)$ fluctuates between its values in the ordered and the disordered states (Fig. 3.3). The time averaged value of the order parameter $\langle V(\eta, L) \rangle$ in the stationary state varies continuously with the noise parameter η as shown in Fig. 3.4(a). It assumes high values for small η and gradually decreases as η increases. Around $\eta_c = 0.140$, its value decreases continuously at the fastest rate. For $\eta > \eta_c$, $\langle V(\eta, L) \rangle$ gradually vanishes. This is also demonstrated in Fig. 3.4(b) where the probability density of $V(\eta, L)$ has been plotted for five different values of η , namely, 0.138, 0.139, 0.140, 0.141 and 0.142. While for $\eta = 0.138$ and 0.142, the distributions have single maxima, for the intermediate values double maxima appears. For example, for $\eta = 0.139$ the height of the right peak is larger than that of the left peak, for $\eta = 0.140$ both peaks are of nearly same heights whereas for $\eta = 0.141$ the left peak is taller than the right peak. This implies that while $\eta = 0.139$ and 0.141 are in the subcritical and supercritical regimes respectively, $\eta = 0.140$ is nearly the value of the critical noise.

The Binder cumulant $U(\eta, L)$ has been displayed in Fig. 3.4(c). Because of the existence of the multiple metastable states, a sharp dip in the Binder cumulant exists. This is the typical signature of a discontinuous transition as observed previously in the metric distance dependent Vicsek model [16] occurring at $\eta \approx 0.140$ for $n = 2$.

To see the spatial structure of the flock one can construct the contact network. It is straight forward to define a Euclidean directed network with the binary flock.

Here the agents are the nodes, and a directed link is introduced from agent i to agent j if j is the topological neighbor of i . In Fig. 3.5 the stationary state spatial patterns of such networks have been shown for the critical noise η_c and for $n = 1$ to 5, and for $L = 512$ and $\rho_0 = 1/8$. The spatial distribution of agents is most uniform for $n = 1$. Then as the value of n increases, the agent distribution become more and more heterogeneous.

3.3.3 The $n \geq 3$ cases

The situation is completely different in the $n \geq 3$ cases when we consider the variation of the order parameter $V(t, \eta, L)$ against time t . Neither we see any switching over from the disordered to the ordered state as in $n = 1$ case, nor we observed incessant flip flop between the metastable states of the ordered and disordered states as in $n = 2$ case. In contrast, it is observed for the cases of $n = 3, 4$ and 5, that the width of fluctuation of $V(t, \eta, L)$ becomes increasingly larger as the critical noise strength $\eta_c(L)$ is approached continuously either from the ordered or from the disordered side. At $\eta = \eta_c(L)$, the fluctuation is maximum (not shown). Very similar are the situation for the cases of $n = 4$ and 5. No discontinuous change in the average value of the order parameter has been detected. In Fig. 3.6(a) we exhibit the variation of $\langle V(\eta, L) \rangle$ against η for $n = 3, 4$ and 5. Its variation near the critical point is the sharpest for $n = 3$, less sharp for $n = 4$ and most flat for $n = 5$. The critical noise strengths η_c has been estimated to be 0.151, 0.162 and 0.180 respectively for $L = 512$. In Fig. 3.6(b), the probability distribution of the order parameter are shown again for $n = 3, 4$ and 5. Each curve has a single maximum, and the peak continuously shifts from high to low value with increasing noise strength. In the ordered state, because of the non-zero value of the order parameter, the locations of the three curves are at the right side of the figure. Similarly, the three peaks on the left side correspond to strong noise so that order parameters are nearly zero. Thus the transition from ordered state to

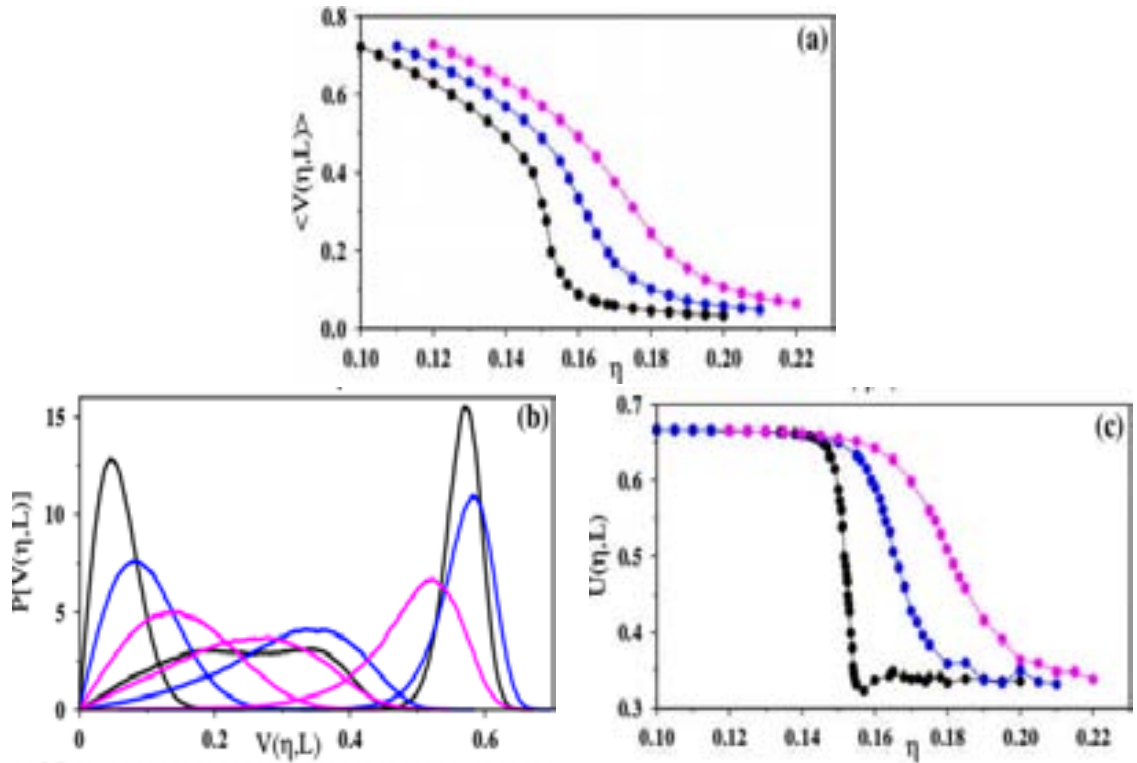


Figure 3.6: For $L = 512$, $\rho_0 = 1/8$ data for $n = 3$ (black), $n = 4$ (blue) and $n = 5$ (magenta) are shown. (a) The order parameter $\langle V(\eta, L) \rangle$ plotted against η , the plots exhibit sharp but continuous decrease around the critical noise strength $\eta_c(L)$. (b) The probability density of the order parameter $P[V(\eta, L)]$ has been plotted against $V(\eta, L)$. The three peaks on the right correspond to the noise levels of the ordered state, three peaks on the left correspond to the disordered phase, whereas the three curves at the intermediate region have been simulated with $\eta \approx \eta_c(L)$. (c) On increasing η , the Binder cumulant $U(\eta, L)$ decreases continuously from ≈ 0.66 and attains its disordered phase value ≈ 0.33 for $\eta > \eta_c(L)$.

a disordered state exhibits the typical signatures of continuous transition.

The fourth order Binder cumulants $U(\eta, L)$ have been exhibited in Fig. 3.6(c). They show a continuous transition from its ordered phase value $2/3$ to its disordered phase value $1/3$ without any sharp discontinuous jump or any dip to a negative value at any intermediate noise strength η . The decrease was most sharp for $n = 3$, less sharp for $n = 4$ and even less sharper for $n = 5$.

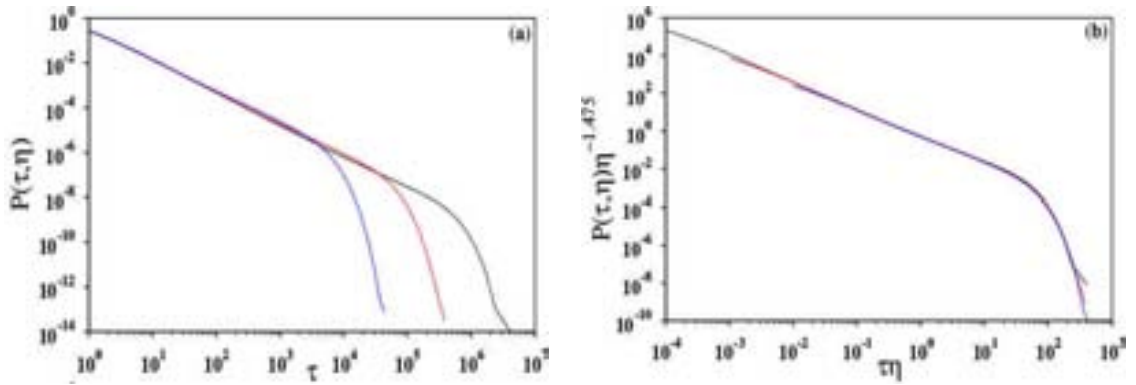


Figure 3.7: For $n = 1$, $L = 128$ and $\rho_0 = 1/8$. (a) The persistence time distribution $P(\tau, \eta)$ plotted against τ for $\eta = 0.0001$ (black), 0.001 (red) and 0.01 (blue) using log–log scale. (b) The coordinate axes have been rescaled using η^{ζ_1} and $\eta^{-\zeta_2}$ with the best estimates of $\zeta_1 = 1.0$ and $\zeta_2 = 1.475$. This gives the persistence time distribution exponent $\gamma_p = \zeta_2/\zeta_1 \approx 1.48(2)$.

3.4 Studying different characteristic times

During flights of such a collectively moving agents a few time scales becomes relevant to understand the dynamics properly. Two such time scales have been analyzed in this section. The first one is the persistence time which somewhat defines and give some idea about the temporal correlation of two moving particles. The second one is the information spreading time scale that gives an approximate idea of the average time scale needed for any information to propagate through the whole flock during the flight.

3.4.1 Persistence times

In this section, we study the persistence time distribution for the agents. Persistence time τ for an agent i is a certain interval of time through which any other agent interacts with i . At each time instant, every agent i has another agent j to interact. The interaction partner of i changes from one agent to another agent, and then to another agent, etc., and therefore the agent i passes through a series of persistence times $\tau_1, \tau_2, \tau_3, \dots$ etc. In the stationary state, we have collected data

of these persistence times for each individual agent and have drawn the probability distribution $P(\tau, \eta)$. We have observed that for a fixed density ρ_0 of agents, this distribution does not depend significantly on the system size L , in contrast, it does depend very strongly on the noise parameter η . It is intuitively apparent that as η decreases, there is less fluctuation in the paths of the agents and therefore the typical persistence time gets longer. Consequently, the persistence time distribution gets elongated over a larger period.

In Fig. 3.7(a) we have shown the plots of persistence time distributions $P(\tau, \eta)$ against τ . On the other hand, three plots for three different values of the noise parameter η differ quite a lot. On a double logarithmic scale, the intermediate region of each curve is quite straight, and the extent of this regime gets elongated as $\eta \rightarrow 0$. This indicates that the persistence time distribution is likely to follow a simple power law distribution in the limit of $\eta \rightarrow 0$

$$P(\tau) \sim \tau^{-\gamma_p}. \quad (3.4)$$

where γ_p is an exponent, and its value has been estimated by the finite-size scaling analysis. As η increases the value of the typical persistence time become shorter, and therefore the extent of the region of validity of the power law also shortens. However, it has been observed that a nice finite-size scaling analysis can be performed on this data. In Fig. 3.7(b) we have re-plotted the same data after scaling the coordinate axes with η^{ζ_1} and $\eta^{-\zeta_2}$ where $\zeta_1 = 1.0$ and $\zeta_2 = 1.475$. Therefore the scaling form is,

$$P(\tau, \eta) \eta^{-\zeta_2} \sim \mathcal{G}[\tau \eta^{\zeta_1}]. \quad (3.5)$$

This gives the persistence time distribution exponent $\gamma_p = \zeta_2/\zeta_1 \approx 1.48(2)$.

3.4.2 Information spreading times

During the dynamical evolution of the binary flock, every agent comes in contact with a large number of other agents. Let us assume that at a certain time instant when the system has settled in its stationary state, a particular agent has some specific information. This information is shared with the topological neighbor with probability one. Generally, at any intermediate time, any agent i that has this piece of information, shares with any other agent j which comes in contact.

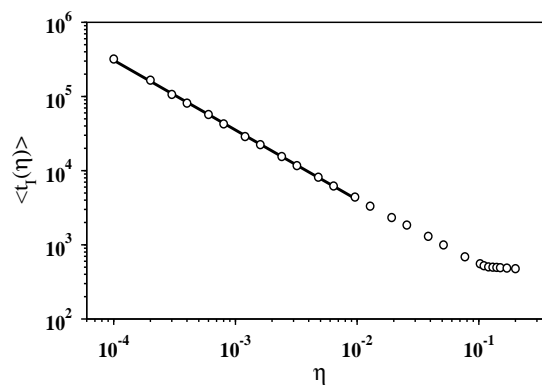


Figure 3.8: For $n = 1$, $L = 256$ and $\rho_0 = 1/8$. The average spreading time $\langle t_I(\eta) \rangle$ has been plotted against η on a double logarithmic scale. The slope of the straight line is the value of the spreading exponent κ defined in Eqn. 3.6 and has the value ≈ 0.94 .

Therefore, after a certain time $t_I(\eta, L)$, the entire collection of agents will have this information. We would like to study how the averaged value $\langle t_I(\eta, L) \rangle$ of information spreading depends on the noise strength η . It is intuitively clear that less the amount of noise, longer is the contact time between the two agents. Therefore we expect that as $\eta \rightarrow 0$, the average contact time would gradually increase. In fact, in the limiting situation of $\eta \rightarrow 0$, all agents will be completely coherent in the stationary state. In this situation, if there are more than one cluster, these clusters would maintain the separate identities and would never merge. In this case the spreading time is infinity, otherwise it is finite. When $\eta > 0$, the spreading time decreases on the average, and we find that it decreases as a power law. In Fig. 3.8

we exhibit the estimates of $\langle t_I(\eta, L) \rangle$ against η on a double logarithmic case. The plot appears to fit a nice straight line, and the linearity ends at $\eta = \eta_c$ where it becomes horizontal. Beyond η_c the flock is randomized, the order parameter has the vanishingly small value. Therefore the average spreading time remains same, and the curve becomes horizontal.

Therefore, within the range $\eta < \eta_c$, the average spreading time follows a power law decay:

$$\langle t_I(\eta, L) \rangle \sim \eta^{-\kappa}, \quad (3.6)$$

where $\kappa \approx 0.94(2)$ has been estimated.

3.5 Theoretical analysis

3.5.1 Hydrodynamic equations of motion for binary flocks

We can also estimate the critical noise strengths as we increase the topological neighbor number n to higher values, using the coarse-grained hydrodynamic equations of motion derived from microscopic rule for particle moving along its heading direction with speed v_0 and orientation update for binary flocks as defined in Eqn. 3.1. In our topology dependent binary interaction model critical point depends on the strength of interaction between the two binary pairs. Strength of interaction can be calculated using angular correlation of two interacting agents. We find the dependence of critical noise strength on interacting binary angular correlation $\alpha(n) = \langle \mathbf{m}_i \mathbf{m}_{in} \rangle$, where $\mathbf{m}_i = (\cos(\theta_i), \sin(\theta_i))$ and \mathbf{m}_{in} is the direction of i -th and its n -th interacting agent, $\langle \dots \rangle$ is average over all possible interacting pairs in the system. We feed the value of $\alpha(n)$ for $n = 1$ to 5 from the microscopic simulation and estimate the critical noise strengths for different n values and compare them with numerical estimates $\eta_c(n)$.

Using the update rule for the position \mathbf{R}_i and orientation θ_i of the i -th agent

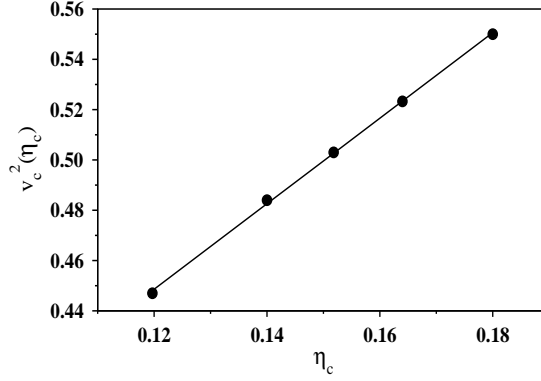


Figure 3.9: Plot of critical v_c^2 vs. η_c for various n values. The value of η_c is estimated from numerical simulation for corresponding n value and the critical v_c is calculated from Eqn. 3.22 for fixed density $\rho_0 = 0.125$.

we can write the coarse-grained hydrodynamic equations of motion for density and polarization order parameter defined as

$$\rho(\mathbf{r}, t) = \sum_i \delta(\mathbf{r} - \mathbf{R}_i(t)) \quad (3.7)$$

$$\mathbf{P}(\mathbf{r}, t)\rho(\mathbf{r}, t) = \sum_i \mathbf{m}_i \delta(\mathbf{r} - \mathbf{R}_i(t)) \quad (3.8)$$

coarse-grained equation for density is same as previously derived in [110] for metric distance model

$$\frac{\partial \rho}{\partial t} = -v_0 \nabla \cdot (\mathbf{P}\rho) + D_\rho \nabla^2 \rho \quad (3.9)$$

but order parameter equation will be different with no explicit density dependence of alignment term

$$\frac{\partial \mathbf{P}\rho}{\partial t} = \left[\frac{(1 - 2\eta^2)2}{\sqrt{2(1 + \alpha)}} - 1 \right] \mathbf{P}\rho - \alpha_2 (\mathbf{P} \cdot \mathbf{P}) \mathbf{P}\rho + -\frac{v_0}{2\rho} \nabla \rho + D_P \nabla^2 P \quad (3.10)$$

where v_0 is the self-propulsion speed of the particle; D_ρ and D_P are the diffusion constants in density and order parameter equations and α_2 is in general a function of microscopic parameters of the model but we treat α_2 as constant. Because of Galilean invariance [32] Eqn. 3.10 in general have convective nonlinearities

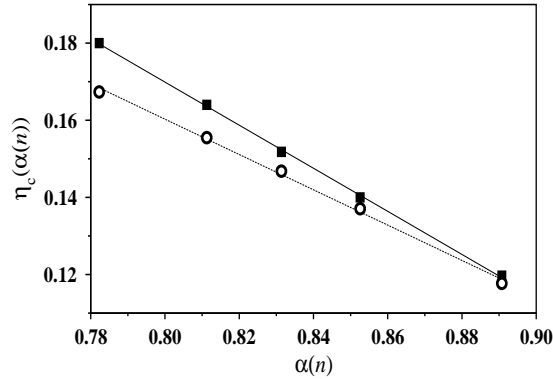


Figure 3.10: Plot of mean field estimate of the critical noise strength $\eta_c(n)$ vs. angle-angle correlation $\alpha(n)$ averaged over all possible interacting pairs. The upper curve (filled squares, solid line) represents the numerical data, whereas, the lower curve (opaque circles, dashed line) represents the analytical result (Eqn. 3.11 in the text).

$\propto \mathbf{PVP}$, but close to order-disorder transition this effect is negligible, hence it has been ignored. The mean field value of critical noise strength η_c is obtained where the coefficient $[\frac{(1-2\eta^2)2}{\sqrt{2(1+\alpha)}} - 1]$ vanishes,

$$\eta_c = \frac{1}{\sqrt{2}} \left[1 - \frac{1}{\sqrt{2}} \sqrt{(1+\alpha)} \right]^{1/2} \quad (3.11)$$

The critical value of noise at which the transition takes place depends very much on the angle-angle correlation $\alpha(n)$ between the agent and its binary pair. More they are correlated, the value of the critical noise strength $\eta_c(n)$ shifts towards the smaller values. In Fig. 3.10 we plot and compare the values of $\eta_c(n)$ obtained analytically as well as numerically for $n = 1$ to 5.

3.5.2 Linear stability of homogeneous polarized state close to order-disorder transition

Steady state solution of homogeneous Eqns. 3.9 and 3.10 are $\rho = \rho_0$ and $\mathbf{P} = P_0 \hat{\mathbf{z}}$. We add small perturbations $\rho = \rho_0 + \delta\rho$ and $\mathbf{P} = (P_0 + \delta P_z) \hat{\mathbf{z}} + \delta P_x \hat{\mathbf{x}}$ and we can write

the linearized equations of motion for small perturbations, $\delta\rho$, δP_x and δP_z

$$\partial_t \delta\rho = -vP_0(\partial_z \delta\rho + \partial_x \delta\rho) - v\rho_0(\partial_z \delta P_z + \partial_x \delta P_x) + D_\rho \nabla^2 \delta\rho \quad (3.12)$$

$$\partial_t \delta P_z = 2P_0^2 \alpha(\eta) \delta P_z - \frac{v}{2\rho_0} \delta_z \delta\rho + D_P \nabla^2 \delta P_z \quad (3.13)$$

$$\partial_t \delta P_x = -\frac{v}{2\rho_0} \delta_x \delta\rho + D_P \nabla^2 \delta P_x \quad (3.14)$$

using Fourier transformation

$$\delta Y(\mathbf{k}, S) = \int d\mathbf{r} \exp(i\mathbf{k} \cdot \mathbf{r}) \exp(St) dt \quad (3.15)$$

we get linear equation in Fourier space.

$$\partial_t \begin{pmatrix} \delta\rho \\ \delta P_z \\ \delta P_x \end{pmatrix} = \mathcal{M} \begin{pmatrix} \delta\rho \\ \delta P_z \\ \delta P_x \end{pmatrix}$$

where matrix \mathcal{M} is given by coefficient of different terms in Eqs. 3.12, 3.13 and 3.14. We can solve above coupled equation for mode S . If the real part of S , $Re[S] > 0$ homogeneous polarized state is unstable and if $Re[S] < 0$, homogeneous polarized state is stable to small perturbation. We can solve for modes analytically for two different directions $\theta = 0$ and $\frac{\pi}{2}$, where θ is the angle between wave vector \mathbf{q} and ordering direction. For $\theta = \frac{\pi}{2}$, S is determined by

$$(S + vP_0 i q + D_\rho q^2)(S + D_P q^2) - \frac{v^2}{2} q^2 = 0 \quad (3.16)$$

and both modes are always stable. For $\theta = 0$

$$(S + vP_0 i q + D_\rho q^2)(S + 2\alpha_1(\eta) + D_P q^2) + \frac{v^2}{2} q^2 = 0 \quad (3.17)$$

Hence

$$2S = -\alpha_1(\eta) - \bar{D}q^2 \pm \frac{\frac{1}{2}v^2q^2(\frac{3}{8}\rho_0^2 + 1)}{2\alpha_1(\eta) + \bar{D}q^2} \quad (3.18)$$

where, $\bar{D} = D_\rho + D_P$, one of the mode can become unstable if

$$\frac{1}{2}v^2q^2(\frac{3}{8}\rho_0^2 + 1) > (\alpha_1(\eta) + \bar{D}q^2)(2\alpha_1(\eta) + \bar{D}q^2) \quad (3.19)$$

as we approach the critical point from the subcritical regime. Very close to critical point, we can write $\eta = \eta_c + \eta - \eta_c = \eta_c + \Delta\eta$, where η_c is the critical value of η at which $\alpha_1(\eta)$ changes sign and $\Delta\eta = \eta - \eta_c$ and since we are approaching critical point from below $\Delta\eta < 0$. Close to critical point we can expand $\alpha_1(\eta)$ about the critical η_c ,

$$\begin{aligned} \alpha_1(\eta) &= \alpha_1(\eta_c) + \alpha'_1(\eta_c)\Delta\eta + \mathcal{O}(\Delta\eta)^2 \\ &= \alpha_1(\eta_c) - \alpha'_1(\eta_c)|\Delta\eta| + \mathcal{O}(\Delta\eta)^2 \end{aligned} \quad (3.20)$$

where $\alpha'_1(\eta_c) = \frac{\partial\alpha_1}{\partial\eta}|_{\eta_c}$. Since $\alpha_1(\eta) = \eta_c^2(1 - \frac{\eta^2}{\eta_c^2})$, hence $\alpha'_1(\eta_c) = -2\eta_c$ and we can write, up to linear order in $\Delta\eta$ as $\eta \rightarrow \eta_c$, as

$$\begin{aligned} \alpha_1(\eta) &= \alpha_1(\eta_c) + 2\eta_c|\Delta\eta| + \mathcal{O}(\Delta\eta)^2 \\ &= |\Delta\eta|((\eta_c + \eta) + 2\eta_c) + \mathcal{O}(\Delta\eta)^2 \\ &= 4|\Delta\eta|\eta_c + \mathcal{O}(\Delta\eta)^2 \end{aligned} \quad (3.21)$$

However, the state is unstable if $Re[S] > 0$ and stable if $Re[S] < 0$. Hence, the condition for instability to leading order in $\Delta\eta$ and for small q limit is,

$$v^2(\frac{3}{8}\rho_0^2 + 1) > 24|\Delta\eta|\eta_c\bar{D} \quad (3.22)$$

As we approach critical point instability is more pronounced and smaller the

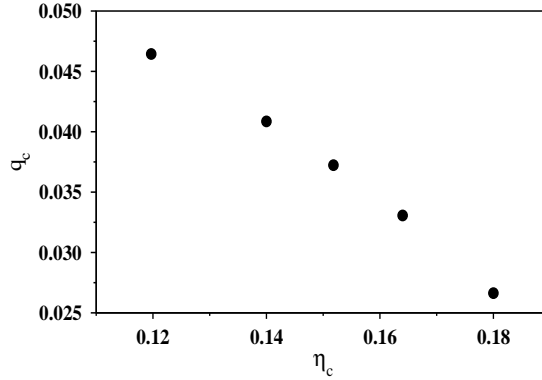


Figure 3.11: Plot of critical wave vector q_c vs. η_c below which instability occur Eq. 3.23 for speed $v = 0.5$ and density $\rho_0 = 0.125$. Critical wave vector decreases with decreasing η_c and hence decreasing n .

value of η_c instability occur at small v value. As shown in Fig. 3.10 and Eqn. 3.11, η_c decreases as we decrease n . Hence for small n instability appears at smaller v as shown in Fig. 3.9. We can also estimate critical wave vector at the onset of instability close to the critical point.

$$\bar{D}^2 q_c^2 = \frac{1}{2} v^2 \left(\frac{3}{8} \rho_0^2 + 1 \right) - 12 \eta_c |\Delta \eta| \bar{D} \quad (3.23)$$

Hence in the subcritical regime, as we approach closer and closer to the critical point $\alpha_1(\eta)$ is small and instability will occur at larger wave vector or smaller length. Also, instability occurs at large q_c for small η_c (Fig. 3.11) and this is in agreement with our numerical simulation where we find formation of bands occurring at larger system size L as we go from the first ($n = 1$) neighbor to the second ($n = 2$) neighbor.

3.6 Summary

We have studied the collective behavior of a binary flock using Vicsek dynamics. In this flock, the velocity of an agent depends on the velocities of its n -th topological neighbor and its own. The velocity field of all agents is updated

synchronously maintaining the periodic boundary condition on a collection of agents confined within a two-dimensional square space. Extensive numerical simulations reveal that for all values of n , an order to disorder phase transition takes place at certain critical threshold η_c of the noise parameter. In particular, for $n = 1$, it is a different kind of discontinuous transition: The long time stationary state of the system is either in the ordered phase or in the disordered phase. At a certain η_c for $n = 1$ it switches over from one phase to the other. The case of $n = 2$ exhibits ordinary discontinuous transition where, around the critical point, the system flip flops between the two metastable states corresponding to the ordered and disordered phases. The probability distribution of the order parameter has been observed to be characterized by double humped function, whereas the fourth order Binder cumulant exhibits a negative dip at the critical noise strength. For $n \geq 3$ the system exhibits continuous transitions, signatures of which are evident in the continuous variation of their order parameters against noise strengths, continuous variation of their Binder cumulants and singly peaked distributions of their order parameters.

Persistence time is the duration of the time interval through which an agent has a specific topological neighbor. The probability distribution of persistence times has been found to follow nice power law decaying functions and independent of the value of the topological neighbor n . Further, we have studied the information spreading dynamics in the binary flocks. How long it takes on the average to spread an information localized at a certain agent to spread to all agents of the system? It has been seen that the mean value of this time decays like a power law as the noise level increases from zero.

Finally, this system of binary flocks has been studied again using the hydrodynamic equations of motion. Linear stability analysis of the homogeneous polarized state close to the order-disorder transition has been done. The average correlation between a pair of agents, who are the topological neighbors, has been

calculated. Using the value of this quantity, the critical noise strength has been estimated, and the correspondence has been found to be good.

4 Band structure in collective motion with quenched range of interaction

4.1 Introduction

As described in the earlier chapters, among many systems that exhibits non-equilibrium phase transitions under driven noise, the phenomenon of Collective Behavior is a familiar example [15, 16, 18–22]. With many prototypical examples of collective motion in nature, such as bacterial colonies [111], insect swarms [112], bird flocks [113], fish schools [114], etc., it has been observed that even a simplified description provides a good starting point for an overall understanding of the collective motion.

With a good portion of studies following the seminal work by Vicsek et. al. [16] and a number of experimental, theoretical and numerical studies been done [32–38, 115], the common prescription in all these models is, agents move with their individual interaction zones. More specifically, an interaction zone is the area within a circle of radius R drawn around each individual agent which is refreshed at each instant of time. An agent interacts with all neighbors within this zone including itself.

In contrast, here in this chapter [46], we present a modified version of the Vicsek model where the zones of interaction are quenched in space. An underlying fixed two-dimensional $L \times L$ lattice, which divides the entire space into L^2 square boxes, constitutes the interaction zones for the study. A moving agent passes through a series of interaction zones.

At a certain instant, an agent interacts with all agents within the interaction zone it is presently residing, and similarly, all agents within this zone interact among themselves. A common direction of motion is determined by these mutual interactions and is assigned to all agents of this zone. At this point, the noise appears into the picture and plays its role. The direction of motion of each individual agent is then updated independently by applying the random scalar noise. The detailed algorithm is as follows.

4.2 Model

A collection of N agents are released within a square box of size $L \times L$ on the $x - y$ plane at the positions $(x_i, y_i), i = 1, \dots, N$. The value of each coordinate is an independent and identically distributed random number between 0 and L . The density $\rho = N/L^2$ of agents has been maintained to be unity in all calculations in this paper. All agents have the same speed $v_0 = 1/2$ always and the orientation angles θ_i of their velocity vectors have been assigned random values between 0 and 2π drawing them from a uniform probability distribution. A configuration of agents prepared in this way, constitute the initial state. The dynamical state of the flock of agents is then evolved using a discrete time synchronous updating rule under periodic boundary condition, the time t being the number of updates per agent.

At any arbitrary time t an agent i interacts with all $n_{\mathcal{R}}(t)$ agents (including itself) within a neighborhood \mathcal{R} around it. Unlike the Vicsek model here the neighborhoods are quenched, i.e., they are fixed in space. We define these neighborhoods as the primitive cells of an underlying imaginary square lattice of size $L \times L$. More specifically, a typical neighborhood \mathcal{R} is the primitive cell whose vertices are located at the coordinates $(x, y), (x + 1, y), (x + 1, y + 1)$, and $(x, y + 1)$ where both x and y are the integer numbers. All $n_{\mathcal{R}}(t)$ agents within a particular cell belong to the same neighborhood and are neighbors of one another.

Under the time evolution the system passes through a series of microstates defined by the specific positions and the directions of motion of the N agents. Let $\mathbf{v}_i(t)$ denote the velocity vector of the i -th agent at time t which has the orientational angle $\theta_i(t)$. The orientational angles $\theta_i(t + 1)$ at the next time step are then estimated for all neighborhoods $\{\mathcal{R}\}$ in a synchronous manner. All agents $n_{\mathcal{R}}(t)$ within a neighborhood mutually interact among themselves. The resultant of the velocity vectors of these agents is determined and its orientational angle $\theta_i(t + 1)$

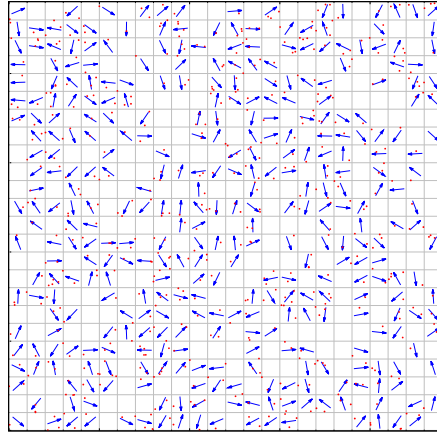


Figure 4.1: A snapshot of the collection of agents at an arbitrary instant of time has been shown, marking them by the red dots, in a two-dimensional system of size $L = 24$ using the periodic boundary condition. The underlying space has been discretized into small neighborhoods by the primitive cells of an $L \times L$ square lattice. For each cell, the direction of the resultant of the velocity vectors of all agents has been shown by a blue arrow.

is assigned to the directions of velocities of all agents (Fig. 4.1) as,

$$\theta_i(t+1) = \tan^{-1} \left[\frac{\sum_{j \in \mathcal{R}} \sin \theta_j(t)}{\sum_{j \in \mathcal{R}} \cos \theta_j(t)} \right], \quad (4.1)$$

where the summation runs over all $n_{\mathcal{R}}(t)$ agents within \mathcal{R} . Therefore, before the noise is switched on, all agents of a neighborhood \mathcal{R} have the same velocity direction which is different in different neighborhoods. This should be compared with the original version of the Vicsek model where even before the application of noise, different agents may have different directions of motion since individual agents have distinctly different neighborhoods in general. This is the main difference between our quenched neighborhood version of the Vicsek model and its original version. This modification has the numerical advantage since before the application of noise, the common direction of motion of all agents within \mathcal{R} is determined only once, which results in the faster execution of the code.

However, on the introduction of scalar noise, the orientational angles become

disordered. Along with the noise the Eqn. 4.1. is modified as:

$$\theta_i(t+1) = \tan^{-1} \left[\frac{\sum_{j \in \mathcal{R}} \sin \theta_j(t)}{\sum_{j \in \mathcal{R}} \cos \theta_j(t)} \right] + \zeta(\eta). \quad (4.2)$$

The noise term $\zeta(\eta)$ quantifies the amount of error that is added to the orientational angle of each agent participating in an interaction. Here η measures the strength of the noise and $\zeta(\eta)$ represents a random angle for each agent drawn from a uniform distribution within $[-\eta/2, \eta/2]$. Each agent is then displaced along its direction of motion $\theta_i(t+1)$. In general, at every time instant, some agents leave a particular neighborhood \mathcal{R} and move to their adjacent neighborhoods. Similarly, another set of agents moves into \mathcal{R} from its adjacent neighborhoods.

The instantaneous global order parameter $\Omega(t, \eta, L)$ is defined for the entire system as the magnitude of the velocity vector of an agent, averaged over all agents and scaled by the speed v_0 .

$$\Omega(t, \eta, L) = \frac{1}{N v_0} \left| \sum_{j \in N} \mathbf{v}_j(t) \right|. \quad (4.3)$$

In the stationary state $\Omega(t, \eta, L)$ is estimated over a long duration of time and is averaged to find $\Omega(\eta, L)$.

4.3 Description of the dynamical evolution

A computer code for the animation of the dynamical evolution of this system starting from the random initial state has been written and is run over long durations for different values of noise strengths. Let us analyze the time evolution of the system for $\eta < \eta_c$. In particular, let us first consider the updating process of the directions of motion of the agents in two adjacent cells at locations (x, y) and $(x+1, y)$. Let the angles $\theta_i(t+1)$ for these cells before the application of the noise is

approximately equal to $\pi/2$. Then after the application of noise and after moving one step, these two cells would exchange some agents. Since their directions are nearly the same, most of the agents of two adjacent cells would move to two new cells at $(x, y+1)$ and $(x+1, y+1)$ which are also adjacent cells. Thus we refer agents in two adjacent cells of nearly parallel directions of motion tend to stick together maintaining their adjacency as the ‘cohesiveness property’ of similarly moving agents in adjacent cells. This cohesiveness is inbuilt in the dynamical rules of the collective motion. Because of this cohesiveness, large clusters of agents gradually form as time passes. They move as a whole and are extended spatially across the direction of motion. Evidently, the most stable conformation of such a cluster appears when two wings of it join together after wrapping the system because of the periodic boundary condition, which then is called the ‘band’.

In the absence of noise, the agents move in the stationary state completely coherently in a ballistic fashion and $\Omega(0, L) = 1$. When the noise is switched on, and its strength η is tuned to a small value, the motion of the individual agents in the stationary state is predominantly directed leading to a high value of the order parameter. In other words, it means that on the average the entire system of N agents moves along a globally fixed direction, but the instantaneous velocity directions of individual agents do fluctuate randomly with a small spread about this global direction. On the other hand, when η is tuned for the large values, individual agent’s motion is grossly diffusive, and this leads to nearly vanishing values of the order parameter. The minimum value of noise parameter $\eta = \eta_c$ where the order parameter vanishes for infinitely large system sizes, is called the critical point of the order-disorder phase transition that takes place in this system of collective motion under the application of noise.

How the system becomes increasingly ordered as the strength of the applied noise is systematically reduced? To understand it we need to follow the formation of bands. When η is tuned to $\eta_c(L)$, a band of agents of high density appears in the

system for the first time. Within a band, the motions of the agents are directed. Such a band has the shape of a thin and straight strip which moves as a whole along a specific direction perpendicular to the length of the band. Because of the imposed periodic boundary condition, the band takes the shape of a closed ring. Consequently, the magnitude of the order parameter jumps discontinuously to a non-zero value when a band appears in the system. In general, for $\eta < \eta_c$ the bands can be oriented along different directions, e.g., parallel to the sides, along the diagonal directions, or even along some other directions. The shapes of the bands become increasingly non-trivial as the system size becomes larger. For such large system sizes, multiple bands can also be simultaneously present.

A band consists of a set of directionally biased agents moving along almost (apart from noise) in the same direction. The entire band moves in a sea of randomly diffusing agents. Thus, the whole $L \times L$ area is divided into two zones: the band, comprised of the directed agents and the diffusive zone, comprising of the rest of the diffusive agents. At every instant the band does two activities simultaneously: (i) It absorbs fresh agents into it at its front edge picking them from the diffusive zone, which executes a directed motion inside the band, and (ii) simultaneously it pushes the directed agents at the back edge of the band into the diffusive zone. The rates of these two processes are equal, and in that way, the width and shape of the band are maintained in the stationary state. The front edge of the band is sharp where as the back edge is hazy. Therefore, when there is only one band present in the system, an arbitrarily tagged agent has two types of motion: for a certain amount of time it executes a diffusive motion, and then it is swallowed by the band at the front edge. It then moves with the band for a little while as a directed agent, and then again dropped out in the diffusive region from the back edge. In the stationary state, this type of motion is repeated ad infinitum for all agents.

In the following, we report the results of our numerical study on three different

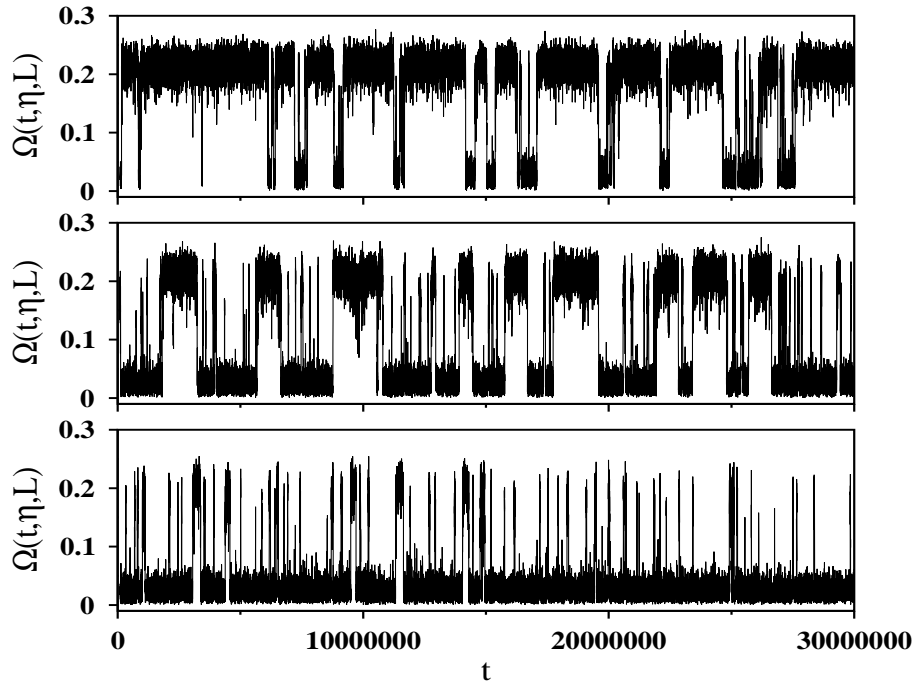


Figure 4.2: $L = 128$: Variation of the instantaneous order parameter $\Omega(t, \eta, L)$ has been shown against time t for the values of the noise strength $\eta = 2.262, 2.266$ and 2.270 (from top to bottom). These η values are very close to $\eta_c = 2.266$. Here the system is seen to flip-flop between the ordered and disordered states corresponding to non-zero and almost zero values of Ω . These states are characterized by the presence and absence of high density correlated bands.

system sizes, namely $L = 128, 256$ and 512 . We have observed how the discontinuous transition becomes more vivid and the band structure become increasingly rich as the system size is systematically enlarged.

4.4 Results

4.4.1 System size $L = 128$

We first exhibit the variation of the instantaneous order parameter $\Omega(t, \eta, L)$ against time t in Fig. 4.2. Three figures corresponding to three closely separated values of the noise parameter $\eta = 2.262, 2.266$ and 2.270 have been shown in the top, middle and bottom panels. The same random initial state has been used in all

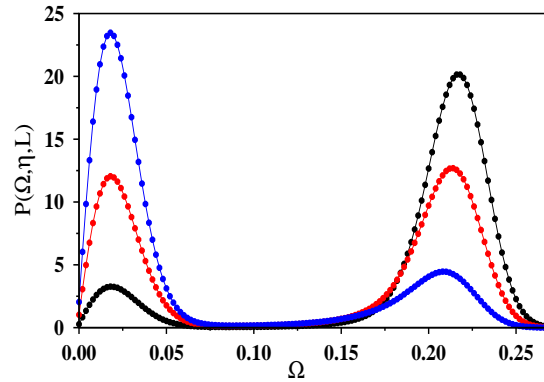


Figure 4.3: $L = 128$: Probability distribution $P(\Omega, \eta, L)$ of the instantaneous order parameter in the stationary state against the order parameter Ω . The three curves (from the right to the left) correspond to $\eta = 2.2610$ (black), 2.2645 (red), and 2.2680 (blue). Each curve has two peaks, one at a large Ω (ordered state) and the other at a small value of Ω (disordered state).

three cases. In each case, the data has been plotted at the interval of every 1000 time steps and the time series has been shown for 30 million time steps. It is apparent from the plot that the system evolves through two possible metastable states, an ordered state with a high value of Ω and a disordered state with a very small value of Ω . The system flip-flops between these two states. It can also be observed that the system spends more time in the ordered state with smaller noise at $\eta = 2.262$. On the other hand, the typical residence time in the disordered state is longer with a larger value of $\eta = 2.270$. However, in between at $\eta = 2.266$, the system resides in both states almost equally frequently. Therefore, we approximately estimate $\eta_c = 2.266$ as the critical noise parameter of the system for $L = 128$.

To quantify the metastable states, we have estimated the probability distribution of the order parameter $P(\Omega, \eta, L)$ (Fig. 4.3). It has been found that for all three noise levels, the probability distribution has double peaks at two distinct values of Ω . These humps correspond to the ordered and disordered states. For small $\eta = 2.2610$, the peak in the ordered state is taller than its peak in the disordered state. On the other hand, for large $\eta = 2.2680$, it is the opposite, i.e., the

peak in the disordered state is taller than its peak in the ordered state. For the third plot with $\eta = 2.2645$ both peaks are of same heights approximately.

In Fig. 4.4 snapshots of fifteen agent configurations have been shown, and the characterization of each figure has been done in Table 1. The presence of bands has been searched for in the stationary states of the system. We started from a high value of η and reduced its value systematically in small intervals. The first high density stable band is observed for $\eta = 2.262$. The flip-flop dynamics of the system exhibited in Fig. 4.2 implies the appearance and disappearance of such bands with time. The orientation of the band is measured by the angle ϕ between the direction of motion of the band and the positive x direction. All bands always move along the normal to the front edge of the band. Therefore, for the first few snapshots of Fig. 4.4, the angle ϕ has the values $\pi, 5\pi/4, 3\pi/2, 3\pi/2, 7\pi/4, \dots$ etc. The first diagonal band appeared at $\eta = 2.140$. The first parallel double bands appeared at $\eta = 1.850$. The next non-trivial band appeared at $\eta = 1.600$ with $\phi = 3\pi/2 - \arctan(1/2)$.

The bands are stable and with the periodic boundary condition imposed, they wrap the system different number of times in different snapshots. For example, if the orientation of the band is neither horizontal nor vertical, it must be oriented at an angle ϕ such that it wraps the system. We characterize such a wrapped band by an integer pair $W(m, n)$ such that the numbers of its intersection are m and n with the x and y axes respectively and ϕ differs from $\arctan(m/n)$ either by $\pm\pi/2$ or by $\pm\pi$. For example, $W(1, 0)$ and $W(0, 1)$ are the vertical and horizontal bands respectively. A single diagonal band is denoted by $W(1, 1)$.

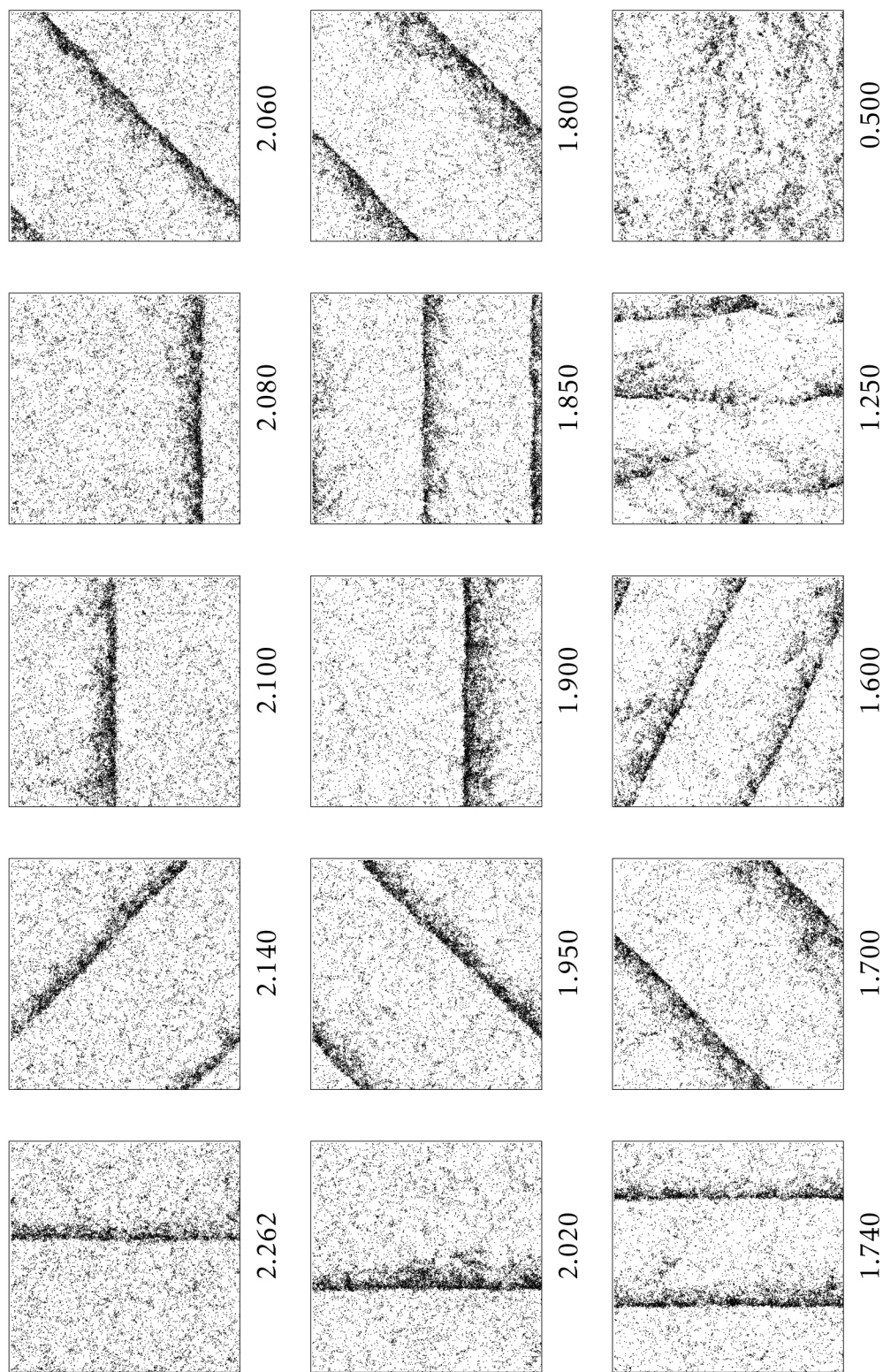


Figure 4.4: $L = 128$: Band structures have been shown for fifteen different stationary states evolved from the same initial state but subjected to noise strength η of different magnitudes mentioned under the figure. Brief description of the individual bands are given in Table I.

η	ϕ	Ω	Wrapping	Description
2.262	π	0.173	W(1,0)	Single vertical band.
2.140	$5\pi/4$	0.303	W(1,1)	Single diagonal band.
2.100	$3\pi/2$	0.329	W(0,1)	Single horizontal band.
2.080	$3\pi/2$	0.342	W(0,1)	Single horizontal band.
2.060	$7\pi/4$	0.382	W(1,1)	Single diagonal band.
2.020	π	0.379	W(1,0)	Single vertical band.
1.950	$3\pi/4$	0.443	W(1,1)	Single diagonal band.
1.900	$\pi/2$	0.450	W(0,1)	Single horizontal band.
1.850	$\pi/2$	0.505	2W(0,1)	Two parallel horizontal bands.
1.800	$7\pi/4$	0.520	W(1,1)	Single diagonal band.
1.740	π	0.562	2W(1,0)	Two vertical bands.
1.700	$7\pi/4$	0.568	W(1,1)	Single diagonal band.
1.600	$3\pi/2 - \arctan(1/2)$	0.617	W(1,2)	Single multiply wrapped band.
1.250		0.761		Parallel bands become blurred.
0.500		0.949		Bands are absent.

Table 4.1: $L = 128$: Brief descriptions of different types of bands.

A set of k parallel $W(m, n)$ bands are denoted by $kW(m, n)$.

Therefore, it is apparent that as η decreases the agents become more strongly correlated. Such stronger correlation appears in longer lengths as well as wider widths of the bands. Long band lengths are accommodated by increasing the number of bands, selecting the non-trivial orientation of the bands, or by increasing the wrapping numbers. When η is tuned down to ≈ 1.250 , the distinct structure of bands start vanishing, i.e., the dismantling process of the bands starts. Evidently, no distinct band was observed when η was set to even smaller values.

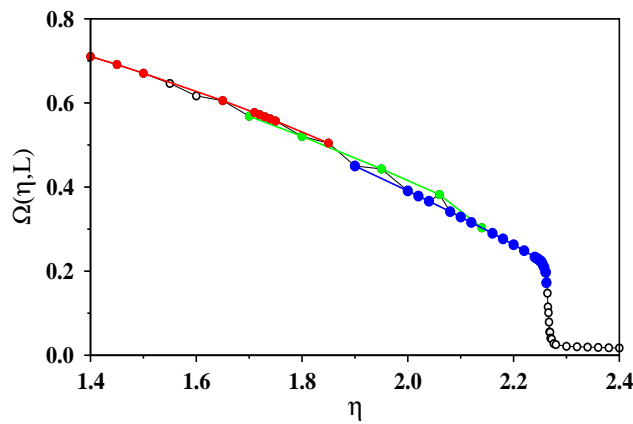


Figure 4.5: $L = 128$: The average value of the order parameter $\Omega(\eta, L)$ in the stationary state has been plotted against the noise strength η using black opaque circles. At the critical noise $\eta_c(L) = 2.2645$ there is a sharp rise in the order parameter. In the sub-critical regime three distinct data sets are identified which correspond to three different shaped bands and are plotted with circles filled with different colors: $W(1, 0)$ and $W(0, 1)$ (blue); $2W(1, 0)$ and $2W(0, 1)$ (red); $W(1, 1)$ (green). In each set the $\Omega(\eta, L)$ increases almost linearly on decreasing η .

The variation of the order parameter $\Omega(\eta, L)$ for $L = 128$ against the noise strength η has been shown in Fig. 4.5. For $\eta < \eta_c(L)$ the order parameter $\Omega(\eta, L)$ increases almost linearly on reducing η . It is clear that the entire plot is the combination of a different subset of points corresponding to different shaped bands. In Fig. 4.5 we have marked three sets of colored circles that represent the data for three types of bands. For $\eta > \eta_c(L)$ the $\Omega(\eta, L)$ assumes a nearly constant value close to zero on increasing η .

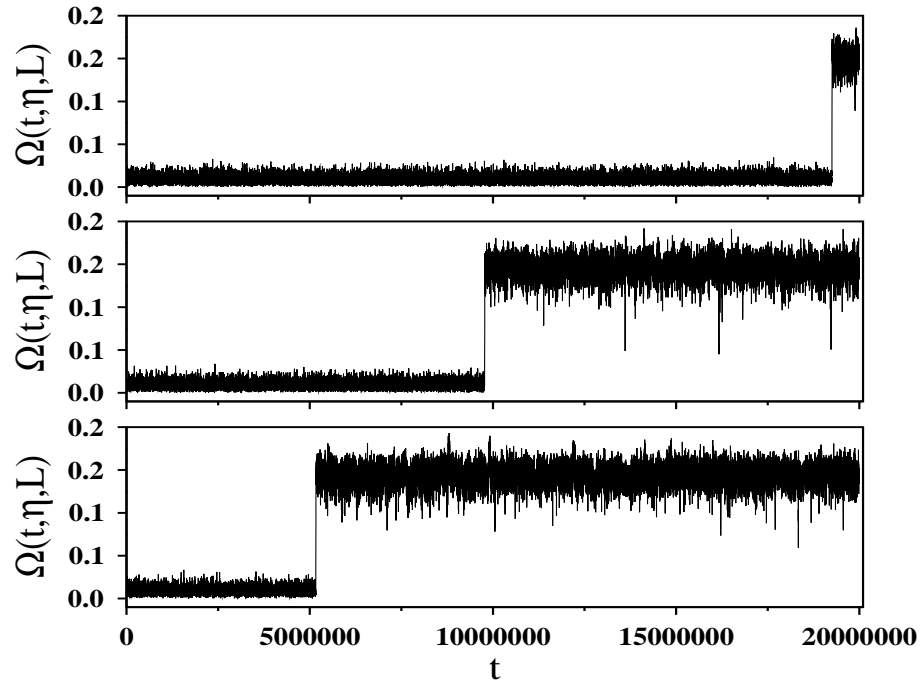


Figure 4.6: $L = 256$: Plot of the instantaneous order parameter $\Omega(t, \eta, L)$ against time as in Fig. 4.2 for $\eta = 2.346, 2.348$ and 2.350 (from top to bottom). Here the system is not seen to flip-flop between two metastable states. Since the system evolves from a randomly selected state, initially the system is in a disordered state without any band having a nearly vanishing value of Ω , but then it suddenly jumps to an ordered state on the appearance of a correlated band.

4.4.2 System size $L = 256$

Here also the dynamics start from the same completely random initial state for all values of the noise strength parameter η , and therefore the motion of the agents are predominantly diffusive at the early stage. As time is elapsed, the system gets time to organize itself. Typically, after a substantial amount of relaxation time, bands are formed here as well. In contrast to the situation in $L = 128$ system, here the system does not flip-flop between two metastable states. Consequently, the magnitude of the order parameter jumps up only for once from a nearly vanishing value to a finite magnitude. Three such jumps have been shown in Fig. 4.6 where the time series for the order parameter has been plotted against time for the 20 million time steps. For the noise level of $\eta = 2.346, 2.348$, and 2.350 the

transitions take place at times $\approx 18, 9$ and 5 million respectively.

Similar to the case of $L = 128$, fifteen snapshots of the agent configurations have been shown in Fig. 4.7. These snapshots are taken at long times after the jumps to the ordered states have taken place. Here a number of bands of different orientations and wrappings have been observed. Compared to $L = 128$ we find here a new type of stationary state where two different sets of bands cross one another. For example, in case of $\eta = 1.800$, we have exhibited a snapshot where a single horizontal band $W(0,1)$ with $\phi = \pi/2$ crosses a single diagonal band $W(1,1)$ with $\phi = \pi/4$. Both bands are stable and move along two different directions, separated by $\pi/4$. In general, for such crossed bands, the order parameter takes slightly smaller values.

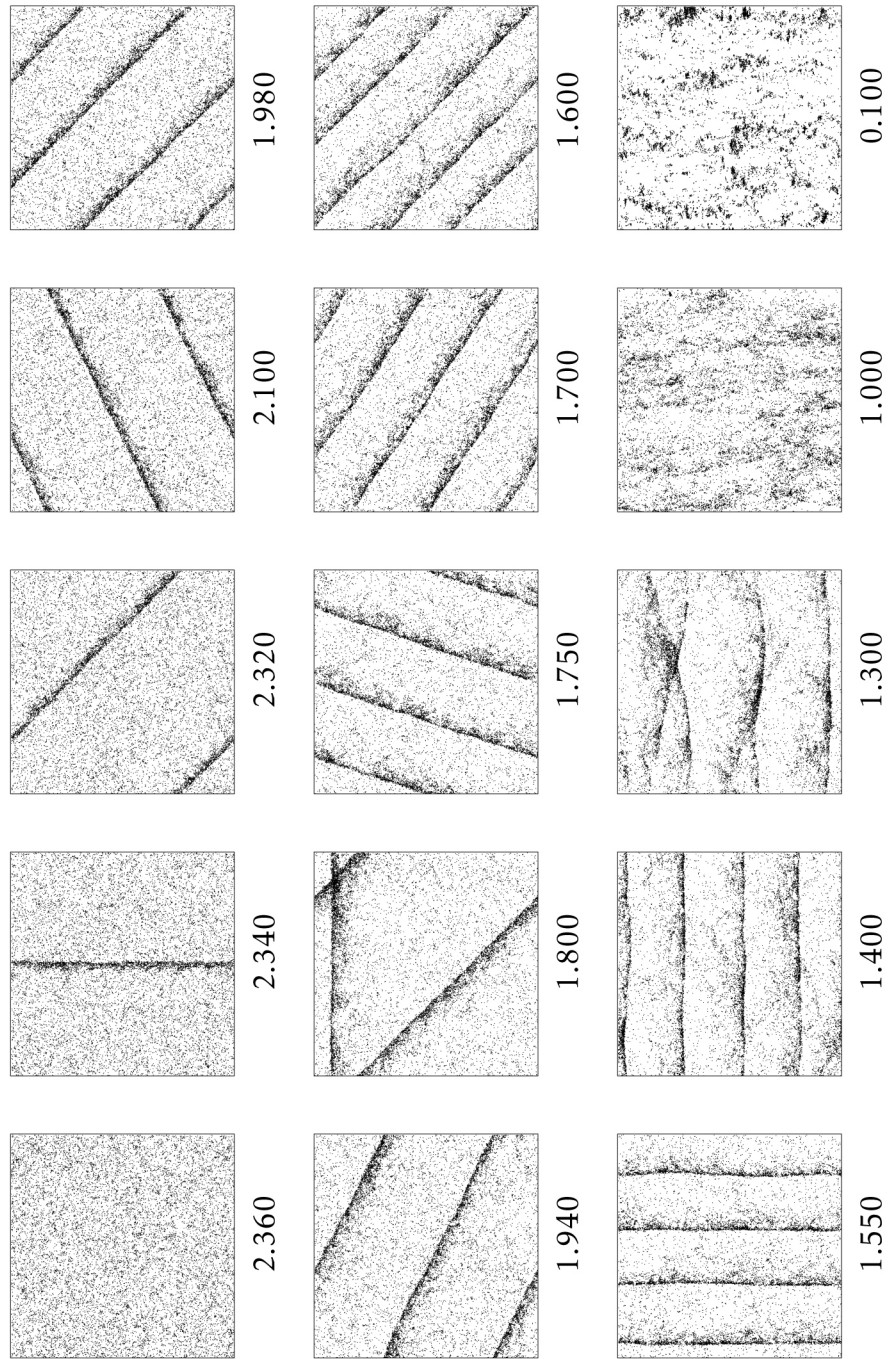


Figure 4.7: $L = 256$: Band structures in fifteen different stationary states evolved from the same initial positions and velocities but subjected to noise η of different strengths have been exhibited using 16384 randomly selected agents. The description of the individual bands are given in Table II.

η	ϕ	Ω	Wrapping	Description
2.360		0.009		Disordered state without band.
2.340	0	0.149	$W(1, 0)$	Single vertical band.
2.320	$5\pi/4$	0.189	$W(1, 1)$	Single diagonal band.
2.100	$\pi/2 + \tan^{-1}(1/2)$	0.345	$W(1, 2)$	Single multiply wrapped band.
1.980	$5\pi/4$	0.429	$2W(1, 1)$	Two parallel diagonal bands.
1.940	$\pi/2 - \tan^{-1}(1/2)$	0.437	$W(1, 2)$	Single multiply wrapped band.
1.800	$\pi/2, \pi/4$	0.488	$W(0, 1), W(1, 1)$	Crossing: A diagonal and a horizontal band.
1.750	$\pi - \tan^{-1}(3)$	0.549	$W(3, 1)$	Single multiply wrapped band.
1.700	$3\pi/2 - \tan^{-1}(2/3)$	0.577	$W(2, 3)$	Single band, wrapped four times.
1.600	$5\pi/4$	0.620	$3W(1, 1)$	Three parallel diagonal bands.
1.550	π	0.647	$4W(1, 0)$	Four parallel vertical bands.
1.400	$3\pi/2$	0.710	$4W(0, 1)$	Four parallel horizontal bands.
1.300		0.739		Some distorted and hazy bands.
1.000		0.838		Ordered state without band.
0.100		0.997		Ordered state without band.

Table 4.2: $L = 256$: Brief descriptions of different types of bands.

In Fig. 4.8 the time averaged value of the order parameter $\Omega(\eta, L)$ has been plotted against η . The sharp fall in the order parameter takes place at $\eta_c(L) \approx 2.350$. Beyond this value of $\eta > \eta_c(L)$, order parameter is nearly zero. For $\eta < \eta_c(L)$ four sets of data points are plotted which correspond to four different band structures as explained in the figure caption.

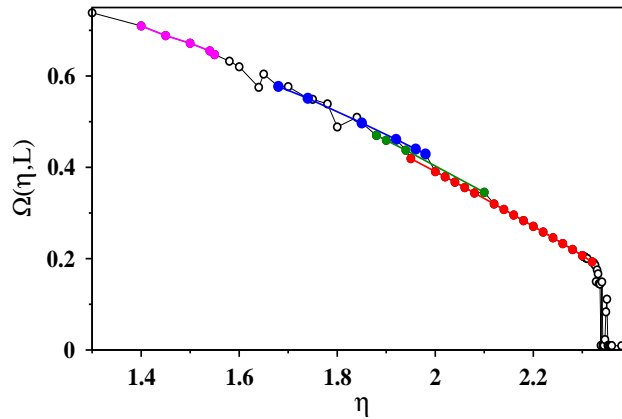


Figure 4.8: $L = 256$: The average value of the order parameter $\Omega(\eta, L)$ in the stationary state has been plotted against the noise strength η using black opaque circles. At the critical noise $\eta_c(L) = 2.350$ there is a sharp rise in the order parameter similar to a discontinuous transition. In the subcritical regime four different data sets are identified with four distinctly different shaped bands and are represented by filled circles of different colors: $W(1,1)$ (red); $2W(1,1)$ (blue); $4W(1,0)$ and $4W(0,1)$ (magenta) and $W(1,2)$ and $W(2,1)$ (green). In each set the $\Omega(\eta, L)$ increases almost linearly on decreasing η .

4.4.3 System size $L = 512$

The bands become most clearly visible for the system size $L = 512$. Because of the choice of random orientation angles of the velocity vectors, the initial state is disordered with a vanishingly small value of the order parameter. Beyond the critical noise value, $\eta_c = 2.368$ the order parameter in the stationary state assumes a very small value. However, when the noise is reduced, $\Omega(\eta_c, L)$ jumps discontinuously at η_c to a finite value. In Fig. 4.9 the instantaneous value of the order parameter $\Omega(t, \eta, L)$ has been plotted against time for long durations. For

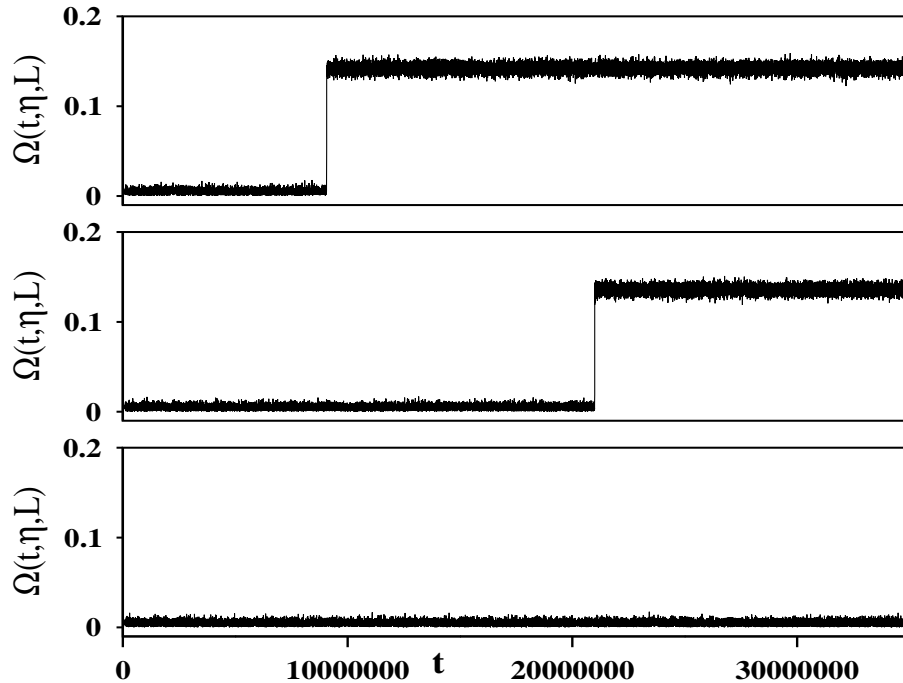


Figure 4.9: $L = 512$: Variation of the instantaneous order parameter $\Omega(t, \eta, L)$ has been shown against time t and for $\eta = 2.350, 2.360,$ and 2.370 (from top to bottom). As η approaches η_c , increasingly longer time is required for switching over from the disordered to the ordered state.

$\eta = 2.350$ and 2.360 discontinuous jumps to the ordered state are observed after approximately 9 and 21 million time steps. In the bottom curve, $\eta = 2.370$ has been used, and no such jump has been observed within the entire duration of observation of 35 million time steps.

Therefore in general, the long time stationary states of all states for $\eta < \eta_c(L) = 2.368$ have been observed to be characterized by the presence of bands of high density directed agents. As the value of the noise strength η is systematically decreased different types of bands appear in the stationary states. In Fig. 4.10 we have exhibited twenty snapshots of agent locations in these stationary states of $L = 512$. We have observed single and multiple bands, diagonal and non-diagonally oriented bands, crossed bands meeting perpendicular to one another or at an angle, and also bands which wrap the system multiple times. For $0 < \eta < 1$ the clearly visible band structure has been missing till our time of observation of 50

million time steps. In Table III we describe the band structures of these twenty stationary states. The value of η has been mentioned below every plot.

In Fig. 4.11 we have plotted $\Omega(\eta, L)$ against η . Here also, in the ordered state the points for different types of bands form different groups. Within one group the band pattern is the same for all values of η but the value of $\Omega(\eta, L)$ increases linearly with decreasing η . Six such group of points have been shown in Fig. 4.11 and the corresponding wrapping numbers have been mentioned in the caption.

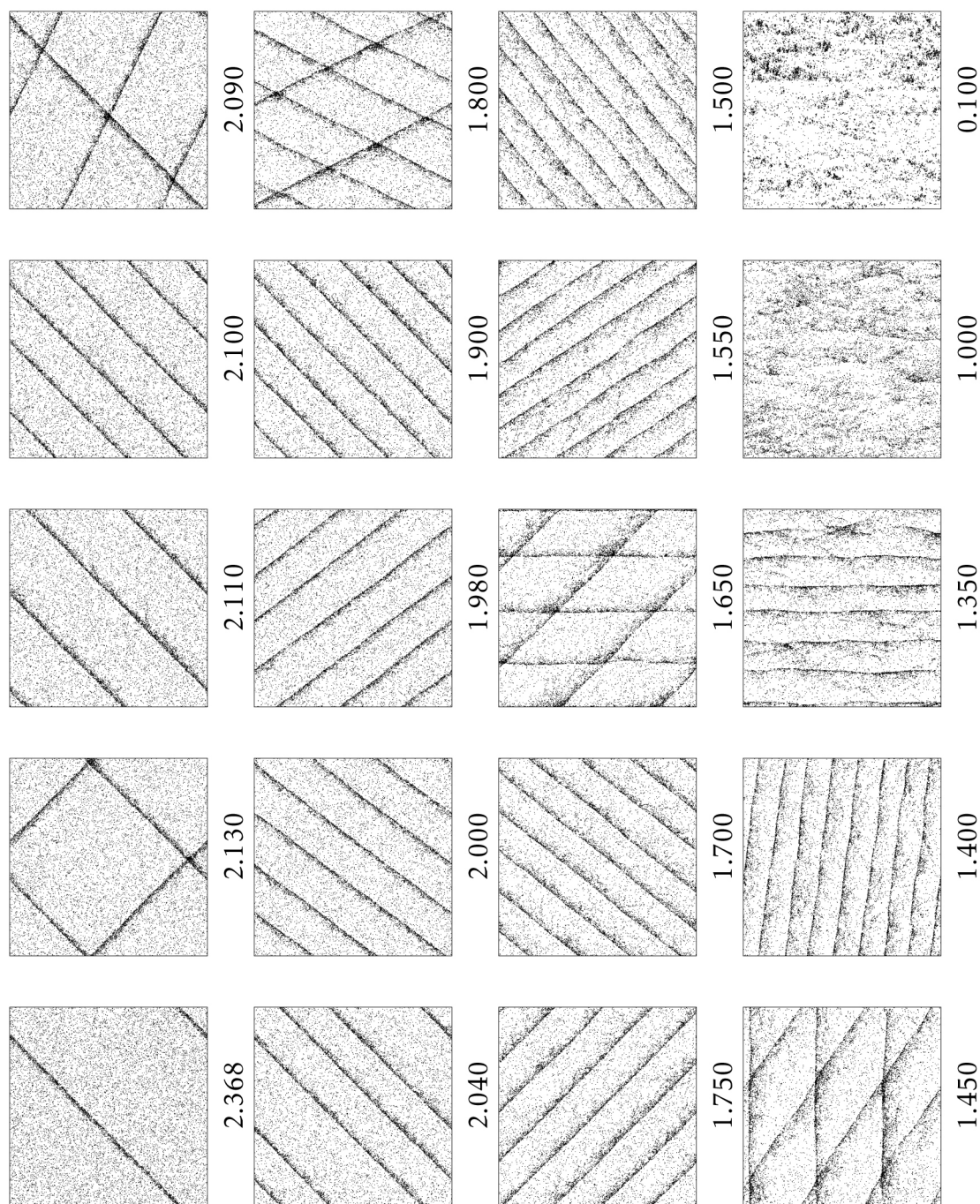


Figure 4.10: $L = 512$: Band structures in twenty different stationary states evolved from the same initial positions and velocities but subjected to noise η of different strengths have been exhibited using 16384 randomly selected agents. The description of the individual bands are given in Table III.

η	ϕ	Ω	Wrapping	Description
2.368	$7\pi/4$	0.115	W(1,1)	Single diagonal band.
2.130	$\pi/4, 3\pi/4$	0.227	W(1,1), W(1,1)	Crossing of two diagonal bands at right angle.
2.110	$3\pi/4$	0.326	2W(1,1)	Two parallel diagonal bands.
2.100	$\pi/4$	0.350	3W(1,1)	Three parallel diagonal bands.
2.090	$7\pi/4, 3\pi/2 - \arctan(1/2)$	0.288	W(1,1), W(1,2)	Crossing of two sets of bands.
2.040	$3\pi/4$	0.384	3W(1,1)	Three parallel diagonal bands.
2.000	$3\pi/2 + \arctan(4/3)$	0.413	W(4,3)	A single multiply wrapping band.
1.980	$\pi/2 - \arctan(4/3)$	0.424	W(4,3)	A single multiply wrapping band.
1.900	$3\pi/4$	0.472	4W(1,1)	Four parallel diagonal bands.
1.800	$\pi/2 - \arctan(2), 3\pi/2 + \arctan(2)$	0.489	W(2,1), 2W(2,1)	Crossing of two sets of bands.
1.750	$5\pi/4$	0.546	4W(1,1)	Four parallel diagonal bands.
1.700	$\pi - \arctan(5/4)$	0.574	W(5,4)	A single multiply wrapping band.
1.650	$\pi, 5\pi/4$	0.570	4W(1,0), 2W(1,1)	Crossing of two sets of bands.
1.550	$\pi/2 - \arctan(6/4)$	0.642	2W(3,2)	Two parallel multiply wrapped bands.
1.500	$3\pi/2 + \arctan(5/6)$	0.663	W(5,6)	A single band that wraps multiple times.
1.450	$\pi/2, \pi/2 - \arctan(3/2)$	0.670	3W(0,1), W(2,3)	Crossing of two sets of bands.
1.400	$\pi/2 - \arctan(1/8)$	0.709	W(1,8)	Single multiply wrapped band.
1.350		0.724	7W(1,0)	Seven parallel vertical bands.
1.000		0.838		No band structure is found.
0.100		0.996		No band structure is found.

Table 4.3: $L = 512$: Brief description of different types of bands.

4.5 Summary

To summarize, we have studied the Vicsek model [16] of collective motion with quenched range of interaction. For studying the two-dimensional version of the model with scalar noise, the underlying plane has been divided into non-overlapping square shaped neighborhoods. All agents residing within a certain square cell at a certain time are mutual neighbors of one another. The direction of the resultant of their velocity vectors is assigned to all agents which are then topped up by applying random noise. In a microscopic description of the model it has been argued that the agents in two adjacent cells, having similar velocity directions, feel certain cohesiveness and therefore continue their motion in the adjacent cells. This cohesiveness property of moving together in the same direction is the original cause for the formation of band structures in the models of collective motion in the framework of the Vicsek model. Within a band, the agents are correlated. As the noise decreases the sub-critical regime, the correlation becomes stronger. Consequently, the system becomes more ordered which is reflected in the non-trivial shaped bands of longer lengths, larger widths, different orientations and wrapping numbers. We have formulated a detailed prescription for the characterization of such bands. Starting from the completely disordered regime, as the strength of the noise is tuned down systematically, the most simple band parallel to the edges pops up abruptly, indicating a discontinuous transition similar to the Vicsek model.

By introducing the quenched range of interaction we have reduced, the individual freedom of the agents. In a way, this can be looked upon as feeding more correlation among the agents. It seems likely, that because of this extra correlation many different shaped bands show up in our model, even for the system size $L = 512$. The appearance of similar bands may be plausible even in the original Vicsek model for the larger system sizes and with smaller noise.

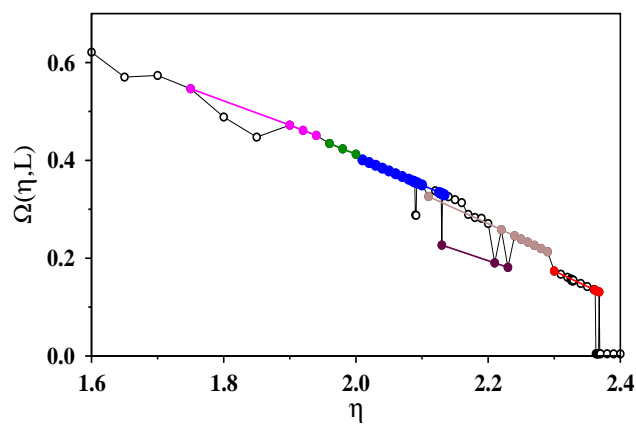


Figure 4.11: $L = 512$: The stationary state order parameter $\Omega(\eta, L)$ has been plotted against the noise strength η . The critical value $\eta_c(L)$ of transition has been found to 2.368. In the sub-critical regime six distinct subsets of data points have been identified for six differently shaped bands. They are grouped together and labeled by their wrapping numbers: $W(1,1)$ (red); $2W(1,1)$ (brown); $3W(1,1)$ (blue); $4W(1,1)$ (magenta); $W(4,3), W(3,4)$ (green) and $W(1,1), W(1,1)$ bands are presented by maroon color.

5 Information sharing and sorting in a community

5.1 Introduction

As we grow up, we learn that objects we observe around us, have their own names by which we identify these objects successfully and are often known locally by the same name. There are many names of any object with each name belonging to a specific group of the community. Socio cultural diversity and lack of communicative origins have often been the reason behind many such nomenclatures of objects present all around. However with time, i.e. with increasing communication and interaction, out of many locally famous names, few become more known among people around the world. There might be many social, economic, political, educational reasons behind, but the development of such a consensus among people of a large community, with each agent often locally interacting with very few other agents, has been a matter of interest to researchers. There have been many models, describing the phenomena of consensus reaching among locally interacting agents in a community, often described as the 'Naming Game'.

One of the simplest framework as described in the previous chapter as the Naming Game (NG) [47,48], progressively leading to the establishment of human-like languages, is a simple multi-agent model in a community of agents employing mutual bipartite interactions within themselves, leading to the emergence of a shared communication scheme.

Formulated by a group of researchers to understand the role of self-organization in evolution of language [49, 50], studies in many directions including semiotic dynamics [51, 52, 55, 116], artificial sensor network as a leader election model [56], social media as an opinion formation model [57] and also more advanced models [58, 59] in attempt to explain various complex processes like categorization, color naming have also been built on top of the basic naming game framework.

Following the basic idea of the naming game, our argument is that learning is reciprocal [117,118] and is not properly incorporated into the dynamical rules of

the Naming Game models available in the literature.

In each game a randomly selected pair of agents interact to negotiate conventions, i.e., associations between forms (names) and meanings (e.g. objects in the environment, linguistic categories etc.) and the negotiation of conventions takes place when one of the agents (termed as a speaker) tries to draw attention of the other agent (termed as the hearer) toward the meaning by producing a conventional form.

If the hearer is capable of expressing the actual meaning of the conventional form uttered by the speaker, the pair of interacting agents are assumed to have a mutual consensus, and the interaction is called a “success”. Consequently, the speaker-hearer pair updates their form-meaning repository by removing all competing forms corresponding to the meaning except the “winning” one currently uttered by the speaker. On the other hand, if the hearer produces a wrong interpretation, he takes a lesson from the interaction by learning this new form-meaning association, and in this case, the interaction is termed as a “failure”. Thus, depending on the success and failure moves of the hearer in producing meaning of the name of any object, both the interacting agents reshape their internal form-meaning association. Through successive interactions, the adjustment of such individual associations collectively leads or should lead to the emergence of a global consensus.

In this chapter, we revisit the basic construction of the model of the naming game and redefine the interaction rules, accordingly in order to address the reciprocity of learning process by having a model with symmetric interactions, based on our work in [60]. It has been argued that it is too stringent in removing all the entries except the winning one from the agent repertoire after a successful interaction between the speaker-hearer pair. Further, note that learning is rarely unidirectional as assumed in the case of a failure move in the original naming game models; in contrast, we believe that learning activity most of the times is

reciprocal.

Therefore, here we redefine the interaction rules in order to address the above limitations by having a symmetric model where on a success both the agents sort out all the common information that they have while on a failure enhance each of their knowledge by learning all the form-meaning associations that the other partner only knew so far. One can intuitively posit that this process should lead to the emergence of a faster consensus than the original naming game owing to the fact that (a) the agents learn more and (b) the agreement criteria is relaxed, thereby, increasing manifold the probability of successful communication. We perform rigorous numerical simulations to obtain the scaling relations for this revised model and explicitly show that for a population of N agents the time to reach global consensus indeed scales as $N^{1.13}$ as opposed to $N^{1.5}$ for the original naming game.

5.2 Model

The dynamics of naming game is defined in terms of a sequence of bipartite interactions in a community of N agents, with each agent i ($i = 1, \dots, N$) having an inventory of words whose length l may be arbitrarily long, initially with empty inventories, i.e., $\ell_i = 0$ for all i . Following the long sequence of mutual bipartite information sharings, the system finally reaches a stable state where all agents have the same set of common words. A ‘pseudo’ time t is defined for the convenience of following the dynamics, equal to the number of interactions. In an interaction, a pair of distinct agents i and j of inventory lengths ℓ_i and ℓ_j , respectively, are selected randomly with uniform probability from all the agents. One of them, say the i^{th} agent, is randomly selected and is termed as the “speaker” whereas the j^{th} agent is called the “hearer”. The interaction between them can

take place in the following three possible ways: A. *Invention*: In this case the inventory list of the speaker is empty. The speaker picks up a new word and keeps it at the bottom of his inventory. Since this is a new word, it cannot be present in the inventory of the j -th agent. Therefore this new word is simply added at the top of the inventory of the j -th agent.

B. *Success*: In this case the inventory length of the speaker is non-zero. The speaker and the hearer share information about their contents, sort out the common contents and only the common words are retained. That means the inventories of lengths ℓ_i and ℓ_j of the speaker and the hearer respectively are compared, and the number n of common words are sorted out. In case $n > 0$ then this possibility is called a success. The inventories of both the speaker and the hearer are then shrunk to n entries where only the common words are kept.

C. *Failure*: If the inventories have non-zero lengths yet there is no common word between them, then the lists are merged together, and both the agents have the same combined list.

It is to be noted that in this model the success and failure rules are symmetric with respect to the speaker and the hearer.

At any arbitrary intermediate time t the total number of words in the community is denoted by $N_w(t)$ and the total number of distinct words is denoted by $N_d(t)$. The dynamics starts with the inventory lengths $\ell_i = 0$ for all i . At very early times almost all interactions are of type A. During this period both $N_w(t)$ and $N_d(t)$ grow very fast, i.e., linearly with time. As time proceeds more and more agents have non-zero inventory lengths and therefore the chances of success and failure moves become increasingly likely. Consequently $N_w(t)$ reaches a maximum at a specific time t_m and then it decreases with time (Fig. 5.1(a)). On the other hand the number of distinct words $N_d(t)$ nearly saturates around a fixed mean value. Eventually $N_d(t)$ also decreases gradually and the community finally converges at the time t_f to a stable state which is a fixed point (Fig. 5.1(b)). In

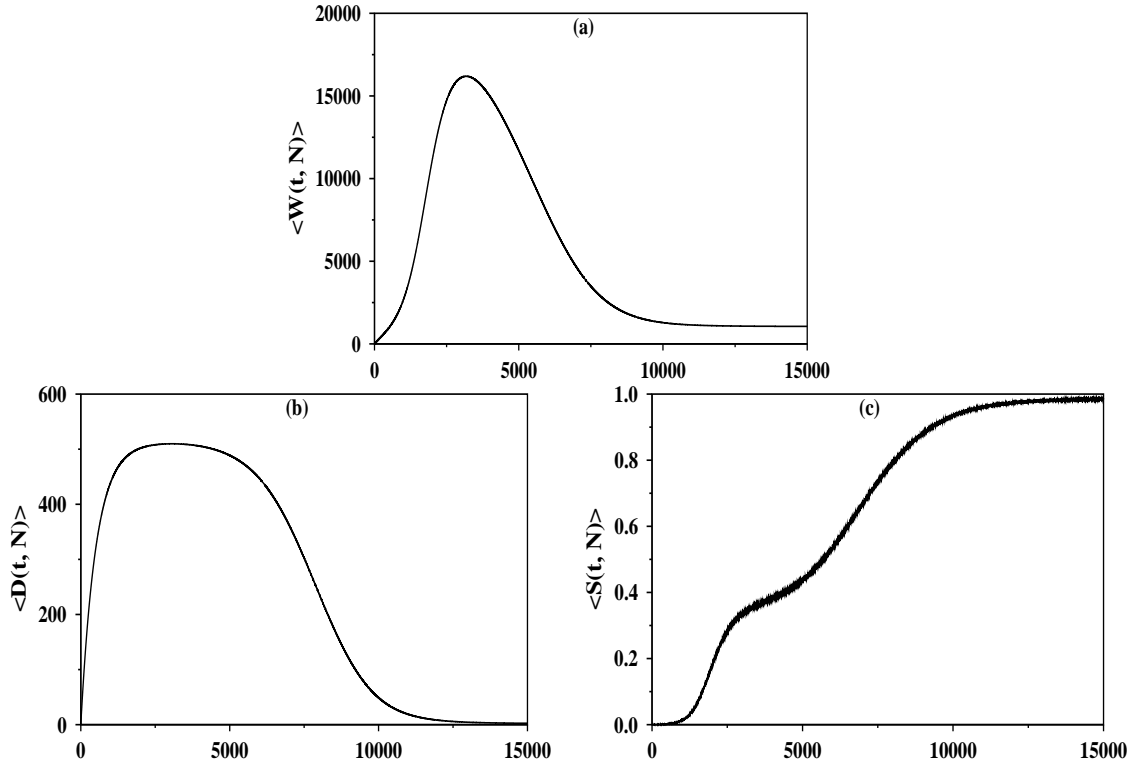


Figure 5.1: Time Variations of the average (a) number of words $\langle W(t, N) \rangle$, (b) number of distinct words $\langle D(t, N) \rangle$ and (c) success rate $\langle S(t, N) \rangle$ with time for a community size $N = 1024$.

this stable state $N_w(t_f)$ takes a value of gN with every inventory having the same set of g common words, g being a small positive integer. Therefore in contrast to the naming game model where $g = 1$ [47], there could be multiple globally common words present in our model i.e., $g > 1$. Consequently $N_d(t)$ finally reaches the value g . In addition a third quantity $\mathcal{S}(t)$ is also calculated which measures the success rate of an interaction at time t . In other words $\mathcal{S}(t)$ is the fraction of a large number of independent runs having successful moves at time t and the variation of this quantity with time is shown in Fig. 5.1(c).

5.3 Algorithm

The algorithm used for the simulation can be described as follows. Positive integer numbers starting from unity are used for representing different words. There-

fore at any arbitrary intermediate stage, if N_d distinct words have already been used, to choose a new word one simply selects the number $N_d + 1$. It turned out that defining an array $b(k)$ is very useful, $b(k)$ keeps track of the number of times the word k has occurred with all agents. In case A, $b(k)$ is increased by 2: $b(k) \rightarrow b(k) + 2$. However to check if an interaction is a case of success or failure, one first compares the inventories of the i -th and the j -th agents. Therefore every word of the list ℓ_i has to be checked in the list ℓ_j and vice versa. This is easily done by using another array $a(k)$ and for every word k in ℓ_i and ℓ_j one makes $a(k) \rightarrow a(k) + 1$. After that, the number of locations with $a(k) = 2$ are the number of common words between ℓ_i and ℓ_j . Let this number be n , and only these common words are kept in another array a_1 . At the same time we also count that out of n such common words how many have b values greater than 2, i.e., these words have not only occurred in ℓ_i and ℓ_j but also in the inventories of other agents. Let this number be n' . If $n > 0$, it is a success but on the other hand if $n = 0$, it is a case of failure.

In the case of successful moves, we first update the array b . For each entry k in ℓ_i and ℓ_j , we make $b(k) \rightarrow b(k) - 1$. Therefore during the updating procedure whenever $b(k)$ becomes zero we reduce N_d by unity: $N_d \rightarrow N_d - 1$. If there are m distinct entries present in the inventories of the agent i and agent j where $b(k)$ becomes zero, then the n common words in the array a_1 , are copied to ℓ_i and ℓ_j . N_w is updated like: $N_w \rightarrow N_w - \ell_i - \ell_j + 2n$ and N_d is updated like: $N_d \rightarrow N_d - m + n - n'$. This completes a successful interaction.

In case of a failure move, the combined list of ℓ_i and ℓ_j are copied to the inventory lists of i and j . For each such word the b value is increased by unity. The total number of words N_w is increased as $N_w \rightarrow N_w + \ell_i + \ell_j$, the number of distinct words N_d remains same. This completes an unsuccessful interaction (see Table I).

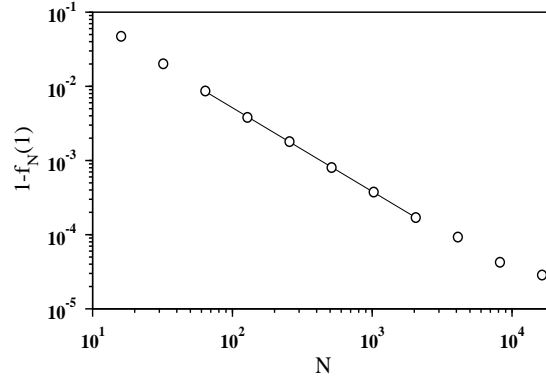


Figure 5.2: The fraction $1 - f_N(1)$ of configurations having more than 1 distinct word per agent in the stable state has been plotted against the community size N . A power law is observed like $1 - f_N(1) \sim N^{-\tau}$ with $\tau \approx 1.13(2)$.

5.4 Results

It is noticed that on increasing the community size N the probability that an arbitrary configuration has the same set of g distinct words per agent in the final stable state decreases for $g > 1$ and it increases to unity for $g = 1$. We have measured the fraction $f_N(g)$ of a large sample of uncorrelated configurations that have g words in the final stable configurations. The variation of $f_N(1)$ has been shown in Fig. 5.2. A plot of $1 - f_N(1)$ vs. N on a log–log scale gives a nice straight line for the intermediate range of N . This indicates that the growth of $f_N(1)$ to unity as N increases follows a power law like $1 - f_N(1) = AN^{-\tau}$ and our measured value of τ is 1.13(2). The mean maximal time $\langle t_m(N) \rangle$ and the mean convergence time $\langle t_f(N) \rangle$ have been measured for different values of N and are plotted using a log–log scale in Fig. 5.3. The community sizes which have been simulated varied

Rule A:	$N_w \rightarrow N_w + 2;$	$N_d \rightarrow N_d + 1$
Rule B:	$N_w \rightarrow N_w - \ell_i - \ell_j + 2n;$	$N_d \rightarrow N_d - m + n - n'$
Rule C:	$N_w \rightarrow N_w + \ell_i + \ell_j;$	$N_d \rightarrow N_d$

Table 5.1: Summary of the rules A, B and C for the changes in the total number of words $N_w(t)$ and the number of distinct words $N_d(t)$ at any arbitrary time t .

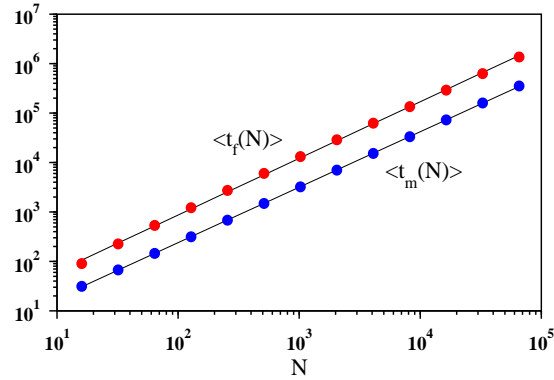


Figure 5.3: The variations of the average maximum time $\langle t_m(N) \rangle$ (blue) and the average convergence time $\langle t_f(N) \rangle$ (red) against the community size N . The exponents are $\alpha = 1.12$ and $\beta = 1.14$ respectively.

from $N = 2^4, 2^5, \dots, 2^{16}$, increased by a factor of 2 in successive steps. These data fit very well to straight lines. Therefore assuming power law variations like

$$\langle t_m(N) \rangle \sim N^\alpha \quad \text{and} \quad \langle t_f(N) \rangle \sim N^\beta \quad (5.1)$$

we obtained $\alpha = 1.12$ and $\beta = 1.14$. This observation leads us to conclude that

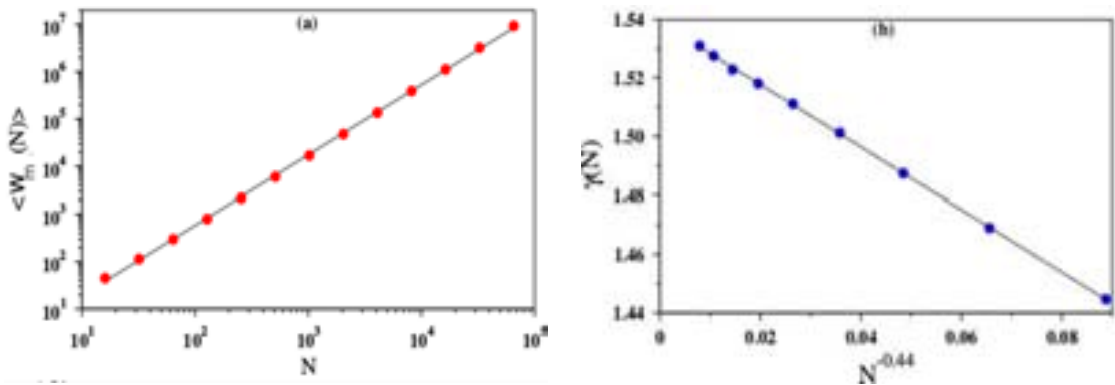


Figure 5.4: (a) Plot of the average maximal number of words $\langle W_m(N) \rangle$ against the community size N on a log–log scale. (b) The slopes $\gamma(N)$ between pairs of successive points in (a) gradually increases with increasing N and has been plotted against $N^{-0.44}$ to obtain the asymptotic value of $\gamma = 1.539$.

both α and β are approximately the same and has a value 1.13(1). It may be noted that these exponents are much smaller than the original naming game (both α and β equal to 1.5) [47]. This faster consensus is possibly a consequence of the

fact that the interaction rule here is symmetric thus increasing the possibility of alignment between the agents through fewer interactions as compared to the original naming game. Further, here the stable state criteria are also relaxed, so the agents are assumed to reach consensus even if they do not agree with only a single word.

Next in Fig 5.4(a). we plotted the average maximal number of words $\langle N_{wm}(N) \rangle$ against N on a log–log scale for the same community sizes. Here again we assumed a power law variation like

$$\langle N_{wm}(N) \rangle \sim N^\gamma \quad (5.2)$$

and the average slope is measured using a least square fit method. We obtained an average value of $\gamma = 1.49$. Further, this analysis has been done in more detail. The intermediate slopes $\gamma(N)$ between successive pairs of points have been measured and extrapolated against $N^{-0.44}$. The extrapolation fits very well to a straight line and in the limit of $N \rightarrow \infty$ the value of $\gamma = \gamma(\infty) = 1.539$ has been obtained. This value of γ is comparable with 1.5 in the original naming game model [47].

5.5 The largest cluster

At an intermediate time t there are $N_d(t)$ distinct words, and in general each word is shared by a number of agents. Similar to the percolation phenomena [119] we define the cluster size s_i associated with the i -th word as the number of distinct agents which have the word i in their inventories. In the algorithm described in the previous section, we have stored the cluster sizes in the array $b(i)$. As time evolves cluster sizes of some words gradually vanish, but at the same time the cluster sizes of the other words grow. Finally, only g distinct words survive whose cluster sizes are exactly N , and at this point of time, the dynamics reach the fixed point. It may be noted that the size of a particular cluster increases in

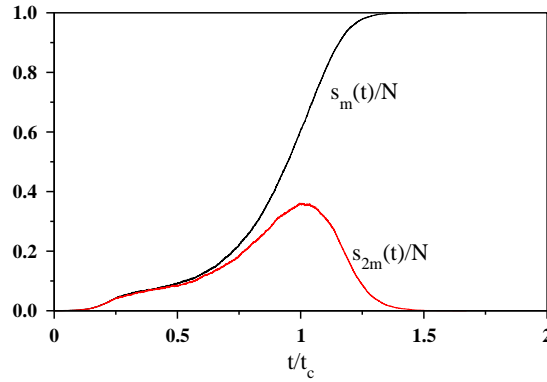


Figure 5.5: For a single run the variations of the scaled sizes of the largest cluster $s_m(t)/N$ and the second largest cluster $s_{2m}(t)/N$ for a community with $N = 16384$ agents. It is seen that while the size of the largest cluster grows almost (but not exactly) monotonically, the size $s_{2m}(t)$ of the second largest cluster reaches a maximum at time t_c and then gradually decreases to zero. The time axes has been scaled by the characteristic time t_c .

the failure rule and decreases in the success rule only by one agent at a time. We keep track of the variation of the size of the largest cluster $s_m(t, N)$ and observe how it almost monotonically increases and assumes the size N at the fixed point (Fig. 5.5). At an intermediate stage, there may be a number of distinct clusters whose sizes are equal to the largest cluster size $s_m(t, N)$. We define the fractional size of the largest cluster at time t averaged over many independent runs as:

$$\mathcal{C}(t, N) = \langle s_m(t, N) \rangle / N. \quad (5.3)$$

In addition, we define the size s_{2m} of the second largest cluster as well. In contrast to s_m , the value of s_{2m} gradually increases to a maximum value and then systematically decreases to zero at the fixed point (Fig. 5.5). We define another characteristic time t_c at which the second largest cluster assumes its maximum value. This is the transition time when the second largest cluster starts dismantling, and the largest cluster grows at its fastest rate which signifies the onset of correlation in the community.

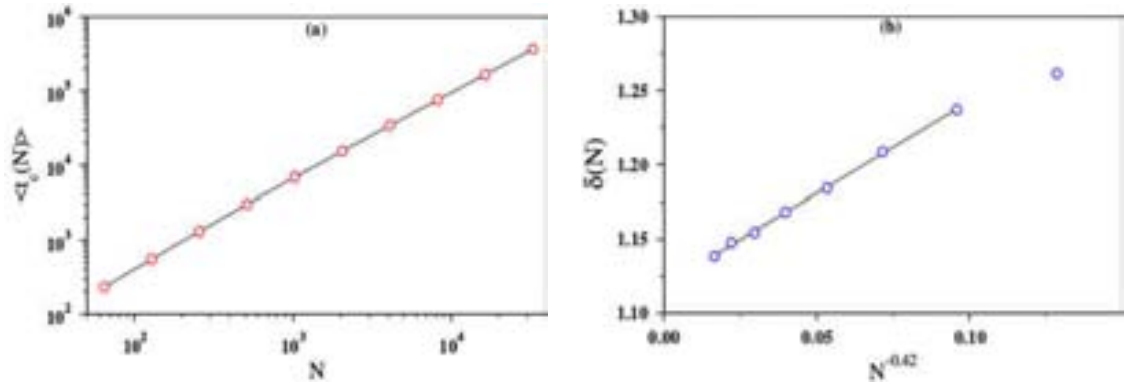


Figure 5.6: (a) The average value of the characteristic time $\langle t_c(N) \rangle$ where the size of the second largest cluster is maximum has been plotted with the community size N on a log–log scale for $N = 2^6, \dots, 2^{15}$. The variation seems to be a power law: $\langle t_c(N) \rangle \sim N^\delta$. (b) Slopes between successive points has N dependence and we plot $\delta(N)$ vs. $N^{-0.42}$ which fits best to a straight line. The extrapolated value $\delta = 1.12$.

In Fig. 5.6(a) the characteristic time $\langle t_c(N) \rangle$ averaged over many independent runs has been plotted on a log–log scale against the community sizes $N = 2^6, 2^7, \dots, 2^{15}$. While the points seem to fit a nice straight line on the average, a closer look reveals that here again the local slopes between successive pairs of points have a systematic variation. Assuming that the functional form would indeed be a power law in the limit of $N \rightarrow \infty$ as

$$\langle t_c(N) \rangle \sim N^\delta \quad (5.4)$$

we have extrapolated the local slopes $\delta(N)$ with a negative power of N . The best value of this correction exponent is 0.42 and in Fig. 5.6(b) a plot of $\delta(N)$ against $N^{-0.42}$ gives a nice straight line for large N values. Extrapolating to $N \rightarrow \infty$ we obtained $\delta = 1.12$.

Finally in Fig. 5.7 the average value of the largest cluster size $\mathcal{C}(t, N)$ has been plotted for three different community sizes $N = 2^{12}, 2^{14}$ and 2^{16} . We first scale the time axis $t/N^{1.13}$ so that the scaled time could be treated similar to the site / bond occupation probability in percolation theory. The scaled axis is then shifted

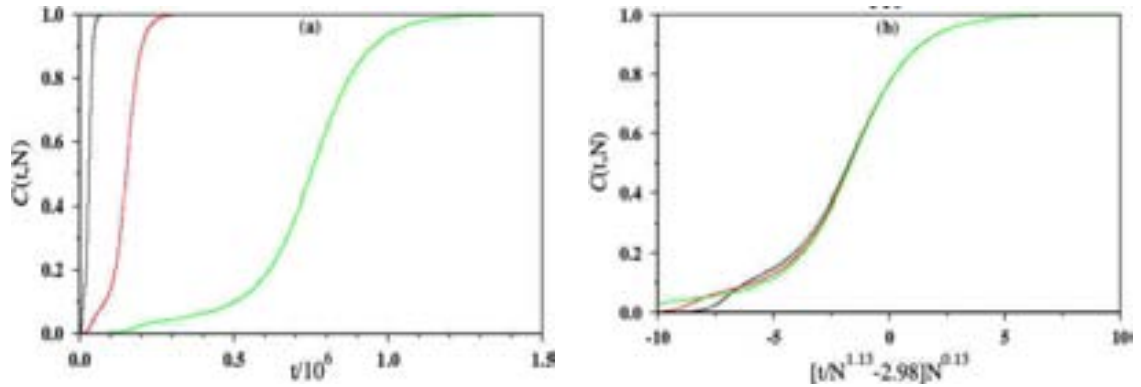


Figure 5.7: (a) Variation of the fractional size of the largest cluster $\mathcal{C}(t,N) = \langle s_m(t,N) \rangle / N$ with time $t/10^6$. (b) Finite size scaling of the data in (a), plot of $\mathcal{C}(t,N)$ vs. $[t/N^{1.13} - 2.98]N^{0.13}$ exhibits a data collapse.

by 2.98 and then again scaled by $N^{0.13}$ to obtain a data collapse.

5.6 Summary

To summarize we devised a new model for information sharing and sorting in a community of agents. Three types of mutual bipartite interactions take place among the randomly selected pairs of agents. Here the interactions are more symmetric and less restricted compared to the ordinary naming game. By Invention new words are created, by Failure inventories are shared, and by Success, only the common words are sorted out. The dynamics of the system is dominated initially by Invention, followed by rapid growth of different words dominated by Failure and finally, the system gradually gets rid of uncommon words dominated by Success moves. The system finally reaches the stable state where each agent has the same set of g words in his inventory. Using extensive numerical studies, we find that the exponents describing the characteristic time scales and the maximum number of words of this model assume a completely distinct set of values compared to the ordinary naming game.

6 Asymptotic properties of restricted naming games

6.1 Introduction

As described in the previous chapters, the aim of the model of the naming game is to study the evolution of consensus opinion in the context of naming a single object in a large community of agents [47, 48]. Different agents refer to the object using different names when the object is introduced initially. Agents interact among themselves and share the names that have been already introduced according to a set of specific rules. At the early stage, the number of distinct names for the object increases as the agents introduces new names for the object. However, as the game progresses, a consensus name gradually emerges, and distinct names disappear. The dynamical evolution of the game terminates when all agents agree upon a single name through mutual interactions and following the rules of the game. At an arbitrary intermediate stage, an agent has a number of names of the same object in his vocabulary suggested by different groups of agents. An agent, under the sharing dynamics, not only learns new names for the object but also shares names from his own vocabulary with other agents.

The dynamics have been studied in various aspects. Starting from the analysis of real world data in [120] to verify the power law exponents of the model, faster convergence in the presence of overhearers [57] and also more general advanced studies of categorization of names and color naming have been performed as well [58, 59, 121] in the same light. However, in all the models studied for the dynamics of naming games in the literature and in other apparent directions, the sizes of the vocabularies of the agents have been assumed to be infinite [49, 50, 60]. In reality, an individual agent has only a finite amount of memory. Therefore, it would be quite appropriate to study the effect of the finiteness of the vocabulary sizes in the dynamics of naming games. In this chapter, based on our work [61], the vocabulary size of every agent is assumed to be finite and has been restricted to a certain fixed cut-off value, which has been suitably tuned.

We have studied the effect of restrictions on both the symmetric [60] and asym-

metric naming games [47, 48]. With the restriction, the asymmetric and the symmetric naming game exhibit very similar type of behavior. However, the power law exponents which characterize the naming games, namely α , β and γ as discussed in chapter 1, of both the games are found to be distinctly different.

6.2 Restricted vocabulary

The naming game is defined in terms of a community of N agents and a new object to name [47]. An agent, either invents a new name for the object, or he learns a name from another agent by the bipartite sharing dynamics. Finally, all the agents come to an agreement and refer the object by a single name. This spontaneous evolution of a consensus name is the objective of the naming game. During the time evolution, pairs of randomly selected distinct agents execute a sequence of interactions to share their stock of the names of the object. In the

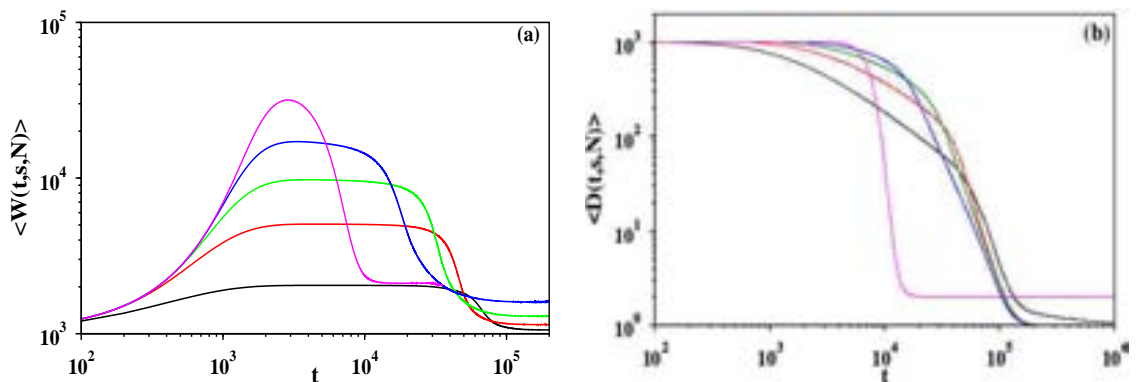


Figure 6.1: (Color online) (a) The time variation of the averaged total number of names $\langle W(t, s, N) \rangle$ for community size $N = 1024$ with the restricted vocabulary sizes $s = 2$ (black), 5 (red), 10 (green), 20 (blue) and ∞ (magenta). (b) The time variation of the averaged total number of distinct names $\langle D(t, s, N) \rangle$ for community size $N = 1024$ with the same set of s values

literature, two models of the naming game have been studied. In the original ‘asymmetric’ naming game, one of the two agents selected for sharing, say the ‘ i ’-th agent, is called the ‘speaker’, whereas the ‘ j ’-th agent is termed as the ‘hearer’

[47]. The speaker first randomly selects a name from his vocabulary and checks if the hearer also has the same name. If the hearer has this name, it is called a successful sharing, and then the vocabulary sizes of both the agents are reduced to unity, both having only the selected name. On the other hand, in the case of a failure, the selected name of the speaker is added to the vocabulary of the hearer.

In comparison, in the ‘symmetric’ naming game [60], there is no distinction between the speaker and the hearer. Here, for a successful move, the entire subset of names that are common in the vocabularies of the agents i and j are retained, and the remaining un-common names are deleted from the vocabularies of both the agents. On the other hand, in the case of a failure, there is no common name, and both the agents get the combined list of both agents’ vocabularies.

6.2.1 The model

We have studied the effect of restrictions on both the symmetric and asymmetric naming games [61]. We describe the game and present the plots of the data for the symmetric naming game only. The plots of the asymmetric naming game exhibit very similar type of behavior. However, the power law exponents of both the games are found to be distinctly different, and we have enlisted them in Table 6.1.

In the symmetric game, we first abolish the step for the invention of names. Instead, we assign every agent a distinct name at the initial stage. Therefore, $\ell_i(t)=1$ for all i at time $t = 0$ and the dynamics starts with N such distinct names. Further, we apply a restriction to the vocabulary size of every agent. The vocabulary size is assigned a maximal cut-off value s , same for all agents at all times, and no agent can accommodate any additional name. We follow the rules of symmetric naming game [60] to describe the dynamics. At every time step two distinct agents i and j are randomly selected and are allowed to interact between themselves. The interaction can be of two types according to which both the agents

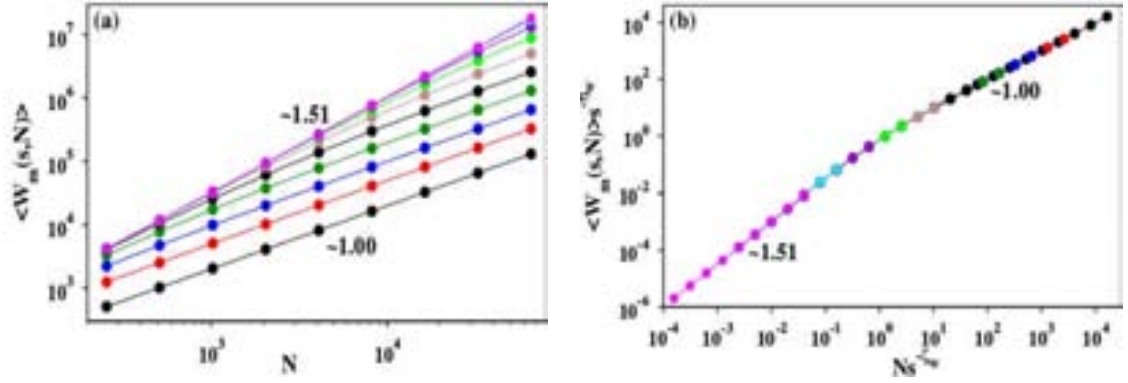


Figure 6.2: (a) The configuration averaged value of the maximum number $\langle W_m(s, N) \rangle$ of names against community size N for different values of the vocabulary sizes: $s = 2$ (black), 5 (red), 10 (blue), 20 (green) etc. and ∞ (magenta) (from bottom to top). (b) Scaling collapse of the same data as $\langle W_m(s, N) \rangle s^{-\eta_W}$ and $Ns^{-\zeta_W}$ with scaling parameters $\eta_W = 3.0$ and $\zeta_W = 2.0$.

update their vocabularies.

A. *Failure*: In this case, none of the names in the vocabulary of the i -th agent is common to the vocabulary of the j -th agent. Therefore, the agents share their vocabularies entirely. Each agent gets the combined list of names of both the agents. In mathematical form:

If $\{\ell_i(t-1)\} \cap \{\ell_j(t-1)\} = \emptyset$, then

$\{\ell_i(t)\} = \{\ell_j(t)\} = \{\ell_i(t-1)\} \cup \{\ell_j(t-1)\}$, where \emptyset is the empty set.

However, if $\ell_i(t-1) + \ell_j(t-1) > s$, only first s names are retained in the vocabularies of both the agents.

B. *Success*: In this case, at least one of the names in the vocabulary of the agent i is common to the vocabulary of the agent j . Then, after sharing both the agents retain only their common names.

If $\{\ell_i(t-1)\} \cap \{\ell_j(t-1)\} \neq \emptyset$, then

$\{\ell_i(t)\} = \{\ell_j(t)\} = \{\ell_i(t-1)\} \cap \{\ell_j(t-1)\}$

Here, the finite size s of the vocabularies does not affect this sharing step.

6.2.2 Results

Here again the variation of the $W(t,s,N)$ and $D(t,s,N)$ are quite similar with the unrestricted asymmetric naming game. But, Due to the abolition of the invention step the $W(t,s,N)$ and $D(t,s,N)$ starts from N instead of zero at $t = 0$. However, this has no effect on the three characteristic exponents.

For smaller vocabulary sizes $s = 2, 5, 10$ etc., $\langle W(t,s,N) \rangle$ quickly reaches its maximum value sN , as individual agent's vocabulary gets filled up (Fig. 6.1(a)) and is then maintained for some time, showing a plateau over the same period. Smaller the value of s longer is the length of the plateau. At a certain initial time t_{in} , $W(t,s,N)$ attains the value sN , remains equal, or very close to it for a long time and then at a latter time t_{out} , $W(t,s,N)$ decreases from sN . Both t_{in} and t_{out} fluctuate over a wide range. We have therefore defined the maximal time t_m for attaining the maximum number of names in the community as mean of these two reference times, i.e., $t_m(s,N) = (t_{in} + t_{out})/2$.

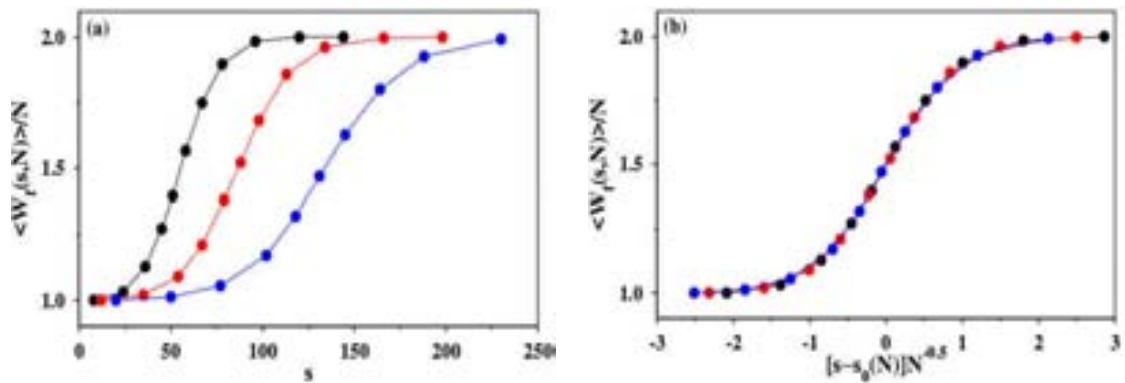


Figure 6.3: (a) The configuration averaged value of the number $\langle W_f(s,N) \rangle$ of names in the converged state against the cut-off vocabulary size s for community sizes $N = 512$ (black), 1024 (red), and 2048 (blue). (b) Data collapse for the finite-size scaling of $\langle W_f(s,N) \rangle / N$ against $[s - s_0(N)]N^{-0.5}$; $s_0(N)$ is found to grow as $N^{0.64}$.

For fixed N , but for relatively larger values of $s = 80$ or 160 , the plateau gradually shrinks as the number of names with an agent hardly reaches its cut-off value s . Instead, a single peak of value $\langle W_m(s,N) \rangle$ starts showing up at $\langle t_m(s,N) \rangle$ as s

increases even further. The unrestricted case of $s \rightarrow \infty$ is the original symmetric naming game (Fig. 6.2). From the averaged slopes of these lines, our estimate for the exponent γ 1.54 (asymptotic), very close to $\gamma = 1.539$ of the symmetric naming game [60]. On the other hand, when s is very small the exponent is found to be $\sim 1.00(1)$. The corresponding γ exponents of the asymmetric naming game are 1.50 and 1.00 respectively.

We observe (Fig. 6.1(b)) that for all values of s , $\langle D(t, s, N) \rangle$ starts from N at time $t = 0$ and then monotonically decreases and at $t = t_f$, converges to either only one or two names. Larger the value of s , sharper is the fall.

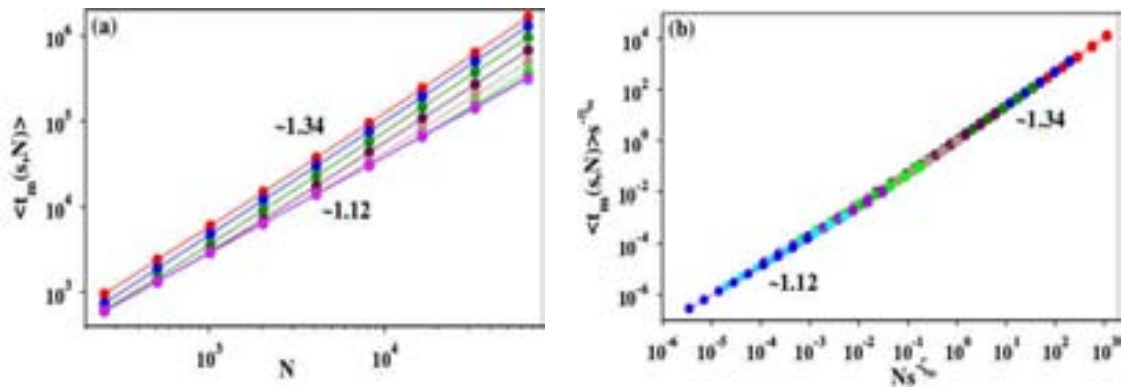


Figure 6.4: (a) The averaged value of the maximal time $\langle t_m(s, N) \rangle$ against N using the same set of vocabulary sizes and colors used in Fig. 4. (b) Scaling of the axes leads to a data collapse with the scaling exponents $\eta_m = 3.0$ and $\zeta_m = 2.53$.

The corresponding exponent of the averaged number $\langle W_f(s, N) \rangle / N$ of names per agent in the converged state, systematically increases from 1.0 to 2.0 and the entire curve shifts to the larger regimes of s values with increasing N (Fig. 6.3(a)). The value of s for which $\langle W_f(s, N) \rangle / N = 3/2$, $s_0(N)$ scales with N as $N^{0.64}$. Further, we have shown a scaling of $\langle W_f(s, N) \rangle / N$ against $[s - s_0(N)]N^{-0.5}$ exhibiting an excellent data collapse (Fig. 6.3(b)). In the $\langle t_m(s, N) \rangle$ vs N plot (Fig. 6.4(a)), for the same values of s , it is observed that for $s = \infty$ and for very small values of s , e.g., $s = 2$ the curves fit to straight lines with α , approximately 1.12(1) and 1.34(1) respectively and the system crosses over from the original symmetric naming game

behavior to the behavior of restricted symmetric naming game. Using scaling analysis (Fig. 6.4(b)) we obtained the dependence of the crossover community size on s as: $N_c(s) \sim s^{\zeta_m}$ with $\eta_m = 3.0$ and $\zeta_m = 2.53$. For the asymmetric naming

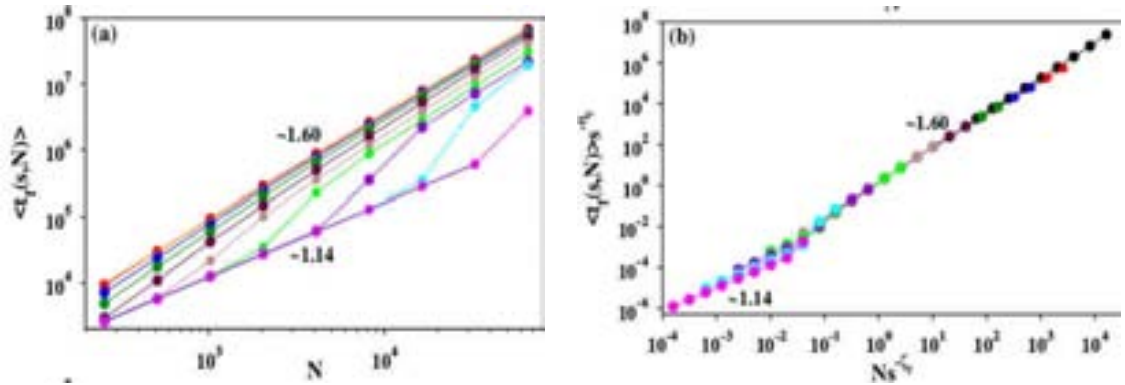


Figure 6.5: (a) The averaged final convergence time $\langle t_f(s, N) \rangle$ plotted, against N using the same set of vocabulary sizes and colors as in Fig. 2. For a specific value of the vocabulary size s , the curve is a straight line with slope ~ 1.14 for $N \ll N_c$ and ~ 1.60 for $N \gg N_c$. (b) Scaling of the axes leads to a data collapse with scaling exponents $\eta_f = 3.0$ and $\zeta_f = 2.0$ respectively.

game, the corresponding α exponents are 1.54 and 1.87 respectively.

Finally, from the plot of $\langle t_f(s, N) \rangle$ against N (Fig. 6.5(a)), we estimated the exponent $\beta \sim 1.60(1)$ for the smallest vocabulary size ($s=2$), where as for $s = \infty$ we get back the exponent of the original symmetric naming game $\beta = 1.14(1)$. A crossover between the two behaviors is present as well. For the asymmetric naming game the corresponding β exponents are 2.18 and 1.48 respectively.

6.3 Symmetric naming game with limited number of distinct names

6.3.1 Model and results

In this modification of the symmetric naming game, initially, each agent starts with a single name, selected randomly from a set of $n < N$ distinct names, in his

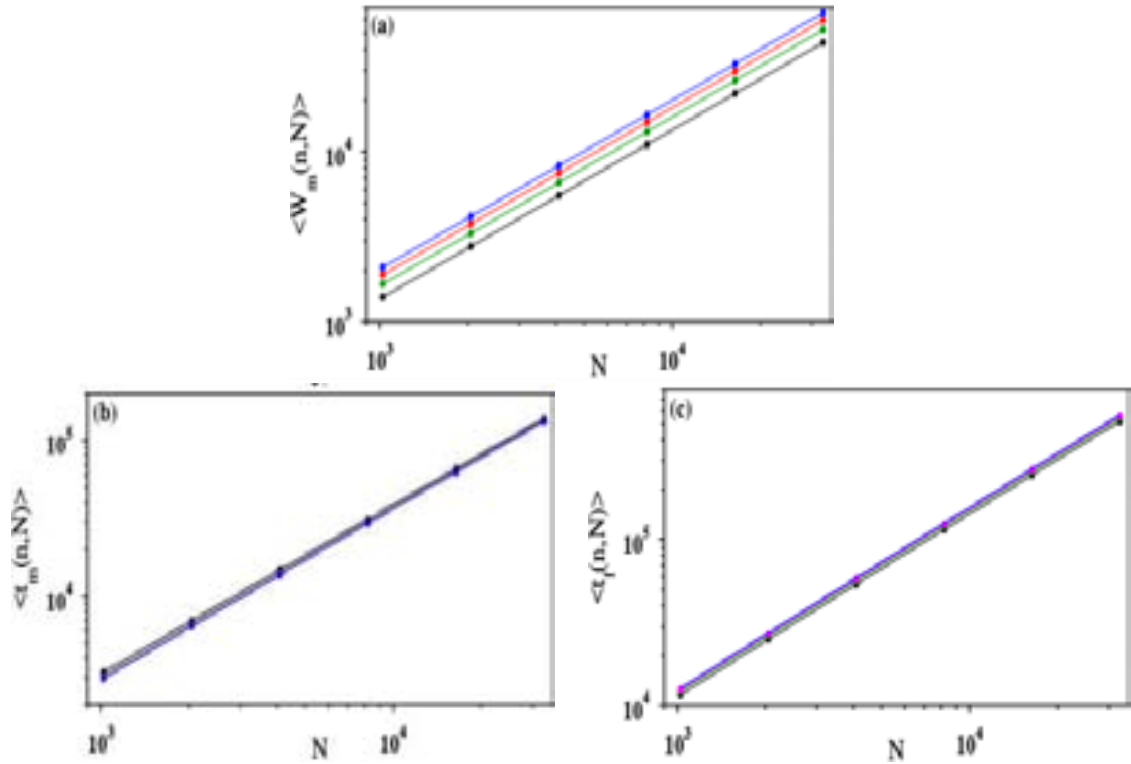


Figure 6.6: (a) The configuration averaged value of the maximum number $\langle W_m(n, N) \rangle$ of names has been plotted with the community size N for different constant values of distinct names: $n = 2$ (black), 3(green), 4(magenta), 5(blue). All of them fit to nearly parallel straight lines and have average slope $\gamma = 0.99(1)$. (b) Similar plot for the maximum time $\langle t_m(n, N) \rangle$ against N for same values of n using same colors. The average value of the slopes gives $\alpha = 1.09(1)$. (c) Similar plot for the convergence time $\langle t_f(n, N) \rangle$ against N for same values of n using same colors. The average value of the slopes gives $\beta = 1.10(1)$.

vocabulary. The set of names, in the vocabularies of agents, evolve by mutual pairwise interactions. At any intermediate time, an agent's vocabulary can only be filled up to n names. The game evolves following the dynamical rules of the symmetric naming game, mentioned above.

In the $N \gg n$ scenario, the average number of names an agent can have is also $\approx n$, implying $\langle W_m(n, N) \rangle \sim N$. Therefore, for a fixed value of n , the growth exponent γ from Eqn. (1) must be equal to unity. This is verified numerically in Fig. 6.6(a).

On the other hand, the case of $n = N$ implies that initially all N agents have

been given N distinct names so that all agents have different initial names. This is the same as the symmetric naming game without the invention step. The vocabulary size can be at most N , but in practice, it is much smaller.

In Fig. 6.6(a) we have plotted the $\langle W_m(n, N) \rangle$ against N for four different values of $n = 2, 3, 4$, and 5 , and for six different community sizes N . On a log-log scale the curves fit nicely with straight lines. The averaged overall slope gives a value for $\gamma = 0.99(1)$. Similar plots of $\langle t_m(n, N) \rangle$ and $\langle t_f(n, N) \rangle$ in Fig. 6.6(b) and Fig. 6.6(c) gives $\alpha = 1.09(1)$ and $\beta = 1.10(1)$ respectively.

Naturally one can ask, what happens if the number n of distinct names grows non-trivially with the number of agents N , e.g., $n = N^\delta$? Here $\delta = 0$ corresponds to the case when n has a fixed value, independent of N . On the other hand, $\delta = 1$ implies the case when $n = N$. For other intermediate values of δ in the range $0 < \delta < 1$, simulations have been performed.

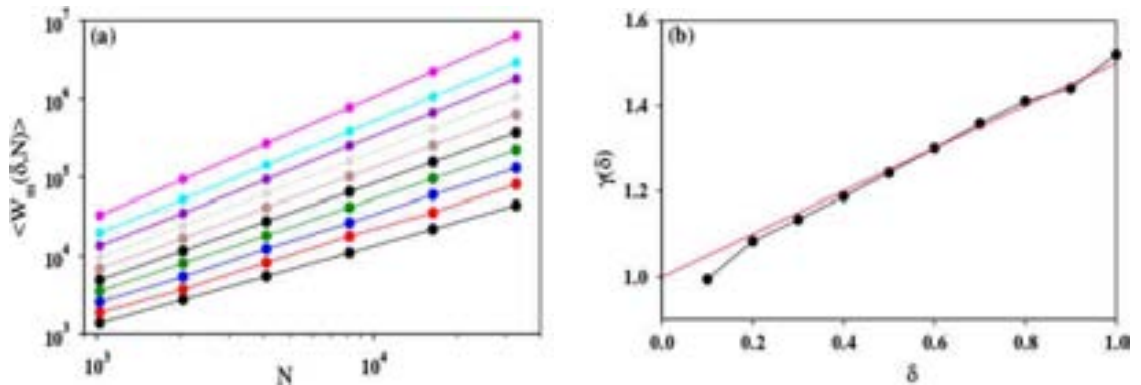


Figure 6.7: (a) The $\langle W_m(\delta, N) \rangle$ against the community size N for different values of the tuning parameter: $\delta = 0.1, 0.2, \dots, 1.0$ (from bottom to top). Slopes of these lines are the values of the power law exponent γ and are different for different values of δ . (b) Plot of the exponent $\gamma(\delta)$ against δ . Except the two end points, the intermediate region fits well with the form in Eqn. (6).

Fig. 6.7(a) exhibits $\langle W_m(\delta, N) \rangle$ against N for $\delta = 0.1, 0.2, \dots, 1.0$. For each value of δ we get one straight line and the slopes of these lines vary with δ between 1.0 and 1.54. A plot of a total of ten different values of the parameter δ yields different values of $\gamma(\delta)$ and in Fig. 6.7(b) we plot $\gamma(\delta)$ against δ . Apart from the

two limiting points at $\delta = 0$ and 1 the plot fits nicely to the following relation

$$\gamma(\delta) = 1 + \delta/2. \quad (6.1)$$

In a similar way we have obtained the variation of the $\alpha(\delta)$ and $\beta(\delta)$ against δ

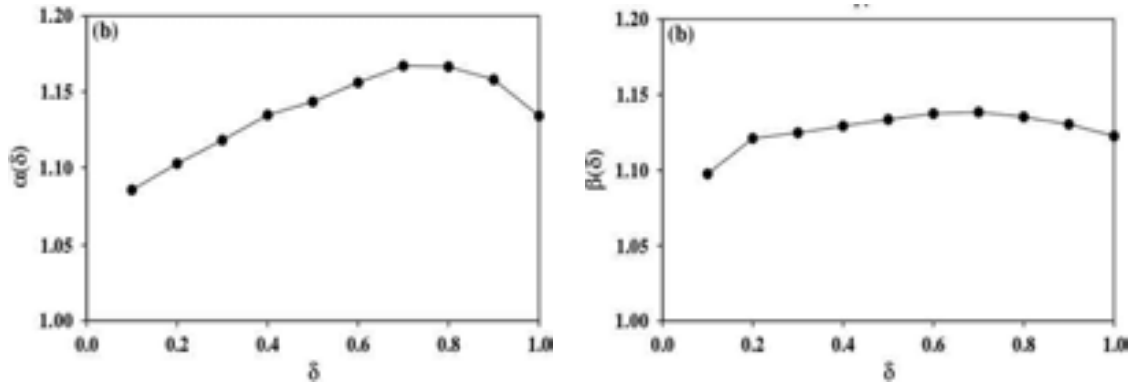


Figure 6.8: (a) Variation of the power law exponent $\alpha(\delta)$ against δ . (b) Variation of the power law exponent $\beta(\delta)$ against δ .

from the $\langle t_m(\delta, N) \rangle$ against N and $\langle t_f(\delta, N) \rangle$ against N plots for the same set of δ values. $\alpha(\delta)$ and $\beta(\delta)$ vary systematically within a short-range. The variation of $\alpha(\delta)$ starts from a value ≈ 1.09 for $\delta = 0.0$, then gradually goes through a maximum at $\delta \approx 0.7$, and then decreases to its value ≈ 1.14 at $\delta = 1$ (Fig. 6.8(a)). $\beta(\delta)$ also shows a similar kind of behavior (Fig. 6.8 (b)) showing a mild variation with δ , with the maximum occurring around $\delta = 0.7$.

6.4 Summary

To summarize, here we have studied two modified version of the symmetric naming game for vocabulary sorting and achieving consensus, with one version exhaustively studied for the asymmetric naming game as well. First, we have introduced a cut-off in the capacity of vocabulary associated with the agents in the community, resulting in a crossover from strong restriction behavior to the weak restriction one. This has been reflected in the characteristic exponents of the

Naming Game	α	β	γ
Asymmetric game [47]	1.5	1.5	1.5
Symmetric game [60]	1.12	1.14	1.539
Rest. vocabulary (Symm)	1.34(1)	1.60(1)	1.00(1)
Rest. vocabulary (Asymm)	1.87(1)	2.18(1)	1.50(1)
Rest. names	1.09(1)	1.10(1)	0.99(1)

Table 6.1: Comparison of the values of different exponents obtained in the restricted asymmetric and symmetric naming games with similar exponents of the original naming games.

game. We observed that the three exponents characterizing the dynamical evolution of the game in the strong restriction case are a different set of values not yet observed in the literature of naming games.

Effect of a second restriction, imposing a limiting value on the number of distinct names to be assigned to the agents, has been studied. In this case, a constant number n (independent of N) of distinct names has been initially given to the agents. This version of the game is much simpler, yet the three characteristic exponents yielded non-trivial values for constant values of n . Further, when we varied n as N^δ , the exponents depend nontrivially on the tuning exponent δ .

Numerical study of the restricted versions of both the symmetric and asymmetric naming games exhibited non-trivial changes in the asymptotic behaviors of the game. Values of the characterizing exponents have been compared in Tab. 6.1 with the asymmetric and the symmetric naming games.

Bibliography

- [1] J. Guckenheimer and J. M. Ottino, *Report from an NSF Workshop September, 2008*.
- [2] P. Agre, *Journal of Learning Sciences*, **12**, 413-426, 2003.
- [3] Simon A. Levin, *Ecosystems* **1**, 431–436 (1998).
- [4] S. Funtowicz and J. R. Ravetz, *Futures* **26(6)**, 568-582 (1994).
- [5] V. Grimm et. al., *Science* **310**, 987-991 (2005).
- [6] George Sugihara et al., *Science* **338**, 496 (2012).
- [7] E. Ostrom, *Science* **325**, 419 (2009).
- [8] J. Doyne Farmer et. al. *Eur. Phys. J. Special Topics* **214**, 295–324 (2012).
- [9] S. Hori, T. Nomura and S. Sakaguchi, *Science*. **299(5609)**, 1057-61 (2003).
- [10] K. Shortman and S. H. Naik, *Nature Reviews Immunology* **7**, 19-30 (2007).
- [11] M. J. S. Johnston, *Surveys in Geophysics* **18**, 441–475 (1997).
- [12] H. Kanamori, *Annu. Rev. Earth Planet. Sci.* **33**, 195-214 (2005).
- [13] J. L. Deneubourg and S. Goss, *Ethology Ecology and Evolution* **1**, 295-311 (1989).
- [14] M. Moussaid, S. Garnier, G. Theraulaz and D. Helbing, *Topics in Cognitive Science* **1**, 469–497 (2009).
- [15] T. Vicsek and A. Zafeiris, *Physics Reports*, **517**, 71-140 (2012).
- [16] T. Vicsek et. al., *Phys. Rev. Lett.*, **75**, 1226-1229 (1995).
- [17] Hidetoshi Nishimori and Gerardo Ortiz, *Elements of Phase Transitions and Critical Phenomena*, (Oxford University Press Inc., New York, 2011).
- [18] J. Toner and Y. Tu, *Phys. Rev. Lett.* **75**, 4326-4329 (1995).
- [19] Y. Tu, *Phys. Rev. Lett.* **80(21)**, 4819-4822 (1998).
- [20] J. Toner and Y. Tu, *Phys. Rev. E* **58**, 4828 (1998).
- [21] G. Grégoire, and H. Chaté, *Phys. Rev. Lett.* **92(2)**, 025702-025705 (2004).

- [22] M. Nagy, I. Daruka and T. Vicsek, *Physica A*, **373**, 445-454 (2007).
- [23] G. Baglietto, E. V. Albano, *Computer Physics Communications* **180(4)**, 527-531 (2009).
- [24] H. Chaté, F. Ginelli, Guillaume Grégoire, and F. Raynaud, *Phys. Rev. E* **77**, 046113 (2008).
- [25] S. Mishra, A. Baskaran and M. C. Marchetti, *Phys. Rev. E* **81**, 061916 (2010).
- [26] M. Ballerini et. al., *Proc. Natl. Acad. Sci.* **105**, 1232-1237 (2008).
- [27] J. Gautrais et. al., *PLoS Comput. Biol.*, **8**, e1002678v (2012).
- [28] F. Ginelli and H. Chateé, *Phys. Rev. Lett.* **105**, 168103-168106 (2010).
- [29] G. Grégoire, H. Chaté and Y. Tu, *Phys. Rev. E* **64**, 011902 (2001).
- [30] A. Peshkov, S. Ngo, E. Bertin, H. Chaté and F. Ginelli, *Phys. Rev. Lett.*, **109**, 098101-098106 (2012).
- [31] C. Heupe and M. Aldana, *Physica A*, **387**, 2809-2822 (2008).
- [32] J. Toner, Y. Tu and S. Ramaswamy, *Ann. Phys.* **318**, 170-244 (2005).
- [33] D.L. Blair and A. Kudrolli, *Phys. Rev. E* **67**, 041301 (2003).
- [34] V. Narayan, N. Menon and S. Ramaswamy, *J. Stat. Mech.* **P01005** (2006).
- [35] V. Narayan, S. Ramaswamy and N. Menon, *Science* **317**, 105 (2007).
- [36] M. C. Marchetti et. al., *Rev. Mod. Phys.* **85**, 1143 (2013).
- [37] A. Czirok, H. E. Stanley, and T. Vicsek, *J. Phys. A* **30**, 1375-1385 (1997).
- [38] M. Aldana, V. Dossetti, C. Huepe, V. M. Kenkre, and H. Larralde, *Phys. Rev. Lett.* **98**, 095702 (2007).
- [39] M. Aldana and C. Huepe, *J. Stat. Phys.* **112**, 135-153 (2003).
- [40] B. Bhattacharjee, K. Bhattacharya and S. S. Manna, *Frontiers in Physics*, **1**, 1 (2014).
- [41] H. Chaté, F. Ginelli and R. Montagne, *Phys. Rev. Lett.*, **96**, 180602-180605 (2006).
- [42] K. Binder, *Phys. Rev. L.* **47**, 9 (1981).
- [43] M. S. S. Challa and D. P. Landau, *Phys. Rev. B* **33**, 1 (1986).
- [44] M. S. S. Challa, D. P. Landau and K. Binder, *Phys. Rev. B* **34**, 3 (1986).
- [45] B. Bhattacharjee, S. Mishra and S. S. Manna, *Phys. Rev. E* **92**, 062134 (2015).

- [46] B. Bhattacharjee and S. S. Manna, *submitted*.
- [47] A. Baronchelli, M. Felici, V. Loreto, E. Caglioti and L. Steels, *J. Stat. Mech.* **P06014** (2006).
- [48] A. Baronchelli, V. Loreto and L. Steels, *Int. J. Mod. Phys. C* **19(05)**, 785-812 (2008).
- [49] L. Steels, *Artificial Life*, **2(3)**, 318-332 (1995).
- [50] L. Steels, *p179 in Artificial Life V*, 1996, Nara, Japan.
- [51] A. Baronchelli, L. Dall'Asta, A. Barrat and V. Loreto, *Phys. Rev. E* **73(1)**, 015102(R) (2006).
- [52] L. Dall'Asta, A. Baronchelli, A. Barrat and V. Loreto, *Phys. Rev. E* **74(3)**, 036105 (2006).
- [53] P. Erdős and A. Rényi, *Publ. Math. (Debrecen)* **6**, 290-297 (1959).
- [54] P. Erdős and A. Rényi, *Publ. Math. Inst. Hung. Acad. Sci.* **5**, 17 (1960).
- [55] L. Dall'Asta and A. Baronchelli, *J. Phys. A*, **39(48)**, 14851 (2006).
- [56] A. Baronchelli, *Phys. Rev. E* **83(4)**, 046103 (2011).
- [57] S. K. Maity, T. V. Manoj and A. Mukherjee, *Phys. Rev. E* **86(3)**, 036110 (2012).
- [58] A. Puglisi, A. Baronchelli and V. Loreto, *Proc. Natl. Acad. Sci.* **105(23)**, 7936-7940 (2008).
- [59] V. Loreto, A. Mukherjee and F. Tria, *Proc. Natl. Acad. Sci.* **109(18)**, 6819-6824 (2012).
- [60] B. Bhattacharjee, S. S. Manna and A. Mukherjee, *Phys. Rev. E* **87(6)**, 062808 (2013).
- [61] B. Bhattacharjee, A. Datta and S. S. Manna, *Physica A* **478**, 177-187 (2017) .
- [62] Nigel Goldenfeld, *Lectures on Phase Transitions and the Renormalization Group*, (Perseus Books, Reading, Massachusetts, 1992).
- [63] Leo P. Kadanoff, *Physics* **2(6)**, 263-272 (1966).
- [64] A. Z. Patashinskii and V. L. Pokrovskii, *J. Exptl. Theoret. Phys. (U.S.S.R.)* **50**, 439-447 (1966).
- [65] M. E. Fisher, *Rep. Prog. Phys.* **30**, 615 (1967).
- [66] L. P. Kadanoff et. al., *Rev. Mod. Phys.* **39**, 395 (1967).
- [67] H. Eugene Stanley *Reviews of Modern Physics*, **71**, 2 (1999).
- [68] David J. Gross and R. Jackiw, *Phys. Rev. D* **6**, 477 (1972).

- [69] P. J. E. Peebles, 1980, *The Large Scale Structure of the Universe*, (Princeton Press, Princeton, (1980)).
- [70] W. Z. Lenz, *Phys.*, **21**, 613 (1920).
- [71] E. Z. Ising, *Physik*, **31**, 253(1925).
- [72] L. Onsager, *Phys. Rev.*, **65**, 117-149 (1944).
- [73] K. G. Wilson, *Phys. Rev. B* **4**, 3174 (1971).
- [74] E. Brežin, D. J. Wallace and K. G Wilson, *Phys. Rev. B* **7**, 232 (1973).
- [75] P. R. Kozak, M. P. Kozlovskii and Z. E. Usatenko, *J. Phys. A, Math. Theor.* **43**, 495001 (2010(19pp)).
- [76] R. H. Swendsen, and J. Wang, *Phys. Rev. Lett.*, **58(2)**, 86-88 (1987).
- [77] C. F. Baillie, D. A. Johnston and G. W. Kilcup, *The Journal of Supercomputing*, **4**, 277-300 (1990).
- [78] R. A. Holley and T. M. Liggett, *The Annals of Probability*, **3**, 4 (1975), pp. 643-663.
- [79] K. Suchecki, Víctor M. Eguíluz and M. S. Miguel, *Phys. Rev. E*, **72**, 036132 (2005).
- [80] V. Sood and S. Redner, *PRL* **94**, 178701 (2005).
- [81] S. Milgram, *Psychology Today*, **1(1)**, 61-67 (1967).
- [82] R. Albert and A. Barabási, *Rev. of Modern Phys.*, **74**, (2002).
- [83] R Albert, H. Jeong and A. Barabási, *Nature* **401**, 130-131 (1999).
- [84] M. Faloutsos, P. Faloutsos and C. Faloutsos, *Comput. Commun. Rev.* **29**, 251 (1999).
- [85] H. Jeong, B. Tombor, R. Albert, Z. N. Oltvai, and A. L. Barabási, *Nature (London)* **407**, 651 (2000).
- [86] A.-L. Barabási and R. Albert, *Science*, **286**, 509 (1999).
- [87] D. J. Watts and S. H. Strogatz, *Nature*, **393**, 4 (1998).
- [88] S. Wasserman and K. Faust, *Social Network Analysis: Methods and Applications*, (Cambridge University Press, 1994).
- [89] A. Barrat and M. Weigt, *Eur. Phys. J. B* **13**, 547–560 (2000).
- [90] D. S. Callaway et. al., *Phys. Rev. Lett.* **85**, 25 (2000).
- [91] Reynolds, C. W. (1987), *Computer Graphics*, **21**, 25-34 (1987).

- [92] F. Ginelli, and H. Chaté, *Phys. Rev. Lett.*, **105**, 168103 (2010).
- [93] J. Buhl et. al., *Science*, **312**, 1402-1406 (2006).
- [94] M. Nagy, Z. Ákos, D. Biro and T. Vicsek, *Nature*, **464**, 890-893 (2010).
- [95] D. P. Croft et. al., *Okios*, **100**, 429 (2003).
- [96] M. Moussaïd et. al., *PLoS ONE*, **5**, e10047 (2010).
- [97] A. Jadbabaie, J. Lin and A. S. Morse, *Automatic Control, IEEE Transactions*, **48**, 988-1001 (2003).
- [98] H. G. Tanner, A. Jadbabaie and G. J. Pappas, *Proceedings of the 42nd IEEE Conference on Decision and Control*, **2**, 2010-2015(2003).
- [99] N. W. F. Bode, A. J. Wood and D. W. Franks, *Anim. Behav.*, **82**, 29-38 (2011).
- [100] J. Dall and M. Christensen, *Phys. Rev. E*, **66**, 016121-016129 (2002).
- [101] H.J. Herrmann, D.C. Hong and H.E. Stanley, *J. Phys. A*, **17**, L261-L266 (1984).
- [102] J. M. Kosterlitz and D. J. Thouless, *J. Phys. C*, **60**, 1181-1203 (1973).
- [103] S. Miyashita, H. Nishimori, A. Kuroda and M. Suzuki, *Prog. Theor. Phys.*, **60**, 1669-1685 (1978).
- [104] J. Tobochnik and G. V. Chester, *Phys. Rev. B*, **20**, 3761-3769 (1979).
- [105] R. Olfati-Saber and R. M. Murray, *Proceedings of the IEEE*, **95**, 215-233 (2007).
- [106] S. Floyd, *IEE/ACM Transactions on networking*, **2**, 122-136 (1994).
- [107] P. Szabó, M. Nagy and T. Vicsek, *Phys. Rev. E* **79**, 021908 (2009).
- [108] H. Chaté, F. Ginelli and G. Grégoire, *Phys. Rev. Lett.* **99**, 229601 (2007).
- [109] K. Binder et. al., *Int. J. Mod. Phys. C* **3**, 1025 (1992).
- [110] E. Bertin, M. Droz, and G. Grégoire, *J. Phys A: Math. Theor.* **42**, 445001 (2009).
- [111] E. Ben-Jacob, I. Cohen, O. Shochet, A. Czirók and T. Vicsek, *Phys. Rev. Lett.* **75**, 2899 (1995).
- [112] E. Rauch, M. Millonas and D. Chialvo, *Phys. Lett. A* **207**, 185 (1995).
- [113] C. Feare, *The Starling* (Oxford: Oxford University Press) (1984).
- [114] S. Hubbard, P. Babak, S. Sigurdsson and K. Magnusson, *Ecol. Model.* **174**, 359 (2004).

- [115] A. Baskaran and M. C. Marchetti, *Phys. Rev. Lett.* **101**, 268101 (2008).
- [116] L. Dall'Asta, A. Baronchelli, A. Barrat and V. Loreto, *Agreement dynamics on small-world networks*, *Europhys. Lett.*, 73.6 (2006) 969.
- [117] W. T. Fitch, L. Huber and T. Bugnyar, *Neuron* **65**, 795 (2010).
- [118] P. Hendriks et. al., in *Conflicts in Interpretation 2010*, Equinox Publishing, London.
- [119] D. Stauffer and A. Aharony, *Introduction to Percolation Theory* (Taylor & Francis, London, 1994).
- [120] S. K. Maity, A. Mukherjee, F. Tria and V. Loreto, *Euro. Phys. Lett.*, **101**, 68004 (2013).
- [121] V. Loreto, A. Baronchelli, A. Mukherjee, A. Pugliesia and F. Tria, *J. Stat. Mech.*, **2011(04)**, P04006, (2011).